UNIVERSITAT DE BARCELONA

Understanding PI3K signalling in vessel growth and pathophysiology

Piotr Kobialka

Doctoral thesis entitled

Understanding PI3K signalling in vessel growth and pathophysiology

for obtaining the

academic degree

Doctor of Philosophy

submitted by

Piotr Kobiałka, MS

Doctoral Programme in Biomedicine

Faculty of Medicine

at the University of Barcelona

UNIVERSITAT DE BARCELONA

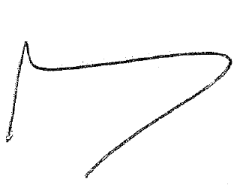

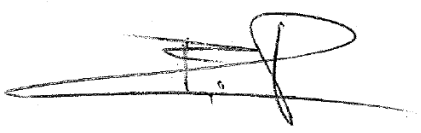

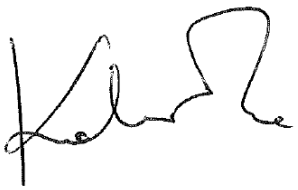

Mariona Graupera i Garcia-Milà, PhD
thesis director

Francesc Viñals Canals, PhD
tutor

Piotr Kobiałka, MS
PhD candidate

Barcelona, 2020

Affidavit

The work entitled “Understanding PI3K signalling in vessel growth and pathophysiology” has been carried out by Piotr Kobiałka in the Vascular Biology and Signalling laboratory at the Bellvitge Institute for Biomedical Research (IDIBELL) under direction of Mariona Graupera. The information derived from the literature has been duly acknowledged in the text and a list of references provided. No part of this work was previously presented for another degree or diploma at this or any other institution.

Financial support

This work received the following financial support:

- European Union’s Horizon 2020 Research and Innovation Programme under the Marie Skłodowska-Curie grant agreement no. 675392 (“PI3K biology in health and disease”)

- ArQule, a wholly owned subsidiary of Merck & Co., Inc., Kenilworth, NJ USA

- La Fundació Bancària Caixa d’Estalvis I Pensions de Barcelona “La Caixa”

Throughout this period, I performed experimental work and training in the laboratories of Len Stephen, PhD (Babraham Institute) and Bart Vanhaesebroeck, PhD (University College London Cancer Institute) as part of secondments funded by “PI3K biology in health and disease” ITN programme (no. 675392).

If you experiment, you have to fail. By definition, experimenting means going to territory where you've never been, where failure is very possible.
How can you know you're going to succeed?
Having the courage to face the unknown is so important.
I love to live in the spaces in between, the places where you leave the comforts of you home and your habits behind and make yourself open to chance.

Marina Abramović
Walk through walls

Abstract

Our knowledge on the molecular basis behind physiological angiogenesis has significantly expanded in the last two decades. This progress also led to improvement in understanding of many vascular-related diseases in which angiogenesis is pathologically altered. Among many molecular regulators of angiogenesis, a family of lipid kinases called phosphatidylinositol 3-kinases (PI3Ks) occupies an important position in controlling endothelial cell functions. Indeed, numerous studies showed that endothelial cells are highly sensitive to fluctuations in the levels of phospholipids generated by these enzymes.

Although highly conservative, the eight PI3K isoforms can produce three different types of phospholipids and this phenomenon formed the basis of the division into three different classes. Two members, class I PI3Kα and class II PI3K-C2α, are essential for proper vascular development. Moreover, somatic activating mutations in the gene encoding PI3Kα (*PIK3CA*) were found to cause 25% of venous malformations – a non-malignant, painful and mainly pediatric vascular disease for which the treatment options are limited. The vascular function of other isoforms, in particular class II PI3K-C2β, remains enigmatic. This is surprising given that this isoform is also express in cultured endothelial cells.

This thesis is composed of two principal objectives objectives which together have been conceived to increase our knowledge on PI3K signaling in the endothelium. In the first part I evaluated the therapeutic efficacy of pan-AKT inhibitor, miransertib, in *Pik3ca*-driven vascular malformations using a preclinical mouse model. I showed that miransertib significantly prevents and reverts *Pik3ca*-associated vascular hyperplasia through inhibition of endothelial cell proliferation. My results provide rationale for the therapeutic intervention of miransertib in treating patients with vascular malformations. The second part of the thesis studies the impact of PI3K-C2β isoform on blood vessel expansion and endothelial cell biology. Using both *in vivo* and *in vitro* models,

I demonstrated for the first time that PI3K-C2β regulates retinal vascularity and vessel width, most likely as result of elevated vascular mTORC1 activity. Moreover, PI3K-C2β kinase inactivation led to increased collagen IV deposition and more stable vascular connections. In parallel, we showed that blood vessel-associated pericytes express high levels of PI3K-C2β and that its loss of function alters their morphology. Finally, we addressed the role of PI3K-C2β in the pathological neoangiogenesis associated with oxygen-induced retinopathy.

Contents

List of figures used in the text

List of tables used in the text

List of non-standard abbreviations

AJ	adherens unction
Alk1	anaplastic lymphoma kinase 1
AMPK	5' AMP-activated protein kinase
Ang	angiopoietin
BMP9	bone morphogenetic protein 9
DLL4	delta-like 4 ligand
DTT	dithiothreitol
DMSO	dimethyl sulfoxide
EC	endothelial cell
ECM	extracellular matrix
EdU	5-ethynyl-2-deoxyuridine
EMP	erythro-myeloid progenitor cell
eNOS	endothelial nitric oxide synthase
FOXO1	forkhead box O transcription factor 1
GPCR	G protein coupled receptor
GSK3	glycogen synthase kinase 3
HDL	high density lipoprotein
HHT	hereditary hemorrhagic telangiectasia
HUVEC	human umbilical vein endothelial cells
IGF	insulin growth factor
LKB1	liver kinase B1
LM	lymphatic malformation
MAPK	mitogen-activated protein kinases
MBPC	mouse brain pericytes
MLEC	mouse lung endothelial cells
MMP	metalloproteinase
mTOR	mammalian target of rapamycin
MYPT	myosin phosphatase targeting protein
NF-κB	nuclear factor kappa-light-chain-enhancer of activated B cells
NICD	Notch intracellular domain
NO	nitric oxide
NRARP	Notch-regulated ankyrin repeat protein
Nrp	neuropilin
PAGE	polyacrylamide gel electrophoresis
PC	pericyte
PDGF-B	platelet derived growth factor-B
PDGFRβ	platelet derived growth factor receptor-beta
PDK1	phosphoinositide-dependent kinase 1
PGF	placental growth factor
PH	plextrin homology (domain)
PHTS	PTEN hamartoma tumour syndrome
PI3K	phosphoinositide 3-kinases

PI(3)P	phosphatidylinositol 3-phosphate
$PI(3,4)P_2$	phosphatidylinositol 4,5-bisphosphate
$PI(3,4,5)P_3$	phosphatidylinositol 3,4,5-trisphosphate
PKB	protein kinase B (known as AKT)
PRAS40	proline-rich AKT substrate of 40 kDa
PROS	*PIK3CA*-related overgrowth spectrum
PTEN	phosphatase and tensin homolog
RBPJ	recombination signal binding protein for immunoglobulin kappa J region
RTK	receptor tyrosine kinase
S1P	sphingosine 1 phosphate
S6	S6 ribosomal protein
SDS	sodium dodecyl sulfate
SHIP1	Src homology 2 domain containing inositol polyphosphate 5-phosphatase 1
TGFβ	transforming growth factor beta
Tie	tyrosine kinase with immunoglobulin-like and EGF-like domains
TJ	tight junction
TSC	tuberous sclerosis complex
VE-cadherin	vascular endothelial cadherin
VEGF	vascular endothelial growth factor
VEGFR	vascular endothelial growth factor receptor
VM	venous malformation
VPS34	vacuolar protein sorting 34
vSMC	vascular smooth muscle cell

CHAPTER 1
Introduction

1.1. Blood vessel development

1.1.1. Circulatory system in mammals

The proper function of the body depends on highly specialised vascular networks – blood vessels and lymphatics. They provide the tissues with necessary nutrients (including hormones and growth factors) and oxygen, remove metabolic waste, but also support cell trafficking and thermoregulation. The importance of the cardiovascular system is reflected in the fact that it is one of the first systems to develop during embryogenesis. The circulatory system consists of a heart and vascular tubes organised into arteries, veins and interconnecting capillary vessels. The blood, transported from the heart through arteries, is distributed across the body and comes back through the veins. The extravasated plasma constitutes the interstitial fluid. Most of it is reabsorbed by venous capillaries, but a small fraction is collected by lymphatics and, upon clearance, is reincorporated into the blood stream [1].

1.1.2. Anatomy and origin of blood vessels

The heterogeneity in vessel types – arteries, veins and capillaries – constitutes an anatomical consequence of the differences in function they serve. In general, all blood vessels are composed of three layers: tunica intima, tunica media and tunica externa. Tunica intima constitutes the innermost layer and is continuously lined by endothelial cells (ECs), covered by the fibrous basement membrane. Tunica media, made of vascular smooth-muscle cells (vSMC) and elastic fibers, varies in thickness depending on the vessel type, being the thickest in arteries. The outermost tunica externa is enriched in collagen that maintains and stabilises the vessel structure [2]. ECs – the main building blocks of vessels – originate mainly from the mesoderm, one of the three main cell layers of the developing embryo. Angioblasts, mesoderm-derived multipotent stem

cells, can differentiate into endothelial cells that form the primitive vascular network. Surprisingly, the most recent studies identified another source of vascular ECs – yolk sac-derived erythro-myeloid progenitor cells (EMPs) – thus demonstrating that ECs may stem from two distinct lineages [3]. This could partially explain why endothelial cells from different niches exhibit substantial molecular and biochemical differences.

1.1.3. Vessel growth in mammals

De novo blood vessel growth occurs during early embryogenesis and involves the assembly of angioblasts-derived ECs into the primordial vascular web – a process called vasculogenesis. Subsequently, most of the vasculature expands through a process of sprouting angiogenesis during which endothelial cells sprout and form new vessels from the existing ones. Interestingly, new blood vessels can also be formed through the splitting of existing tubes. This process, called intussusceptive angiogenesis, requires the formation of the endothelial intraluminal pillar that protrudes across the tube resulting in vessel duplication, bifurcation or pruning (vessel remodelling) [4-5]. While most ECs during adulthood are quiescent, they maintain a high plasticity and capacity to respond to proangiogenic factors upon certain circumstances. Those might be of physiological nature, such as endometrial angiogenesis during menstrual cycles or muscle angiogenesis upon regular exercise, but they are also often associated with pathological vessel growth in wound healing, solid tumours, vascular malformations and eye-associated disorders (e.g. retinopathy) [6].

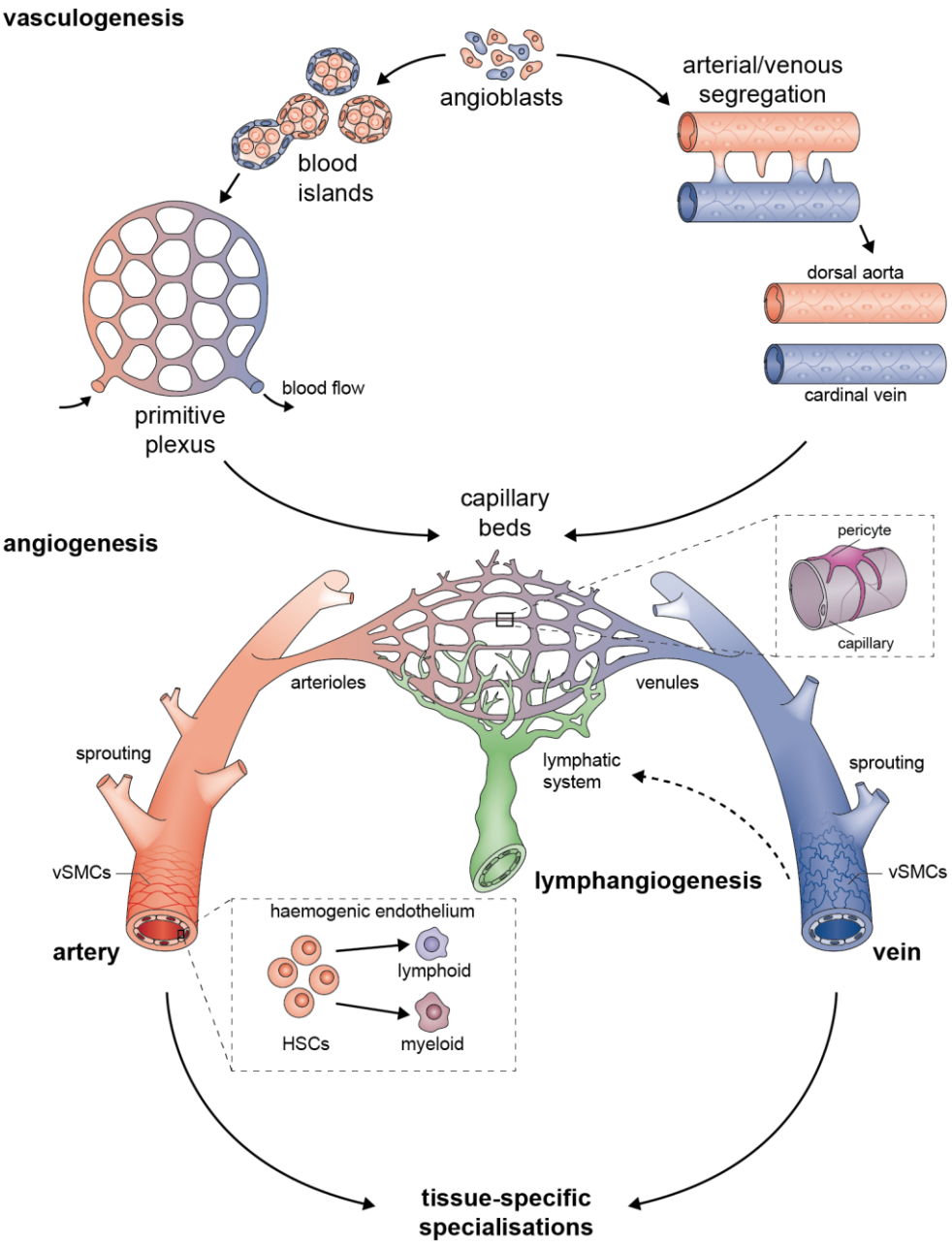

Figure 1. 1. Blood vessel formation during development.

Mesoderm-derived endothelial cell progenitors, angioblasts, form so-called blood islands that subsequently grow into a primitive vascular plexus, consisting of both arteries and veins. Arterial- and venous-fated angioblasts may also coalesce to develop the first embryonic blood vessels – dorsal aorta and cardinal vein. Upon their assembly and consequent angiogenic expansion and remodelling, the complex and hierarchical vascular network of arteries, arterioles, capillaries, venules and veins is formed. Vessel maturation and stabilisation is achieved through the recruitment of mural cells (vascular smooth-muscle cells and pericytes). Vein-derived lymphatic ECs give rise to the lymphatic system (lymphangiogenesis). Blood vessels acquire their tissue-specific properties through a process of endothelial specialisation that changes the molecular signature and consequently biophysical properties of the cells (adapted and modified from [7]).

1.1.4. Sprouting angiogenesis at a glance

Sprouting angiogenesis is a dynamic process that requires strict control on both the cellular and molecular level. It consists of many consecutive steps, each differentially regulated, that include: 1) sprout initiation, 2) sprout elongation, 3) sprout anastomosis and lumen formation, 4) vessel maturation and remodelling and 5) reestablishment of the vessel quiescence. The initiation of angiogenesis may occur independently in many vessels, therefore a finely tuned cooperation between cells involved in this process is crucial.

1.1.4.1. Initiation of vessel sprouting and elongation

Upon activation by proangiogenic stimuli, ECs undergo complex morpho-biochemical changes that allow them to invade and expand in avascularised tissues. Activated ECs secrete metalloproteinases (MMPs) that partially degrade the basement membrane, providing space for ECs to penetrate the hypoxic area. Hypoxia, the key factor stimulating angiogenesis, strongly induces the expression and release of vascular endothelial growth factor (VEGF) that binds and activates the vascular endothelial growth factor receptor 2 (VEGFR2), highly enriched in the endothelium. This spearheads a profound change in EC morphology, behaviour and metabolism. VEGF-A-activated ECs protrude filopodia and acquire migratory properties. These, so-called, tip cells upregulate the expression of the Delta-like 4 (Dll4) ligand that, subsequently, binds to the Notch1 receptor on adjacent cells (so-called stalk cells). While tip cells lead the migration towards proangiogenic environment, stalk cells elongate and actively proliferate to build up a structure of the new vascular tube [6]. To prevent from uncontrolled growth, Notch1 signalling in stalk cells downregulates the expression of VEGFR2, thus restrains the tip cell specification (lateral inhibition) [8-9]. On the other hand, it upregulates VEGFR1, a decoy receptor with high affinity to VEGF-A. Indeed, previous studies showed that genetic and pharmacological inactivation of both Dll4 and Notch1 resulted in vascular hypertrophy due to increased number of filopodia-enriched tip cells, indicating that Notch signalling negatively regulates vessel sprouting and branching [10-12]. In fact, tip/stalk cell phenotypes are dynamically interchangeable through VEGFR2-Dll4-Notch1 circuit, but not genetically predetermined [13].

Proliferation and elongation capacities of the stalk cells drive the extension of new sprouts. Activation of Notch signalling in stalk cells triggers the expression of Notch-regulated ankyrin repeat-containing protein (NRARP) that turns on the Wnt/β-catenin signalling pathway to regulate ECs proliferation and vessel stability. High Notch activity leads to cell cycle arrest, while Wnt signalling promotes ECs proliferation (through Lef1/Cyclin D1) and cell-cell interaction, hence Notch-active stalk cells remain proliferative despite receiving a suppressive signal [14]. Moreover, actin-mediated changes in stalk cell shape drive the elongation of the nascent sprout. This process requires dynamic endothelial cell shuffling and remodelling of cell junctions, and is modulated by the activity of VE-cadherin [15]. Finally, stalk cells produce the basement membrane that stabilises the stem of the newly formed vessel.

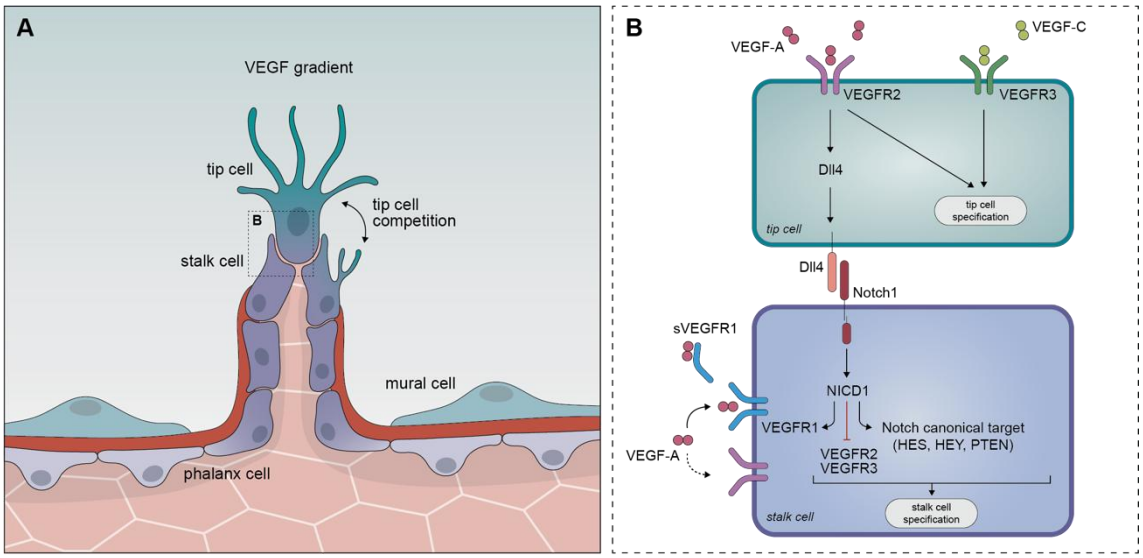

Figure 1. 2. Tip/stalk cell specification during sprouting angiogenesis.
(A) Upon VEGF stimulation, ECs acquire migratory (tip cells) and proliferative properties (stalk cells). VEGF-A/VEGFR2 (or VEGF-C/VEGFR3 in lymphatics) signalling induces tip/stalk cell specification programme. **(B)** Tip cells overexpress Dll4 ligand that binds to Notch1 receptor on adjacent cells. To ensure that no other tip cells are being formed, activated Notch1 signalling downregulates the expression of VEGFR2 and VEGFR3, while upregulating the expression of a decoy receptor VEGFR1. Moreover, Notch-mediated transcription of HES, HEY, PTEN and NRARP, among others, is activated thus promoting stalk cell specification.

1.1.4.2. Anastomosis and lumen formation

Vessel fusion (anastomosis) occurs when the tip cells from distant sprouts encounter and form an apical membrane, with stable cell-cell VE-cadherin junctions (end-to-end fashion). Additionally, tip cells can join a pre-existing blood vessel (end-to-side fashion). Depending on whether the sprouts are already lumenised or not, two different cellular mechanisms have been proposed. Anastomosis of lumenised vessels is driven by blood flow-triggered shear stress within the tube. In non-lumenised sprouts, the apical membrane slowly expands across the vessel [16]. Interestingly, tissue macrophages were shown to facilitate anastomosis through the interaction with the tip cells [17].

The proper function of vessels requires the nascent sprouts to be luminised. Although still little is known about lumen formation in the newly formed vessels, several studies proposed possible mechanisms through which this process can occur. The most common mechanisms include cell and cord hollowing, respectively. During cell hollowing, the lumen is formed through the intracellular fusion of pinocytic vacuoles within neighbouring ECs that, subsequently, expand across the nascent vessel. On the other hand, the development of the vessel cord through the establishment of junction-mediated apical polarity between adjacent ECs is followed by dynamic cell rearrangements to generate an extracellular lumen. While the molecular control behind lumen formation still remains obscure, it is generally accepted that different types of vascular beds use alternative mechanisms to establish the proper lumen [6,18-19].

1.1.4.3. Vessel maturation and remodelling

Maturation is crucial for the vessels to function and it encompasses the formation of cell junctions between ECs, recruitment of mural cells that regulate the endothelium and stabilise the vessel (further discussed in the section 1.1.5.), reconstruction of the extracellular matrix (ECM) as well as establishment of the vessel identity and acquirement of the tissue-specific phenotype [20].

Endothelial cell junctions not only facilitate cell attachment to regulate vessel integrity and permeability, they also constitute vital players in inter- and intracellular communication. There are two main types of cell junctions in the endothelium – tight (TJs) and adherens junctions (AJs) – and they are determined by the type of proteins involved. TJs are primarily involved in the regulation of vessel permeability, thus their fundamental role in blood-brain barrier formation. They often include members of claudin protein family, occludin and junctional adhesion molecules. On the other hand, AJs initiate cell contact, regulate cytoskeletal rearrangement and highly contribute to cell signalling. These protein complexes are composed of cadherins and catenins that form homophillic interactions [21-22]. One of the main AJ-associated protein – VE-cadherin – was shown to be of particular importance in EC biology. VE-cadherin deficiency or truncation result in mice embryonic lethality due to severe vascular defects [23-24]. The protein controls endothelial cell integrity, polarity, lumen formation and cell rearrangements and delivers survival signals to endothelial cells and restricts uncontrolled vessel growth [25].

Both the basement membrane and the interstitial ECM constitute the vascular ECM. This network, highly enriched in protein polymers, macromolecules, enzymes and growth factors, serves mostly as a protection against blood flow-induced shear stress, providing mechanical strength to the vascular tubes. The basement membrane encapsulates both ECs and mural cells, thus facilitating the tight cooperation between those cell types during vessel maturation. Interestingly, vascular ECM is not only involved in vessel maturation, but it also actively modulates the sprouting of the new vessels – it is an important source of proangiogenic growth factors (VEGFs, IGFs, PDGF-B, angiopoietins and TGF-βs) [1,26].

Newly formed vasculature undergoes dynamic changes, known as vessel remodelling, to meet the demands of the tissues. Therefore, unnecessary vascular branches are constantly being removed (vessel pruning and regression) [27]. Low levels of VEGF may induce EC apoptosis and thus vessel pruning [28], but recent studies also suggest that ECs actively re-migrate to well-perfused vascular compartments, indicating that cell rearrangements also contribute to vessel remodelling [29].

1.1.4.4. Reestablishment of vessel quiescence

Once the tissue is vascularised and its demands for oxygen and nutrients are fulfilled, ECs resume their quiescence (so-called phalanx cells) as a result of reduced availability of external proangiogenic signals. The importance of this state is particularly stressed in vascular overgrowth pathologies, e.g. vascular malformations, where ECs fail to respond to 'stop signals' [6]. Nevertheless, ECs constantly receive intra-, auto- and paracrine survival cues to maintain cell viability and vessel integrity. Intracrine and

autocrine VEGF was shown to protect ECs from apoptosis and autophagy by activating PI3K/AKT/FOXO1 signalling [30]. Moreover, EC survival is also mediated by Ang1/Tie2 [31] and BMP9/Alk1 signalling pathways as well as blood flow-associated shear stress [2].

1.1.5. The role of mural cells in vessel growth

Vascular tubes are surrounded by mural cells that are subdivided into vascular smooth-muscle cells (vSMCs) and pericytes (PCs). While vSMCs surround vessels of a big caliber, like arteries and veins, PCs can be found mostly in small arterioles, venules and capillaries. The differences in the location of the mural cells within the vascular niche are reflected by the variety in their morphology as well as molecular signature. Therefore, to discriminate vSMCs from PCs, different molecular markers (both membrane and cytosolic) are used. PCs are embedded in the basement membrane and they directly interact with ECs through AJs (so-called peg-sockets), occluding junctions as well as adhesions plaques. They constitute an essential element in the vascular development and homeostasis, playing a role in angiogenesis, regulation of blood flow, coagulation and immune response [32-33].

Several studies identified molecular mechanisms through which PCs monitor the vessel growth. A sophisticated, paracrine communication between PCs and ECs is required in the beginning of vessel sprouting as well as during maturation and quiescence. Migratory tip cells secrete platelet-derived growth factor B (PDGF-B) that attracts expressing its receptor (PDGFRβ) PCs, resulting in the instant stabilisation of the nascent vessel. Moreover, PC-secreted Ang1 binds to Tie2 receptors on ECs and promotes their survival and quiescence. On a contrary, Ang2 – an antagonist of Tie2 – is secreted by ECs during the initiation of angiogenesis as it allows PCs detachment [1,6]. This implies that a balance between Ang1 and Ang2 needs to be controlled for a proper vascular function. Indeed, upregulated levels of Ang2 are commonly seen in vascular pathologies, with diabetic retinopathy among them.

1.1.6. Molecular regulation of angiogenesis

The complexity of vascular development is reflected in its strict control. Indeed, several signalling pathways have been implicated in the regulation of vessel sprouting, remodelling, maturation and identity. Over the past few decades, two particular signalling cues – VEGF/VEGFR and Notch – have emerged as essential drivers of angiogenesis and vessel function (discussed in the sections 1.1.6.1 and 1.1.6.2.). Other essential signals include PDGF-B and its receptor PDGFRβ, TGFβ and Ephrin/Eph [34]. Furthermore, the last decade of research identified PI3K signalling as another key hub controlling EC biology, and thus angiogenesis (further discussed in detail in the section 1.2.).

1.1.6.1. VEGF/VEGFR signalling

There are five vascular endothelial growth factor ligands in mammals (VEGF-A with its many splicing variants, VEGF-B, VEGF-C, VEGF-D and PGF) that can bind to three vascular endothelial growth factor receptors (VEGFR1, VEGFR2 and VEGFR3). VEGF-A,

the prototype protein of the VEGF family, highly controls vessel permeability as well as EC migration and proliferation during vessel sprouting. In fact, VEGF-A haploinsufficiency leads to embryonic lethality due to abnormal blood vessel formation at mid-gestation [35]. It exists in many isoforms – a result of RNA alternative splicing – that differ in their affinity to the receptors. VEGF-A variants generate a gradient important for the vascular development and patterning by binding to the membrane- and/or ECM-associated heparan sulfate proteoglycans [36].

VEGF-A (and its different forms) can bind to both VEGFR1 and VEGFR2, having the higher affinity to the former. Interestingly, VEGFR1 has much weaker tyrosine kinase activity compared to VEGFR2 and can also exist in its secreted, inactive form, therefore acting as a decoy receptor regulating the magnitude of proangiogenic response. *In vivo* studies in mice highlighted the indispensable functions of all receptors in vessel growth. Both VEGFR1- and VEGFR2-deficient mice die during early embryonic development due to severe vascular defects, but exhibit distinct phenotypes – while VEGFR2 knockout mice showed no vascular development as a result of impaired endothelial cell sprouting and proliferation [37-38], VEGFR1 deficiency led to excessive endothelial cell production, sprouting and vascular disorganisation [39-40].

VEGFR3 is mostly present in lymphatic ECs, thus its essential role in lymphangiogenesis. Its high expression was also shown in tip ECs, suggesting its putative function during blood vessel formation [32,36]. Indeed, VEGFR3 blockade with monoclonal antibodies suppressed angiogenic sprouting and branching in the mouse retina [41]. Surprisingly, the opposite has been observed upon genetic EC-specific *Vegfr3* deletion, indicating a dual nature of the receptor and suggesting its ligand-dependent and ligand-independent functions in angiogenesis [42]. Moreover, it has recently been shown that VEGFR3 controls VEGF-A/VEGFR2 signalling and vessel permeability [43]. To fully define the context-dependent isoform-specific functions of VEGFs and their receptors as well as their interactions, more studies are still needed.

1.1.6.2. Notch signalling

Notch constitutes a crucial signalling cue during embryogenesis, including cardiovascular system development. In mammals, this highly evolutionary conserved signalling pathway consists of four Notch receptors (Notch1, Notch2, Notch3 and Notch4) and five ligands (Dll1, Dll3, Dll4, Jagged1 and Jagged2). The activation of the pathway is initiated by a direct cell-cell contact, a membrane-bound ligand of a signal-sending cell interacts with a membrane-bound receptor of adjacent, signal-receiving cell. This triggers the release of the Notch Intracellular Domain (NICD) that translocates to the nucleus, couples with a DNA-binding protein (RBPJ) and subsequently induces the transcription of several Notch-modulated genes, including *Hes*, *Hey* and *Dll4* [44].

ECs predominantly express Notch1 and Notch4 receptors and their ligands – Dll1, Dll3 and Jagged1. Several *in vivo* and *in vitro* studies, using loss- and gain-of-function strategies, demonstrated a fundamental role of Notch signalling during angiogenesis. Inactivation of Notch components (Notch1 and/or Dll4) leads to an excessive vessel sprouting, branching and filopodia formation, while activating Notch results in the opposite phenotype [11,38,45]. Dll4/Notch1 axis governs EC specification by driving

tip/stalk cell selection during vessel sprouting (see section 1.1.4.1.). This activates Jagged1 that counteracts Dll4/Notch1 signalling, ultimately balancing the angiogenic growth and maturation [46].

Interestingly, strong Notch signalling drives the arterial differentiation of EC progenitors during early embryogenesis, but it is not required in the postnatal artery formation. On the contrary, Notch signalling plays a key role in the remodelling of vein and venous capillaries. It also contributes to vessel maturation and quiescence [47-48].

1.2. PI3K signalling network

The origin of multicellular organisms required the simultaneous evolution of molecular regulatory systems that would coordinate growth, cell division and survival with a response to nutrients and growth factors. Phosphatidylinositol 3-kinase (PI3K) signalling emerged as one of the central signalling networks that translates the extracellular signals into intracellular actions. It regulates nearly all biological responses, from cell division, growth and differentiation to cell death, motility and vesicle traffic. It is of little surprise then that deregulation of this pathway stands behind many pathologies, such as cancer, overgrowth syndromes, immunological and neurological disorders or diabetes, to name just few [49-50].

PI3Ks are lipid kinases that generate a pool of different phosphatidylinositol derivates, all phosphorylated at the third position of the inositol headgroup. This highly conserved family of enzymes counts eight catalytically active isoforms that, on the basis of substrate preferences, are grouped into three main classes. Class I PI3Ks act as heterodimers, where one of the four catalytic subunits is always bound by one of the corresponding regulators. Based on the regulatory subunit binding, class I is further divided into two subclasses – IA and IB. Class IA includes three isoforms, PI3Kα, PI3Kβ, PI3Kδ (encoded by *PIK3CA*, *PIK3CB*, *PIK3CD* genes, respectively) that bind to one of the five p85 regulatory subunits (p85α, p55α, p50α, p85β and p55γ). Class IB, on the other hand, constitutes only one catalytic isoform, PI3Kγ (encoded by *PIK3CG*), that couples with either p84 or p101 regulatory subunit. These regulatory subunits provide stability to the quickly degradable catalytic subunits, control their kinase activity at basal state as well as allow the recruitment to the phosphorylated tyrosine residues in activated membrane receptors. All class I PI3Ks produce $PI(3,4,5)P_3$ phospholipids. Class II comprises three members – PI3K-C2α, PI3K-C2β and PI3K-C2γ – that act as monomers and give rise to two distinct lipid products, $PI(3,4)P_2$ and PI(3)P. The sole class III enzyme – VPS34 – produces only PI(3)P and is the only isoform shared by all eukaryotic cells [51-52].

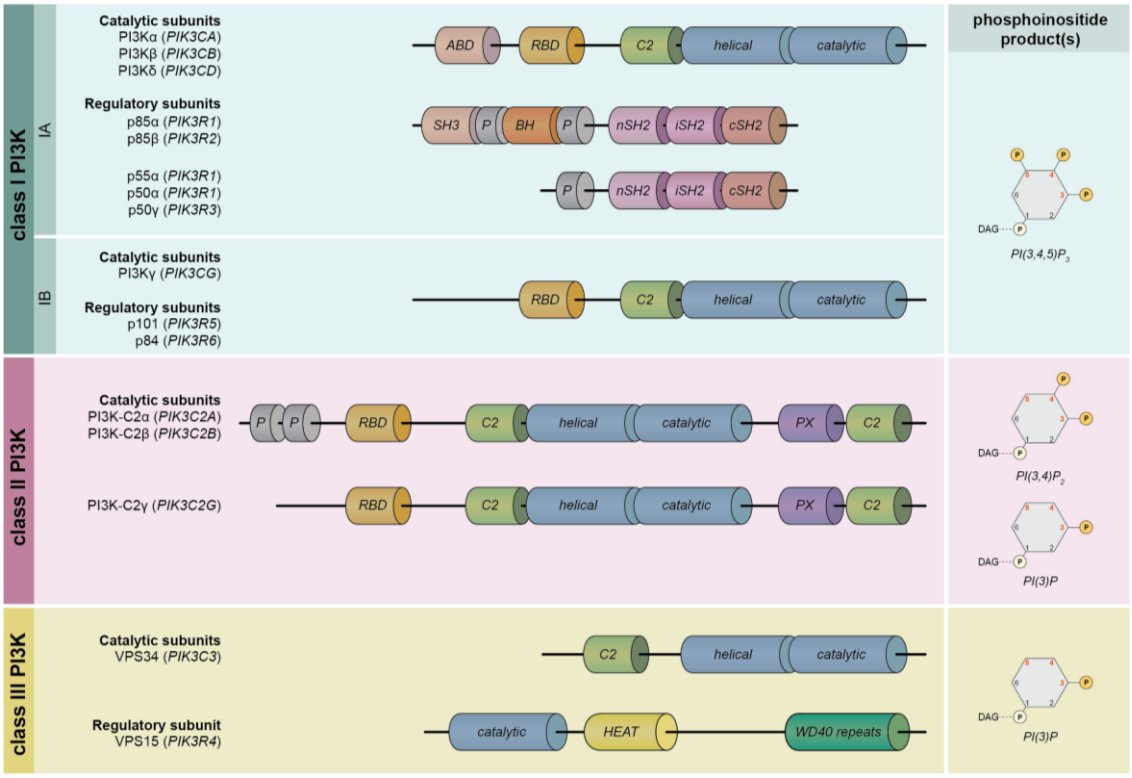

Figure 1. 3. Classification of PI3K enzymes and their catalytic products.
Phosphatidylinositol 3-kinases are grouped into three classes, based on their lipid substrate preferences. All PI3Ks contain the so-called PI3K core, composed of helical, catalytic and C2 domains. Except for class II, PI3Ks act as heterodimers where catalytic subunits couple with their regulator. Class I PI3Ks are subdivided into two groups: class IA where the catalytic subunits (PI3Kα, PI3Kβ, PI3Kδ) bind to one of the p85 regulatory subunits and class IB where the solely catalytic subunit PI3Kγ binds to either p84 or p101 regulatory subunits (not shown). Class II PI3Ks act as holoenzymes. The only class III PI3K isoform, VPS34, couples with the VPS15 regulator. All PI3Ks phosphorylate phosphatidylinositols at the third position of the inositol headgroup. While class I and III generate only one type of lipid ($PI(3,4,5)P_3$ and PI(3)P, respectively), class II PI3Ks can produce both PI(3)P and $PI(3,4)P_2$ phospholipids.

1.2.1. Class I PI3K signalling

Thus far, class I isoforms are the best characterised PI3Ks. Despite some differences in modes of activation, class I PI3Ks engage in signalling downstream of receptor tyrosine kinases (RTKs), G protein-coupled receptors (GPCRs), integrins and small GTPases. Their activation attracts PI3K heterodimers to the plasma membrane through its regulatory subunit, where the enzymatic conversion of $PI(4,5)P_2$ to $PI(3,4,5)P_3$ occurs. This newly produced lipidic secondary messenger allows the recruitment and subsequent activation of serine/threonine kinases – PDK1 and AKT – the latter controlling the activity of major cellular proteins, including GSK3, FOXO transcription factors, TSC2 and mTORC1 as well as eNOS, thus regulating a multitude of cellular responses. The production of $PI(3,4,5)P_3$ is counteracted by lipid phosphatases, such as

PTEN and SHIP, that revert the reaction and give rise to $PI(4,5)P_2$ and $PI(3,4)P_2$, respectively.

Serine/threonine protein kinase AKT, also known as PKB, is a bona fide effector of PI3K. In mammals, it exists in three isoforms – AKT1, AKT2 and AKT3 – encoded by three, evolutionarily conserved genes. While AKT1 and AKT2 are ubiquitously expressed, AKT3 dominates in brain, liver and endocrine tissues. The inactive form of AKT binds to $PI(3,4,5)P_3$ lipid through its N-terminal plextrin homology (PH) domain, and the subsequent phosphorylation of threonine and serine residues (T308 and S473 in AKT1), by PDK1 and mTORC2 respectively, fully activates its kinase potential. There are nearly 100 known protein substrates of AKT that span all functional classes, from protein/lipid kinases and phosphatases, transcription factors to metabolic enzymes, cell cycle regulators and many others [53-54]. Selected processes whose main corresponding proteins are regulated by AKT are summarised in Table 1.

Table 1. Selected AKT substrates and the effect of their regulation on cellular processes.

process	protein involved	AKT-mediated mechanism	reference
cell growth	TSC2	phosphorylation on S939 and T1462 inhibits TSC2, a negative regulator of mTORC1 signalling, thus allowing ribosome biogenesis and translation initiation	[55]
	PRAS40	phosphorylation on T246 inactivates PRAS40, a negative regulator of mTORC1 signalling, thus stimulating cell growth	[56-57]
survival	BAD	phosphorylation on S136 by AKT inactivates BAD and leads to 14-3-3-mediated sequestration, thus inhibiting the proapoptotic function of BAD	[58-59]
	FOXO	phosphorylation on T24 and S256 by AKT leads to 14-3-3-mediated sequestration, thus blockade of FOXO-driven transcription of proapoptotic proteins (e.g. BIM)	[60]
	HDM2	AKT-mediated phosphorylation on S166 and S186 allows nuclear entry and negative regulation of proapoptotic p53	[61]
proliferation	$p27^{Kip1}$	phosphorylation on T167 leads to cytosol sequestration (by 14-3-3), preventing from cell-cycle inhibitory effects of p27	[62-63]
	$p21^{Cip1/WAF1}$	phosphorylation on T145 leads to 14-3-3-mediated cytosol sequestration, preventing from cell-cycle inhibitory effects of p21	[64]
	GSK3	phosphorylation indirectly attenuates the GSK-3-mediated inhibition of cyclin D and E, c-jun and c-myc	[65-66]
metabolism	TBC1D4	phosphorylation permits Rab-mediated translocation of Glut4 to the membrane, thus increasing glucose uptake	[67-68]
	GSK3	phosphorylation inactivates the kinase, therefore promoting glycogen synthesis and lipid production	[69]

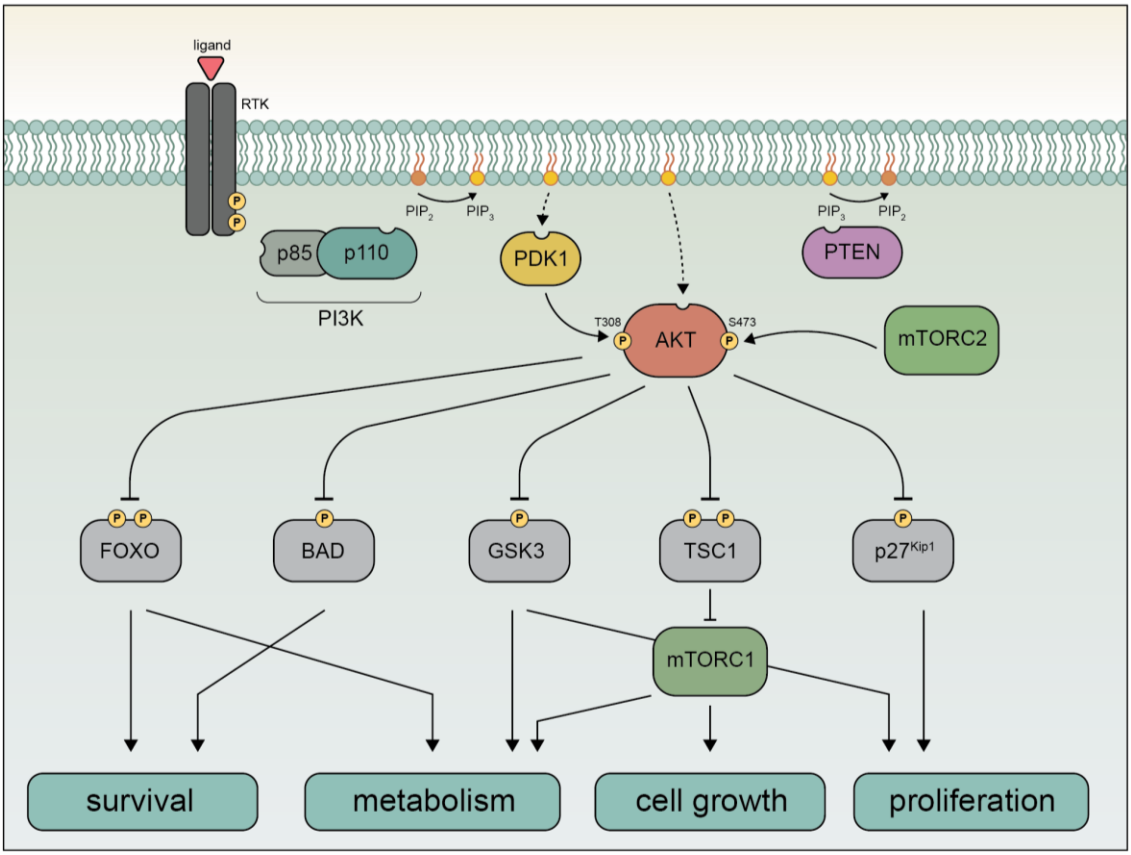

Figure 1. 4. Class I PI3K signalling.

Ligand-mediated stimulation (e.g. insulin) leads to autophosphorylation and activation of a receptor tyrosine kinase (RTK). For simplicity, other modes of activation of class I PI3Ks have been omitted. This indirectly attracts PI3K heterodimers (through p85 regulatory subunit) to the plasma membrane, where the enzymatic conversion of $PI(4,5)P_2$ to $PI(3,4,5)P_3$ occurs. This lipidic secondary messenger attracts PDK1 and AKT (through their PH domains) to the membrane, resulting in AKT phosphorylation at T308. A second phosphorylation at S473 by mTORC2 is necessary for the full activation of the protein. AKT phosphorylates and regulates a plethora of protein substrates, consequently mediating fundamental cellular processes such as survival, cell growth, proliferation and metabolism, to name just few.

1.2.1.1. mTOR signalling

Another signalling hub downstream of PI3K, mTOR (mechanistic target of rapamycin), plays a fundamental role in the regulation of cell growth and metabolism in response to environmental and intracellular stimuli. Isolation of bacterial rapamycin (an antifungal compound with strong immunosuppressive and antiproliferative properties) in 1975 led to identification of mTOR and further accelerated characterisation of its downstream signalling and regulation [70]. Today, it is known that in mammals this serine/threonine kinase forms two protein complexes, namely mTORC1 and mTORC2, that differ in composition and function. While mTORC1 modulates anabolic (biomass synthesis) and catabolic (autophagy) processes, mTORC2 mostly regulates cell proliferation and survival. Both complexes contain mTOR kinase, mLST8 and DEPTOR. mTORC1 additionally binds Raptor and PRAS40, while mTORC2 couples with Rictor, Protor and mSin1. The structure of these complexes and the function of each component are summarised in Figure 1.5. A. High nutrient availability and growth factors stimulation activate mTORC1-dependent signalling and promote protein,

nucleotide, fatty acid and cholesterol biosynthesis, mitochondrial biogenesis as well as glycolysis. On the other hand, nutrient deprivation, energy shortage, cell stress or hypoxia dampen mTORC1 activity, thereby driving catabolic processes and autophagy [71]. Figure 1.5. B schematically illustrates the upstream signals regulating mTORC1 and its downstream targets.

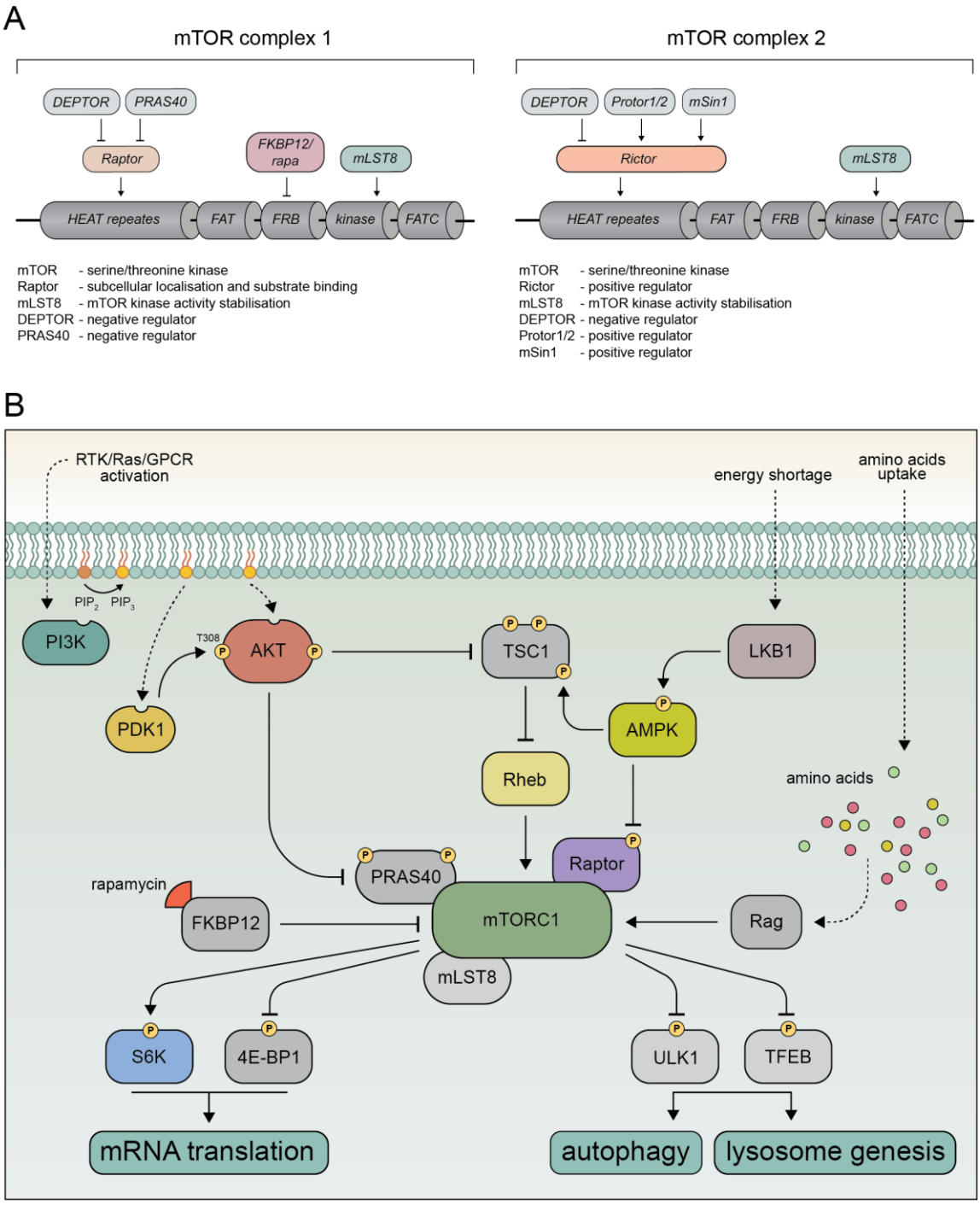

Figure 1. 5. mTOR as a cellular sensor of nutrients, growth factors and energy.
(A) mTORC1 and mTORC2 structure and components. (B) Schematic illustration of different modes of activation of mTORC1 signalling and its main outputs. Growth factors and nutrients stimulate mTORC1,

while energy shortage inhibits its activity. mTOR complex I promotes protein, lipid and nucleotide biosynthesis, while inhibiting catabolic processes such as autophagy and lysosome genesis.

It is important to highlight here that PI3K signalling does not operate in isolation, but in fact is a part of a complex signalling network, with other pathways, such as MAPK/ERK, AMPK and NFκB, intersecting [72].

1.2.2. Class II PI3Ks

For a long time, class II PI3Ks have remained enigmatic and underrated, and it was only recently when their isoform-specific functions have started to emerge. Unlike class I, these isoforms do not act as typical signal transducers. Instead, they regulate vesicular traffic and membrane dynamics, although recent findings indicate that their catalytic activity may indirectly influence cell signalling as well. The two members of class II PI3Ks, PI3K-C2α and PI3K-C2β, are ubiquitously expressed, whereas the expression of PI3K-C2γ is restricted to the liver. So far, no regulatory subunits acting along with these enzymes have been reported. Despite the fact that all class II PI3Ks produce the same pool of phospholipids, PI(3,4)P_2 and PI(3)P, they seem to perform distinct, non-redundant, and at times even opposite functions [52]. PI3K-C2α mainly operates at the cell membrane where it mediates the clathrin-dependent endocytosis. The PI(3,4)P_2 phospholipid is required for the maturation and scission of clathrin-coated pits. On the contrary, PI3K-C2α-produced PI(3)P facilitates the early endosomal sorting and recycling, thus allowing the transit of its contents to the plasma membrane [73]. The cellular role of PI3K-C2β appears to be more elusive, but a recent study showed that it translocates to the membrane of late endosomes/lysosomes, where its lipid product (PI(3,4)P_2) negatively regulates the activity of mTORC1 [74]. This is surprising, since both class I and III PI3Ks are known to activate the mTORC1 signalling cascade instead. Interestingly, both PI3K-C2β and PI3K-C2γ catalytic activities affect insulin-stimulated AKT signalling specifically in hepatocytes, although in an opposite manner. While inactivation of PI3K-C2β leads to an enhanced AKT activity as a result of an early endosomal enlargement [75], blocking the kinase-activity of PI3K-C2γ was shown to inhibit insulin-induced AKT2 activation [76]. Some studies highlighted that PI(3)P produced by PI3K-C2β promote cell migration [77-79], but others reported that PI3K-C2α also regulates this cellular process [80], suggesting that both isoforms may have overlapping functions and their specific function might depend on cell type and environmental context. This implies that the reported roles of class II PI3Ks, and especially their biological consequence on the organismal level, still require further corroboration.

Apart from the lipid kinase activity, class II PI3K-C2α also have a well demonstrated scaffolding function during mitotic spindle formation. Interestingly, reduced expression of PI3K-C2α causes genomic instability in tumour cells and sensitises tumours to paclitaxel, a chemotherapeutic used to treat breast and lung cancers, among others [81].

1.2.3. Class III PI3K

The highly conservative class III PI3K VPS34, in mammals encoded by the *PIK3C3* gene, can operate in two distinct, tetrameric protein complexes – complex I and II. They are composed of VPS34 bound to the VPS15 regulatory subunit and Beclin 1 and are associated to either ATG14 (complex I) or UVRAG (complex II). The only lipid produced by this enzyme – PI(3)P – plays a role in the regulation of vesicular traffic, in particular endocytosis, phagocytosis (complex II) and autophagosome formation (complex I) [52]. The importance of this isoform has been reflected in several *in vivo* mouse models. Indeed, murine VPS34 knock out results in embryonic lethality due to defects in endocytic trafficking and developmental autophagy [82-83]. Moreover, some studies showed that VPS34 complexes, under certain conditions, enhance SGK3-, LKB1/AMPK- and mTORC1-mediated signalling [84-85].

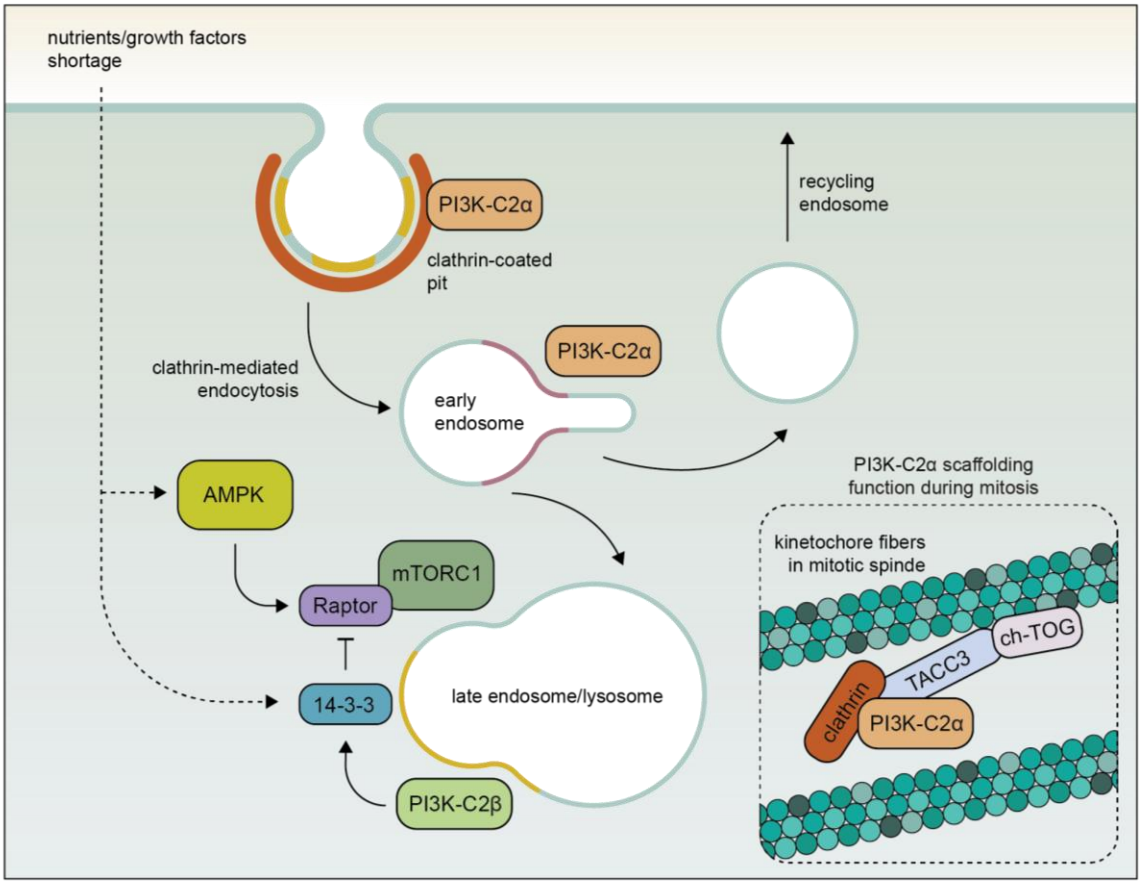

Figure 1. 6. Catalytic and scaffolding roles of II PI3Ks.
The physiological and organismal functions of class II PI3Ks are still unclear. PI3K-C2α-generated $PI(3,4)P_2$ was shown to initiate clathrin-mediated endocytosis and the formation of early endosomes. A different lipid, PI(3)P, produced by PI3K-C2α, facilitates early endosomal sorting and endosome recycling to the plasma membrane. Beyond its catalytic activity, PI3K-C2α interacts with clathrin and TACC3 proteins to stabilize ch-TOG, TACC3 and clathrin complexes on kinetochore fibres during mitosis. Under nutrient shortage, PI3K-C2β-generated $PI(3,4)P_2$ was shown to dissociate mTORC1 from late endosomes/lysosomes (and thus inhibit mTORC1 signalling) by facilitating sequestering of Raptor by 14-3-3 protein.

1.3. PI3K signalling in blood vessel development and EC biology

1.3.1. Class I PI3Ks and their effectors

Many cell signals and receptors that orchestrate EC biology and their response during vessel growth were shown to feed into class I PI3K signalling. These include VEGFs/VEGFRs (excluding VEGFR1 that does not signal through PI3K), Ang/Tie signalling, Ephrin-B2 and VE-cadherin, among others. Interestingly, VEGFR2 was also shown to couple with integrins, VE-cadherin and Nrp1 further extending the list of class I PI3K signalling inputs in ECs [86].

Among class I PI3Ks, only PI3Kα selectively governs ECs behaviour during sprouting angiogenesis. Indeed, both constitutive and EC-specific PI3Kα inactivation in mice led to embryonic lethality due to severe vascular defects in head and trunk [87]. Importantly, this phenotype has not been observed when other class I isoforms have been inactivated specifically in ECs. Detailed studies demonstrated that PI3Kα regulates ECs collective cell migration, rearrangements as well as junctional remodelling. Moreover, high-throughput phosphoproteomic screening revealed that endothelial PI3Kα restrains NUAK1-dependent phosphorylation of MYPT (myosin light chain phosphatase regulatory subunit), thus controlling actomyosin contractility [88]. PI3K signalling was also shown to drive venous differentiation during blood vessel formation in zebrafish [89]. On the contrary, suppression of PI3K signalling stimulated arteriogenesis [90], corroborating a key function of PI3K in the control of vessel identity. EC-specific genetic ablation of four class IA regulatory subunits, namely p85α, p55α, p50α and p85β, resulted in acute haemorrhaging and subsequent embryonic death. This phenotype was rescued upon a single p85α copy retention, indicating a compensatory mechanism between the regulatory subunits [86]. Recent and surprising findings showed that PI3Kβ, although dispensable for ECs, controls PCs proliferation and maturation in a cell-autonomous manner. PC-specific (but not EC) inactivation of this isoform results in an early maturation of PCs that leads to EC quiescence [91]. This implicates that class I PI3K isoforms can regulate sprouting angiogenesis beyond ECs.

PTEN, a negative regulator of PI3K signalling, also plays a pivotal role in angiogenesis. EC-specific Pten loss-of-function mice show that deregulated turnover of $PI(3,4,5)P_3$ leads to deadly haemorrhages and cardiac dysfunction during early embryogenesis [92]. Inactivation of Pten in zebrafish resulted in accelerated angiogenesis [93], and re-introduction of WT and protein phosphatase-deficient Pten significantly rescued the phenotype, indicating that Pten lipid-phosphatase activity is crucial for EC sprouting [94]. Other studies in mice also reported that Pten blocks stalk EC proliferation in angiogenic sprouts downstream of Notch, thus fine-tuning tip and stalk cell selection. Interestingly, Pten arrests EC cell cycle through both its catalytic and scaffolding properties [95].

The EC-specific knockout mouse models showed that not Akt2, but Akt1 isoform plays an essential role in EC biology, phosphorylating and thus affecting many downstream proteins, including eNOS with its pivotal function in the vascular system, mTOR complexes and FOXO transcription factor. Retinal vasculature development is significantly affected in ECs-specific Akt1-deficient mice [96]. Interestingly, despite the

fact that global Akt1 knockout mice show growth retardation, they are viable with a functional vascular system [97].

The inhibition of mTOR complex I by rapamycin in ECs causes impaired proliferation, migration and increased susceptibility to apoptosis as a result of reduced AKT, FOXO1 and FOXO3a phosphorylation, indicating mTORC1-dependent AKT activation [98]. A depletion of endothelial DEPTOR, the negative regulator of both mTORC1 and mTORC2, was shown to promote angiogenesis in heart, kidney and liver tissues through increased production of VEGF [99]. On the other side, recent *in vitro* studies on endothelial cells pointed at mTORC2 in the regulation of actin polymerisation and focal adhesion assembly, and thus migration of those cells [100].

The dynamic response of ECs to proangiogenic factors triggers a profound change in metabolic behaviour that is highly controlled by PI3K-regulated enzymes, e.g. GSK3 or FOXO members. AKT-mediated phosphorylation of FOXO transcription factors dampens their activity as phosphorylated FOXO members are sequestered in the cytoplasm and assigned for degradation. Indeed, FOXO1 was shown to restrict EC proliferation by hampering glycolysis and oxidative phosphorylation through MYC [101]. Moreover, endothelial Foxo1-deprived mice die at mid-gestation as a result of defective vascular growth [101]. *In vitro* assays on FOXO1-knocked down ECs showed reduced capacity for sprout formation and migration, indicating that the FOXO1 transcription factor constitutes a molecular guard of EC activation [102].

1.3.1. Class II PI3Ks

The three rather unexplored and enigmatic isoforms of class II PI3Ks have recently received more attention. In particular, PI3K-C2α isoform has been shown to be crucial for proper vasculature development. EC-specific deficiency of PI3K-C2α leads to embryonic lethality in mice as a result of defective angiogenesis and vessels integrity. On a cellular level, PI3K-C2α participates in delivering an essential junctional protein, VE-cadherin, to the endothelial plasma membrane by controlling endosomal traffic. It is also involved in internalisation of activated VEGF receptors [103].

Very little is known whether and how does PI3K-C2β affect endothelial cell biology. Some studies reported that it is selectively required for S1P- and HDL-induced migration [104]. Interestingly, others showed that S1P-induced EC migration requires the activity of PI3K-C2α as well [80], suggesting that both isoforms might have overlapping functions, and it is likely the cell type and/or environmental context that may determine which of the isoforms takes a lead. Unfortunately, the continuous lack of selective inhibitors of class II PI3Ks poses a real challenge for the interpretation of these data.

1.4. Vascular-related pathologies and their molecular mechanisms

Despite increasing cancer incidence rates, cardiovascular diseases are still number one cause of death worldwide, according to the World Health Organisation. A subgroup of cardiovascular diseases – vascular diseases – are caused by the dysfunction in endothelial and supporting cells. Abnormal vessel growth, observed in many diseases, results from malfunction of angiogenesis that can lead to either vascular insufficiency

(e.g. in ischemia) or vascular overgrowth (e.g. in haemangiomas, retinopathies or vascular malformations). Blood vessels are also an important element of tumour stroma and their structure and function are commonly aberrant, with many vessels being tortuous, hyperpermeable and disorganised. Overall, this highlights that deep understanding of the molecular mechanisms behind vascular diseases and EC dysfunction is essential and may lead to the development of novel therapeutic interventions.

1.4.1. Vascular malformations and associated syndromes

Vascular malformations belong to vascular anomalies, a heterogenous group of congenital diseases characterised by an abnormal growth of the vascular tissue and of different severity, from a simple birthmark to a highly aggressive angiosarcoma. According to the International Society for the Study of Vascular Anomalies, simple vascular malformations can be classified, upon histological analysis, into venous, capillary and lymphatic (so-called low-flow) as well as arteriovenous (so-called high-flow) malformations. Moreover, vascular lesions can manifest in more than one type (e.g. capillary-venous or lymphatic-venous) and can associate with other complex syndromes, encompassing many tissues such as muscles, skin or adipose tissue [105].

Venous malformations (VMs), the most common type of vascular malformations, consist of abnormally dilated venous channels with scarce mural cell coverage. They can be of different sizes and be present in any tissue, such as subcutaneous tissue or internal organs. VMs are painful and disfiguring, with many leading to bleeding and obstruction of organs, thus posing a danger to life. Similarly, lymphatic malformations (LMs) are characterised by dilated lymphatic channels as a result of defects in the development of the lymphatics and can be present in any part of the body. Recent studies identified that the majority of patients (over 80%) with diagnosed LMs carry somatic, mosaic mutations within PI3Kα-encoding gene, *PIK3CA*, and similar mutations were found in around 30% of patients with VMs. Of note, these mutations were among the most common *PIK3CA* mutations (so-called hotspot mutations) found in human cancers – E542K and E542K in the helical domain and H1047R and H1047L in the kinase domain [106-109]. Interestingly, no hotspot *PIK3CA* mutations have been found in germ cells till now. Moreover, *in vivo* experiments in mice showed that activating germline mutations in *Pik3ca* leads to severe vascular damage resulting in embryonic death [110]. These findings suggest that the germline transmission of activating *PIK3CA* mutations is incompatible with life. Postnatal EC-specific *Pik3ca*^{H1047R} mutation was shown to trigger a dramatic vascular hyperplasia in mouse retina as a result of elevated EC proliferation, followed by decreased mural cells (both VSMCs and PCs) coverage and arteriovenous differentiation markers – all features being pathognomonic of VMs [108].

Cancer-associated *PIK3CA* mutations are also present in rare overgrowth disorders, collectively known under the umbrella term *PIK3CA*-Related Overgrowth Spectrum (PROS). PROS exhibits high diversity, regarding the location of the altered tissue and the severity of the disease. *PIK3CA* mutations occur in a mosaic fashion and can affect

nearly all cell types, resulting in an overgrowth that can be either localised (affecting single tissue) or can encompass many tissues and organs and pose a real threat for the proper function of the body. Many PROS patients present vascular malformations of venous, capillary and lymphatic origin [111].

TEK, encoding for Tie2 receptor, constitutes another highly mutated gene found among VMs patients (around 50% of cases), resulting in hyperactivation of PI3K signalling. Interestingly, the hotspot mutations in both *TEK* and *PIK3CA* genes never occur together, indicating a mutual exclusivity [107-108]. Although it is still unclear when and how does the oncogenic PI3Kα trigger the formation of vascular malformations, some studies on mouse embryonic fibroblasts showed that *PIK3CA*^{H1047R} evokes centrosome amplification and genome doubling that cause chromosomal instability in cancer [112]. Of note, many PI3K signalling related genes are commonly mutated in other overgrowth- and vascular malformations-associated syndromes, such as Proteus, PTEN hamartoma tumour syndrome (PHTS) or hereditary haemorrhagic telangiectasia (HHT), with mutations in *AKT1* [113], *PTEN* [114] and *ENG*/*ACVRL1* [115-116] respectively. Together, these findings further cement the unique position of PI3K signalling in ECs and their high sensitivity to $PI(3,4,5)P_3$ fluctuations.

1.4.2. Clinical application of PI3K pathway inhibitors

Owing to the central role of the PI3K signalling pathway in the control of cell growth and proliferation, it is of little surprise that deregulation of this molecular cue leads to severe pathological consequences. Indeed, nearly all human cancers exhibit hyperactive PI3K signalling, and recently many rare overgrowth syndromes, for which no treatment is available thus far, were also shown to carry activating genetic alterations in key PI3K signalling genes, including *PIK3CA*, *AKT*, *PTEN* and *MTOR*. These observations further boosted the urge for development and use of PI3K/AKT/mTOR inhibitors in the clinic, both in oncological and rare disease contexts [117].

Until now, several pan- and isoform-specific PI3K inhibitors have been developed and are either under (pre)clinical investigation or in use. PI3K inhibitors, when used as monotherapy in solid tumours, showed modest therapeutic benefits. This is likely due to insufficient on-target inhibition, tumour intrinsic and acquired resistance, off-target effects and systemic toxicity, when used in higher doses [118]. Nevertheless, two isoform-specific inhibitors have been successfully implemented in the anticancer therapy – alpelisib (PI3Kα-specific) in combination with fulvestrant for breast tumour [119] and idelalisib (PI3Kδ-specific) in combination with rituximab for chronic lymphocytic leukaemia [120]. Considering the importance of PI3K signalling in the endothelium, PI3K inhibitors have been proposed to target tumour stroma, in particular the vasculature. Indeed, some studies showed that high doses of pan-PI3K inhibitors resulted in tumour vessel prunin, and thus, reduced tumour size, but this effect was milder compared to other anti-angiogenic therapies (e.g. VEGF-targeted therapies), therefore limiting its clinical applicability [121-124]. On the contrary, low doses of PI3K inhibitors improved vessel function and hence drug delivery to the tumour [125-126].

This indicates that PI3K inhibitors might be used to modulate tumour stroma and promote vessel normalisation to facilitate chemotherapy.

Recently, a few pre-clinical and clinical studies reported the therapeutic benefit of PI3K inhibition in the treatment of rare diseases, such as HHT and PROS. Blocking the activity of PI3K using pan-inhibitors efficiently prevented the formation of new arteriovenous malformations in an HHT mouse model, but also reverted the already established ones [127]. Moreover, daily administration of alpelisib, a PI3Kα-specific inhibitor, resulted in reduced size and number of multiple tumours and vascular abnormalities in a mouse model of PROS. An impressive clinical improvement was also noticed in alpelisib-treated PROS patients, thus opening a new therapeutic window for the treatment of PROS and related syndromes [128].

Rapamycin, an mTORC1 allosteric inhibitor, is a potent immunosuppressant and anti-proliferative compound. The three rapamycin analogs – sirolimus, everolimus and temsirolumus – have already been approved and are successfully used in the clinic for the treatment of breast cancer, renal cell carcinoma and neuroendocrine tumours as well as in transplant rejections [117]. Apart from oncology, rapamycin was shown to be efficacious in the preclinical treatment of *Pik3ca*- and *Tek*-driven VMs in mice [107-108,129]. Data from phase II clinical trials corroborated a therapeutic benefit and good tolerability of rapamycin in patients with various vascular anomalies, including venous and lymphatic vascular malformation [130-131].

AKT, a PI3K signalling workhorse, poses an attractive therapeutic target for both cancer and overgrowth disorders. Therefore, many inhibitors that either block the ATP-binding site (competitive inhibition) or bind to the allosteric site of AKT have been developed and are being investigated [132]. Miransertib, also known as ARQ 092, an allosteric pan-AKT inhibitor, potently suppresses AKT kinase activity by dephosphorylating the membrane-associated active form, but also by preventing the inactive form from its localisation into the plasma membrane [133]. This inhibitor has shown its promising efficacy in preclinical and clinical studies in cancer [134-135], PROS [136] and Proteus syndrome, a rare disease caused by somatic activating mutations in *AKT1* gene [137-138]. Moreover, miransertib is currently in clinical studies in patients with PROS (NCT03094832) and Proteus syndrome (NCT02594215).

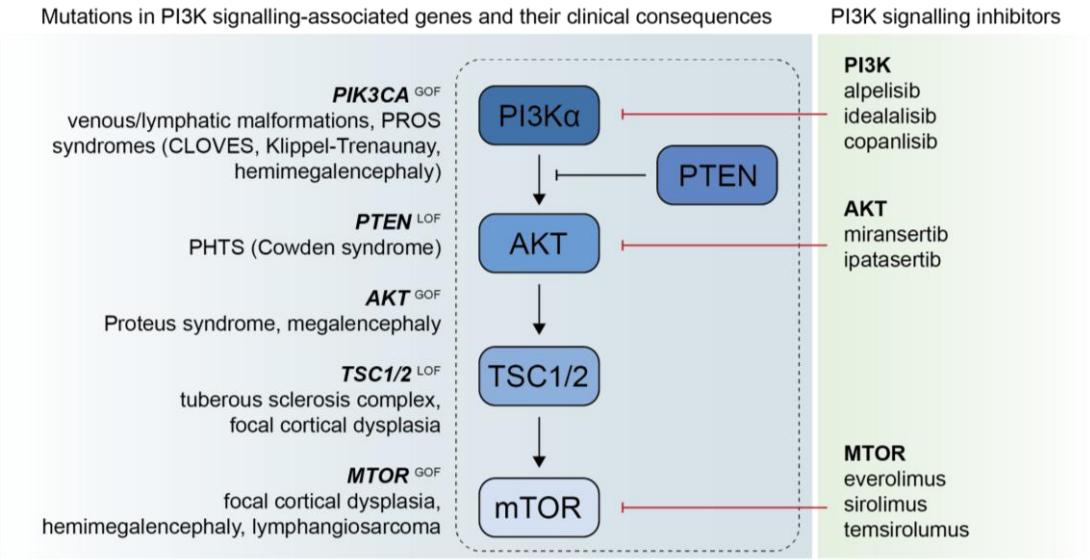

Figure 1. 7. Clinical consequences of somatic mutations in PI3K signalling-associated genes.

CHAPTER 2
Objectives

The last decade in the cardiovascular research has given new insights into how blood vessels are formed and, in particularly, what is the role of PI3K signalling during this process. Two PI3K isoenzymes – class I PI3Kα and class II PI3K-C2α – have emerged to be indispensable for the vascular development, but since the discoveries that somatic activating mutations in *PIK3CA* gene cause venous malformations, it is tempting to speculate that PI3Kα plays a dominant role in endothelial cell biology. These findings opened a new therapeutic window as many PI3K signalling inhibitors have already been developed. Therefore, it is of utmost importance to evaluate their clinical potential in preclinical, both *in vitro* and *in vivo*, models.

Despite of the recent discoveries on the relevance of PI3K-C2α in angiogenesis, there is a substantial shortage of knowledge on the role of class II and class III. In particular, the vascular function of PI3K-C2β still remains elusive, despite recent reports showing that this isoform might play a role in the regulation of EC biology. It is therefore essential to address the uncharacterised isoforms to further extend the knowledge.

Based on the current state of the art on the role of PI3K isoforms in angiogenesis, this thesis dissertation has been organized to address two objectives:

Objective 1: To study new therapeutic potential of pan-AKT inhibitor – miransertib – for *PIK3CA*-related venous malformations. For this, both *in vivo* (mouse retina) and *in vitro* mouse will be used.

Objective 2: To ascertain the role of class II PI3K-C2β in blood vessel development and EC biology using both *in vivo* (mouse retina) and *in vitro* systems.

CHAPTER 3
Materials and methods

3.1. Reagents

All chemical reagents and siRNAs were purchased from Sigma-Aldrich, unless stated otherwise. Providers of antibodies for immunofluorescence and immunoblotting are included in Tables 3., 4., 6. And 7. Cell culture media and buffers were from purchased from Lonza and Gibco. Primers were from Invitrogen.

3.2. *In vivo* studies

3.2.1. Mice husbandry and care

Mice were kept in individually ventilated cages under specific pathogen-free conditions. All experiments were performed in agreement with the guidelines and legislations of the Catalan Ministry of Agriculture, Livestock, Fisheries and Food (Catalonia, Spain), following protocols approved by the local Ethics Committees of IDIBELL-CEEA.

3.2.2. Mouse models

To perform *in vivo* studies, different transgenic mouse (*Mus musculus*) models have been used (listed and described below). All mouse lines were crossed onto C57BL/6J genetic background.

3.2.2.1. *Pik3ca*$^{iH1047R/WT}$ knock-in

Mice carrying a Cre-inducible, gain-of-function point mutation (iH1047R) in the protein´s catalytic domain in one of the *Pik3ca* alleles. The mutation substantially enhances the activity of PI3Kα isoform by increasing its lipid binding and basal activity. The mutation is monoallelic in order to resemble the *Pik3ca*-driven vascular malformations in humans.

3.2.2.2. *Pik3c2b*$^{D1212A/D1212A}$ knock-in

Mice carrying constitutive point mutations (D1212A) in the protein´s catalytic domain in both *Pik3c2b* alleles. This model allows studying the lipid kinase activity of PI3K-C2β, on contrary to a knock-out strategy, as PI3K-C2β is still properly expressed in all cell types despite the introduction of inactivating mutation.

3.2.2.3. *Pdgfb*-Cre^{ERT2}

Mice expressing a tamoxifen-inducible variant of Cre recombinase under the EC-specific promoter *Pdgfb*.

3.2.3. Mouse genotyping (tails lysis and PCR)

Tail biopsies collected from either adult (upon weaning) or newborn mice (upon culling for retina isolation) were lysed with 50 mM NaOH at 100°C for 15 minutes, following neutralisation with 1 M Tris-HCl pH 7.4. Samples were vortexed, centrifuged at maximum speed for 1 minute and used in polymerase chain reaction (PCR) for DNA amplification. Primers sequences and PCR conditions are summarised in a Table 2. PCR products were separated on 1.5% agarose gel and visualised with ethidium bromide.

Table 2. Primers sequences and PCR conditions for mouse lines genotyping.

gene	primer sequence (5′-3′)	PCR composition	PCR conditions
Pik3ca^{iH1047R}	FW 1: TTGGTTCCAGCCTGAATAAAGC FW 2: TCCACACCATCAAGCAGCA RV: GTCCAAGGCTAGAGTCTTTCGG	1.5 µl sample DNA 2.5 µl 10X buffer 2.5 µl 10 µM dNTPs 2.5 µl 10 µM primers mix 0.125 µl Titanium DNA polymerase 15.875 µl H_2O	95°C, 10 min 95°C, 30 sec 55°C, 30 sec 72°C, 40 sec } 35X 72°C, 5 min
Pik3c2b^{D1212A}	FW: CACTGCAGGAAGTGTGAAGC RV: GTGGACAGAAAGGCTGATGC	1.5 µl sample DNA 2.5 µl 10X buffer 2.5 µl 10 µM dNTPs 2.5 µl 10 µM primers mix 0.125 µl Titanium DNA polymerase 15.875 µl H_2O	95°C, 5 min 95°C, 30 sec 65°C, 30 sec 72°C, 1 min } 35X 72°C, 2 min
Pdgfb-Cre	FW: CCAGCCGCCGTCGCAACT RV: GCCGCCGGGATCACTCTCG	2 µl sample DNA 3 µl 10X buffer w/o Mg^{2+} 3 µl 15 mM $MgCl_2$ 3 µl 10 µM dNTPs 3 µl 10 µM primers mix 0.25 µl EcoTaq DNA polymerase 15.75 µl H_2O	94°C, 4 min 94°C, 30 sec 57.5°C, 45 sec 72°C 1 min } 34X 72°C, 5 min

3.2.4. *In vivo* Cre-mediated induction of Pik3ca^{H1047R} mutation

Cre recombination in *Pik3ca*$^{iH1047R/WT}$ mice was induced by intraperitoneal administration of 0.125 mg/kg of 4-hydroxytamoxifen into postnatal day 1 (P1) mice.

3.2.2. Pharmacological treatment

3.2.4.1. Miransertib (ARQ 092)

Miransertib (ARQ 092·2MSA salt) (ArQule, a subsidiary of Merck, Kenilworth, NJ, USA) was prepared at the stock concentration of 10 mgA/ml in 20% Captisol (m/v) in 0.02 M citrate/saline buffer. 20% Captisol (m/v) in 0.02 M citrate/saline buffer was used as a vehicle. Mice were injected intraperitoneally with either 75 mg/kg (high dose) or 35 mg/kg (low dose). Two experimental setups have been designed: a) prevention and b) regression of *Pik3ca*^{H1047R}-driven vascular malformations using the previously described mouse model (see sections 3.2.2.1. and 3.2.4.). For the prevention studies mice were treated with either ARQ 092 or vehicle at postnatal day 1 (P1) and P2, followed by retinas isolation at P6. For the regression studies, mice were treated at P4 and P5 with ARQ 092 or vehicle, followed by retinas isolation at P6.

3.2.4.2. Methylarginine (L-NMMA)

Methylarginine L-NMMA inhibitor was prepared in PBS at the stock concentration of 5 mg/ml. Postnatal day 8 pups were injected intraperitoneally with a single dose of 50 mg/kg/injection and kept for 2 hours prior to retinas isolation. PBS-injected mice were used as a control.

3.2.5. Mouse retina isolation and immunostaining

Mice were sacrificed by decapitation and eyes were isolated, followed by an hour incubation on ice in 4% PFA in PBS. Isolated retinas were fixed for additional hour, washed once with PBS and permeabilised overnight at 4°C in permabilisation/blocking buffer (1% BSA, 0.3% Triton X-100 in PBS). Afterwards, the retinas were incubated overnight at 4°C with specific primary antibodies, diluted in permabilisation/blocking buffer. Table 3. lists the antibodies used in the study, together with appropriate dilutions. The next day, samples were washed three times in PBS containing 1% Tween-20 (PBST), following incubation with PBlec buffer (1% Triton X- 100, 1 mM $CaCl_2$, 1 mM $MgCl_2$ and 1 mM $MnCl_2$ in PBS, pH 6.8) for 30 minutes at RT. Secondary antibodies, diluted in PBlec (Table 4.), were added to the retinas and incubated for another 2 hours. Following triple washes with PBST, the tissues were flat-mounted on a microscope slide.

Table 3. List of primary antibodies and fluorescent agents used for tissue and cell immunofluorescence.

antigen	host species	dilution	company	catalog number
BrdU	mouse	1:50	BD Biosciences	347580
Collagen IV	rabbit	1:50	Millipore	AB756P
Erg 1,2,3	rabbit	1:400	Abcam	ab92513
Isolectin B4 (488, 568)	-	1:300	Molecular Probes	I21411, I21412
NG2	rabbit	1:100	Millipore	AB5320
Paxillin	mouse	1:100	BD Biosciences	610051
p-S6 (235/236)	rabbit	1:100	Cell Signalling Technology	4857
p-S6 (240/244)	rabbit	1:100	Cell Signalling Technology	2215S
β-catenin	mouse	1:200	BD Biosciences	610153

Table 4. List of fluorophore-conjugated secondary antibodies used for immunofluorescence.

antibody	fluorophore	dilution	company	catalog number
goat anti-mouse	Alexa Fluor 488	1:300	Invitrogen	A11001
goat anti-mouse	Alexa Fluor 568	1:300	Invitrogen	A21236
goat anti-mouse	Alexa Fluor 647	1:300	Invitrogen	A11031
goat anti-rabbit	Alexa Fluor 488	1:300	Invitrogen	A11008
goat anti-rabbit	Alexa Fluor 568	1:300	Invitrogen	A11011
donkey anti-rabbit	Alexa Fluor 647	1:300	Invitrogen	A31573

3.2.6. EdU incorporation assay

In order to study EC proliferation capacity, 5-ethynyl-2'-deoxyuridine (EdU) incorporation assay has been performed using a commercially available kit (*Invitrogen*). EdU (5-ethynyl-2'-deoxyuridine) is an analog of thymidine that is incorporated into genomic DNA during S phase of cell cycle. Briefly, animals were injected intraperitoneally with 60 µl of EdU (0.5 mg/ml in 50% DMSO and 50% PBS solution) and after 2 hours the animals were sacrificed, and retinas isolated (see: 3.2.5.). Prior to immunostaining, EdU incorporation was detected with Click-iT EdU Alexa Fluor-647 Imaging Kit, following manufactures instructions. Afterwards, standard protocol for retina immunostaining was applied (see: 3.2.5.).

3.2.7. Oxygen-induced retinopathy

Oxygen-induced retinopathy was used to model retinopathy of prematurity in mice. For this, postnatal day 8 (P8) littermates were exposed to 85% oxygen (hyperoxia) and kept under those conditions till P11. No more than 7 pups per litter were placed in the chamber, in order to ensure sufficient feeding and normal weight gain. While the pups were exposed to hyperoxia, the nursing mother was rested in room air for 2 hours daily. Following exposure to hyperoxia, mice were kept under normoxic conditions (21% oxygen) together with the nursing mother until the pups reach P17. Upon completion, all animals (including the nursing mother) were sacrificed and the retinas from the littermates were isolated. Immunostained tissues (see: 3.2.5.) were flat-mounted and tile-scanning confocal imaging was performed to capture whole retinas.

3.2.8. Confocal imaging, image analysis and quantification

Sample imaging was done with Leica TCS SP5 confocal microscope, using 10X, 40X (oil immersion) and 63X (oil immersion) objectives. For the measurement of vascular outgrowth, 4X images were obtained using Nikon 801 microscope. Maximal projections of confocal images were made using *Volocity* software and saved as .tif files. *Adobe Photoshop CC2018* and *ImageJ* softwares were used for image editing and quantification, respectively. Five to six images per retina of at least five samples of each genotype from at least three independent experiments were captured. Three independent areas of 10^4 μm^2 were selected from each image taken with 40X objective for quantifications (sections from 3.2.8.1. to 3.2.8.10.). Vascular outgrowth was measured directly from 4X images.

3.2.8.1. Retina vascular outgrowth

The vascular outgrowth is a distance from the optic nerve towards the sprouting front of the retina. Four measurements have been taken manually from each retina and

the mean was calculated. The results were presented as a fold change between control and mutant groups. Error bars represent s.e.m.

3.2.8.2. Retina vascularity

The vascularity of the retinas was measured manually from IB4 channel by adjusting the threshold to select a positive area. The mean percentage of IB4-positive area from the total area (10^4 μm^2) was calculated and results were presented as a fold change between control and mutant groups. Error bars represent s.e.m.

3.2.8.3. Vessel sprouts number

Vessel sprouts seen throughout the sprouting front were calculated manually using IB4 channel. The length of the sprouting front was measured manually. The mean was calculated and presented as a number of sprouts per 100 μm of the sprouting front.

3.2.8.4. Vessel width

Vessel width (μm) was determined manually from 10^4 μm^2 images using a proper scale setup. Five different measurements per image were taken and the mean was calculated. Error bars represent s.e.m.

3.2.8.5. Endothelial cell number

The number of endothelial cells was determined manually based on EC-specific nuclei staining (Erg) in 10^4 μm^2 area. The results were presented as a mean. Error bars represent s.e.m.

3.2.8.6. Phospho-S6 intensity in vascular area

The vascular area has been selected and measured from IB4 channel by adjusting the threshold. The selected area was used to measure the integrated density of phosho-S6 level in phosho-S6 channel. Additionally, mean gray value of the background (avascular area) was measured from phosho-S6 channel. The corrected total fluorescence (CTF) was calculated based on the equation below:

$$CTF = \text{integrated density} - (\text{vascular area} \times \text{mean gray background value})$$

The results were presented as a fold change between control and mutant groups with error bars representing s.e.m.

3.2.8.7. Endothelial cell proliferation

EdU immunostaining was used to assess the endothelial cell proliferation capacity (see: 3.2.6.). Both EdU- and Erg-positive cells were quantified as in **3.2.8.5.** and results were presented as a number of EdU-positive cells per 10^4 μm^2. Error bars represent s.e.m.

3.2.8.8. Pericytes coverage

The coverage of vessels by pericytes was quantified from both, NG2 and IB4 channel by adjusting threshold and selecting the positive area. Then the NG2 to IB4 ratio was calculated and presented as a percentage. Error bars represent s.e.m.

3.2.8.9. Collagen IV deposition and empty sleeves

The vascular area has been selected from IB4 channel by adjusting the threshold. The selected area was used to measure the integrated density of collagen IV (ColIV) staining. Mean gray value of the background (avascular area) was measured from ColIV channel. The corrected total fluorescence (CTF) was calculated based on the equation below:

$$\text{CTF} = \text{integrated density} - (\text{vascular area} \times \text{mean gray background value})$$

The results were presented as a fold change between control and mutant groups with error bars representing s.e.m.

Vascular empty sleeves were calculated manually from 40X images of the retina sprouting front using both IB4 and ColIV channels. ColIV^+ and IB4^- tubes were referred to as empty sleeves. Vascular structures positive for both markers were considered functional. The mean value was determined. Error bars represent s.e.m.

3.2.8.10. Quantification of avascular and neovascular areas

Vascular changes upon high oxygen level were determined using IB4 channel. Both avascular (IB4^- area within the retina) and neovascular (vascular hyperplasia and tufts) areas were measured and presented as a percentage of the total retina area. Error bars represent s.e.m.

3.3. *In vitro* studies

3.3.1. Mouse Lung Endothelial Cells (MLEC) isolation and culture

Mouse Lung Endothelial Cells (MLEC) were isolated from adult mice between 3- and 6-week-old. Briefly, lungs were homogenized with a scalpel blade and incubated in dispase II (Gibco, #17105-041) in Hank's Balanced Salt Solution (4 U/ml) for 1 hour at 37°C. The digested tissue was disintegrated by pipetting into a single-cell solution, following enzyme inactivation with DMEM supplemented with 10% FBS and 1% penicillin/streptomycin. Cells were resuspended in 100 µl of PBS and incubated with rat anti-CD144 antibody-coated magnetic beads for 30 minutes at room temperature. CD-144 positive fraction was washed with PBS with 0.5% BSA and sorted using a magnet. Cells were resuspended and cultured in 0.5% gelatin-coated culture well (12-well format) in F12/DMEM medium supplemented with 20% FBS, 1% penicillin/streptomycin and 4 ml endothelial cell growth factors, later referred to as F12 complete (PromoCell, #C30140) until they reached 80-90% confluency. Cells were subjected for a second

selection with the CD-144 antibody-coated magnetic beads for 1 hour at room temperature, then tripsinised, magnetic-sorted and resuspended in F12 complete medium and further cultured (6-well format). Cells were cultured at 37°C in 5% CO_2 atmosphere until passage 5.

3.3.1.1. *In vitro* Cre-mediated induction of Pik3ca^{H1047R} mutation

MLEC isolated from *Pdgfb*-Cre^{ERT2};*Pik3ca*$^{H1047R/WT}$ mice were treated with 2 µM 4-hydroxytamoxifen for 6 hours. Ethanol-treated cells were used as a control. Recombined cells were re-seeded for an experiment and cultured at 37°C in 5% CO_2 atmosphere for 24 hours.

3.3.2. Primary Mouse Brain Pericytes (MBPC) isolation and culture

To isolate brain pericytes, 5 to 6 brains from up to 4-week-old mice were used. Briefly, tissues were thoroughly homogenized with a scalpel blade and incubated in an enzymatic solution (Worthington, LK003150). After several rounds of centrifugation, cells were resuspended in EGM2 complete medium and plated on 2% collagen I-coated plates (BD Biosciences, 354249). Cells were cultured at 37°C in 5% CO_2 atmosphere in EBM-2 supplemented with EGM-2 BulletKit (Lonza, #CC-3162), 20% FBS and 1% penicillin/streptomycin, with the medium changed every 3 days until reaching confluency, followed by a passage into a new well in order to expand the culture. After the third passage, cells were maintained and propagated in PC medium composed of a basal medium supplemented with growth factors (ScienCell, 1201), 2% FBS and 1% penicillin/streptomycin. Primary MBPC were cultured until passage 12.

3.3.3. Primary Human Umbilical Vein Endothelial Cells (HUVEC) culture

Primary Human Umbilical Vein Endothelial Cells (HUVEC) were purchased from Lonza (#C2519A) and cultured in 0.5% gelatin-coated plates in EBM-2 supplemented with EGM-2 BulletKit (Lonza, #CC-3162), 20% FBS and 1% penicillin/streptomycin, later referred to as complete EGM-2. Primary HUVEC were cultured until passage 6.

3.3.3.1. PI3K-C2β knockdown in primary HUVEC using siRNA

$0.4 \cdot 10^5$ cells were seeded onto 0.5% gelatin-coated well (6-well format) and cultured overnight at 37°C in 5% CO_2 atmosphere. The next day, cells were transfected with two different siRNAs against PI3K-C2β using Lipofectamine® RNAiMAX (Invitrogen, 13778075). Scrambled (nontargeting) oligonucleotide was used as a control. Briefly, 2 µl of each oligonucleotide (100 µM) were diluted in 200 µl of OptiMEM. Similarly, 4 µl of Lipofectamine® RNAiMAX were diluted in 200 µl of OptiMEM. The tubes were incubated for 5 minutes and mixed thoroughly together afterwards, following 25 minutes incubation at room temperature. The culture medium has been changed for a complete EGM-2 deprived from penicillin/streptomycin and heparin. The transfection solution was added dropwise onto cells, following 5-6 hours incubation. Cells were

refreshed with complete EGM-2 medium and cultured for additional 72 hours. Prior to further experiments, cells were reseeded onto 0.5% gelatin-coated dishes.

Table 5. siRNA used to generate PI3K-C2β knockdown in HUVEC.

siRNA	oligonucleotide sequence (5'-3')
scrambled	GUAACUGUCGGCUCGUGGU[dT][dT]
PI3K-C2β #1	GUUCGACACUUACCACAAU-[dT][dT]
PI3K-C2β #2	GCUACCAGCUAUGAAGAUU[dT][dT]

3.3.4. MTS assay and determination of IC50

MTS assay was used in order to determine cell proliferation and viability. Viable cells are converting the MTS tetrazolium reagent to a coloured formazan that is soluble in cell culture medium. Briefly, $0.2 \cdot 10^4$ cells were seeded on gelatin-coated 96-well plates (6 technical replicates per condition) and incubated overnight at 37°C in 5% CO_2 atmosphere. The next day, cells were treated for 3 days with either ARQ 092 or BYL 719 inhibitor at indicated concentrations: 0.03, 0.1, 0.3, 1, 3, 10, 50, 100, and 150 μM. Vehicle-treated cells are used as a control. MTS assay (Abcam, ab197010) was performed for 3 hours and the absorbance was measured at 490 nm. Data (the percentage of a vehicle) from three independent experiments were plotted against the logarithm of inhibitor concentration. Error bars represent s.e.m. IC50 values from three independent experiments were calculated by non-linear regression (variable slope) using GraphPad Prism software and presented in a bar graph.

3.3.5. BrdU-incorporation assay (cell proliferation)

To study EC proliferation, bromodeoxyuridine (BrdU)-incorporation assay has been performed. Briefly, $0.5 \cdot 10^5$ cells were seeded onto a gelatin-coated cover slips and incubated overnight at 37°C in 5% CO_2. The next day, BrdU reagent (ThermoFisher, B23151) was added for 2.5 hours at 10 μM concentration. The cells were then fixed with 4% PFA for 10 minutes followed by triple wash with PBS. Cell were permeabilised with 0.2% Triton X-100 in PBS for 30 min and incubated with 2 M HCl for 10 minutes at room temperature. After 45 minutes of blocking in 3% BSA in PBS, cover slips were incubated with a primary mouse anti-BrdU antibody (diluted 1:50 in the blocking solution) overnight at 4°C. The following day, the cells were washed three times in 0.5% Tween-20 in PBS solution and incubated with a secondary AlexaFluor488-conjugated rat anti-mouse secondary antibody (1:200) for 1 hour at room temperature, followed by 5 minutes incubation with DAPI (1:10 000). BrdU-positive cells were quantified and presented as a percentage of all cells.

3.3.6. Wound healing assay (collective cell migration)

Collective cell migration capacity of endothelial cells was measured in wound healing assay. Briefly, $0.25 \cdot 10^5$ cells were seeded onto gelatin-coated plate (12-well format) and cultured at 37°C in 5% CO_2 atmosphere until confluency. Prior to the experiment, cells were incubated for 30 minutes with 1 µg/ml mitomycin C in order to inhibit cell proliferation. The scratch has been made with a help of a pipette tip and bright field images have been taken at three time points: T0 (reference point), T7 and T24. Data were presented as the percentage of a wound area with SEM as error bars.

3.3.7. Immunocytochemistry for β-catenin

Cells were seeded on gelatin-coated cover slips to reach sub- or confluency the next day and incubated overnight at 37°C in 5% CO_2 atmosphere. Then, cells were fixed with 4% PFA for 15 minutes, followed by triple wash with PBS. Cover slips were permeabilised with PBS containing 0.1% Triton X-100 for 30 minutes and blocked with 3% BSA in PBS for 1 hour at room temperature. Cells were incubated with primary mouse anti-β-catenin antibody (diluted 1:200 in blocking solution) at 4°C overnight. The next day, the cover slips were washed three times with PBST followed by 1h incubation at RT with AlexaFluor488-conjugated rat anti-mouse secondary antibody (1:300).

3.3.8. Immunocytochemistry for focal adhesions

$0.7 \cdot 10^5$ cells were seeded on gelatin-coated cover slips and incubated overnight at 37°C in 5% CO_2 atmosphere. Then, cells were fixed with 4% PFA for 15 minutes, followed by triple wash with PBS. Cover slips were permeabilised with PBS containing 0.1% Triton X-100 for 30 minutes and blocked with 3% BSA in PBS for 1 hour at room temperature. Cells were incubated with primary mouse anti-paxillin antibody (diluted 1:100 in blocking solution) at 4°C overnight. The next day, the cover slips were washed three times with PBST followed by 1h incubation at RT with AlexaFluor488-conjugated rat anti-mouse secondary antibody (1:300). Cell nuclei were stained for 5 minutes with DAPI (1:10 000).

3.3.9. RNA extraction, cDNA synthesis and qPCR

Total RNA was isolated from cells with RNeasy Plus kit (Qiagen, 74136) according to the manufacture´s protocol. RNA concentration and quality were measured with NanoDrop 1000 UV-Vis spectrophotometer (Thermo Scientific). 0.5 µg of RNA was processed for cDNA synthesis using the High Capacity cDNA Reverse Transcription kit (Applied Biosystems, 4368814) following manufacturer´s protocol. Quantitative PCR was performed using LightCycler 480 SYBR Green I Master kit and LightCycler 480 System

(Roche). *Rpl32* was used as a housekeeping gene. All primer sequences are listed in Table 6.

Table 6. List of primers and their sequences used for qPCR.

gene name	protein name	primers sequences (5'-3')
Cd248	endosialin	FW: GTTGGTGGCTTTGAGTGTTACTGCA RV: CCTCCCCTTCTTCTCCATCATCCAG
Cspg4	NG2	FW: GCAGGATGGCTGTCTGATCAAACTG RV: TCCTTCCCCATCATGTCTCCGTAAC
Des	desmin	FW: TCAGACTTGACTCAGGCAGCCAATA RV: AATCTCGCAGGTGTAGGACTGGATC
Pdgfrb	PDGFRβ	FW: TCTGCCTGAAGTGTGTACCTACCAC RV: TGGTCCCCAGAGAGAACAAGGAAAG
Pecam1	CD31	FW: GTGGTTGTCATTGGAGTGGTCATCG RV: GACATCTCCACGGGTTTCTGTTTGG
Pik3c2b	PI3K-C2β	FW: CTCCTCGTGTCTCTATCTGGGATGC RV: CTAGCAGTTTGTCAGGTGGCTGTTC
Rpl32	RL32	FW: AACCCAGAGGCATTGACAAC RV: ATTGTGGACCAGGAACTTGC

3.4. Cell signalling studies

3.4.1. Cell stimulation

Prior to cell stimulation, MLEC or HUVEC were serum starved for 5 hours followed by an incubation with either 100 ng/ml recombinant VEGF-A (mouse for MLEC and human for HUVEC, respectively) or 1% FBS for 15 minutes. Serum starved and non-stimulated cells were used as a control. Afterwards, cells were washed immediately with cold PBS and lysed for protein extraction.

3.4.2. Protein extraction and immunoblotting

Cells were lysed in ice cold lysis buffer (50 mM Tris-HCl pH 7.4, 5 mM EDTA, 150 mM NaCl and 1% Triton X-100 supplemented with 2 mg/ml aprotinin, 1 mM sodium fluoride, 1 mM pepstatin, 1 ng/ml leupeptin, 1 mM phenylmethanesulfonyl fluoride (PMSF), 10 g/ml Nα-tosyl-L-lysine chloromethyl ketone hydrochloride (TLCK), 1 mM sodium orthovanadat, 1 µM okadaic acid and 1 mM dithiothreitol) for 15 minutes followed by high speed centrifugation (> 16 000 g) for 15 minutes at 4°C. Protein concentration was measured in the supernatant using Pierce BCA Protein Assay Kit (Thermo Scientific™, 23225) following manufacturer's instructions. Total cell lysates were resolved on 8% or 10% SDS-containing polyacrylamide gels and transferred onto nitrocellulose membranes (Pall Corporation, 66485) for 2 hours at 250 mA. The membranes were blocked in 5% milk in TBS-T (TBS buffer with 0.1% Tween 20) for 1 hour following overnight incubation with specific primary antibodies (Table 7. lists all the antibodies used with appropriate dilutions) diluted in 2% BSA in TBS-T. After triple wash in TBS-T, the membranes were incubated with appropriate horseradish peroxidase

(HRP)-conjugated secondary antibody (Table 8.), washed 5 times in TBS-T and developed with reagents for enhanced chemiluminescence.

Table 7. List of primary antibodies used for immunoblotting.

antigen	host species	dilution	company	catalog number
β-actin	mouse	1:10000	Abcam	ab49900
C2β	mouse	1:1000	BD Transduction Lab.	611342
AKT	rabbit	1:2000	Cell Signaling Technology	9272
PI3Kα (p110α subunit)	mouse	1:500	hybridoma, clone U3A	-
p-AKT T308	rabbit	1:500	Cell Signaling Technology	4056S
p-AKT S473	rabbit	1:1000	Cell Signaling Technology	4060
p-PRAS40 T2456	rabbit	1:1000	Cell Signaling Technology	9202
p-S6 S235/236	rabbit	1:1000	Cell Signaling Technology	4857
p-S6 S240/244	rabbit	1:1000	Cell Signaling Technology	2215S
S6	rabbit	1:1000	Cell Signaling Technology	2212
vinculin	mouse	1:10000	Abcam	ab49900

Table 8. List of secondary antibodies used for immunoblotting.

antigen	host species	dilution	company	catalog number
anti-mouse HRP	rabbit	1:5000	Dako	P0260
anti-rabbit HRP	swine	1:5000	Dako	P0399

3.5. Statistical analysis

Statistical analysis was performed by nonparametric Mann Whitney's test using Prism 8 (GraphPad Software Inc.) unless indicated otherwise. All figures are displayed with individual data points that indicate biological replicates with standard error of the mean (s.e.m.) as errors bars. P values considered as statistically significant were as follows: *$p < 0.05$; **$p < 0.01$ and ***$p < 0.0001$.

CHAPTER 4
Results

4.1. Objective 1: Therapeutic potential of miransertib in the treatment of *Pik3ca*-driven vascular malformations

4.1.1. The impact of miransertib treatment on ECs in vitro

3.3.1.1. Pik3ca^{H1047R} *mouse model*

The potential relevance of targeting AKT in *PIK3CA*-related vascular malformations has not been tested so far. Here, we aimed to evaluate the impact of miransertib (an allosteric pan-AKT inhibitor) on a unique mouse model generated in the laboratory that allows to reproduce the etiology of *Pik3ca*-realted venous malformations in a spatiotemporal manner. Specifically, we crossed mice expressing Cre^{ERT2} recombinase under the EC-specific *Pdgfb* promoter (referred to as *Pdgfb*-Cre^{ERT2}) to mice heterozygous for Cre-inducible *Pik3ca*^{iH1047R} allele (referred to as *Pik3ca*$^{iH1047R/WT}$). The Cre^{ERT2} activity is induced specifically in ECs by 4-hydroxitamoxifen (4-OHT) administration, resulting in the expression of a recombined *Pik3ca*^{iH1047R} allele variant in those cells only (Figure 4.1.1.). Previous studies using a retina model have shown that this leads to the development of a massive vascular hyperplasia as a result of hyperactive PI3K signalling [108].

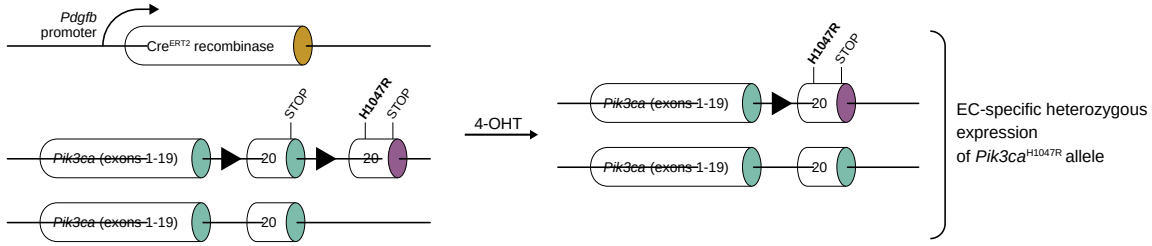

Figure 4. 1. 1. EC-specific *Pik3ca*^{H1047R} mouse model.
Upon 4-hydroxytamoxifen (4-OHT) administration, Cre^{ERT2} recombinase is expressed under EC-specific *Pdgfb* promoter. Cre^{ERT2} recombinase translocates to the nucleus, where it recombines exon 20 of one of the alleles of *Pik3ca* gene due to presence of loxP sites (depicted as triangles). This results in the expression of an additional (knock-in) exon 20 carrying a point mutation that leads to an amino acid substitution (H1047R).

4.1.1.2. Miransertib inhibits AKT-mediated signalling in ECs

First, we wanted to evaluate PI3K/AKT signalling by miransertib *in vitro* using mouse lung endothelial cells (MLEC) isolated from 6-week-old *Pdgfb*-Cre^{ERT2};*Pik3ca*$^{iH1047R/WT}$ mice (referred to as EC- *Pik3ca*$^{iH1047R/WT}$). To induce Cre activity *in vitro*, MLEC were treated with 2 µM 4-OHT for 6 hours and ethanol-treated cells were used as a negative control. We treated the cells with miransertib for 2 hours at four different concentrations: 0 µM, 0.5 µM, 1 µM and 2 µM. Protein lysates were separated by SDS-PAGE and the proteins were transferred onto a membrane, followed by immunoblotting with phosphoprotein-specific antibodies. We confirmed that expression of *Pik3ca*^{H1047R} mutation in MLEC substantially enhances PI3K signalling as seen in increased p-AKT (both S473 and T308) and p-S6 (S235/236) levels, but not p-S6 (S240/244). PRAS, a downstream target of AKT, has also shown increased phosphorylation at T246 upon hyperactivating mutation in *Pik3ca* gene. Treatment with miransertib efficiently reduced the phosphorylation of AKT and PRAS but had minor effect on p-S6 (**Figure 4.1.2.**), indicating that mTOR signalling is less affected by AKT inhibition with miransertib in MLEC. Noteworthy, PI3K/AKT signalling was more sensitive to lower doses of miransertib in *Pik3ca*^{H1047R} than in control MLEC.

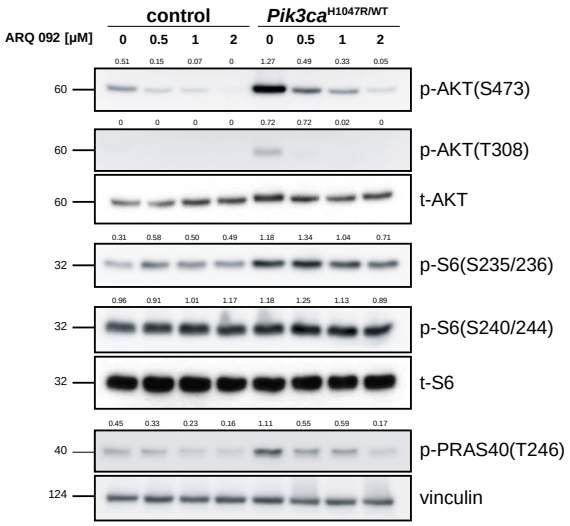

Figure 4. 1. 2. Impact of miransertib on AKT signalling in *Pik3ca*^{H1047R} MLEC.
Class I PI3K signalling pathway assessment by immunoblotting of control and *Pik3ca*$^{H1047R/WT}$ MLEC treated with three different concentration of miransertib (ARQ 092). Non-treated cells were used as a control (0 μM). The quantification of the relative phosphorylation of each protein was normalised to corresponding total proteins (except for p-PRAS40 which was normalised to β-actin) is presented as the mean of three independent experiments (n = 3).

4.1.1.3. AKT inhibition by miransertib reduces ECs viability

Next, we sought to analyse the cellular consequence of AKT inhibition, focusing on its antiproliferative effect. Therefore, we performed the MTS assay using both *Pik3ca*^{H1047R} and control MLEC. Rapamycin, a specific mTORC1 inhibitor currently being tested in clinical trials for vascular malformations treatment, was used for comparison with miransertib. Based on collected data, we determined IC_{50} values for both miransertib and rapamycin in control and *Pik3ca*^{H1047R} MLEC. In both cases, rapamycin showed around 8-fold higher IC50 values compared to miransertib (**Figure 4.1.3.**), indicating that the AKT inhibitor has a significantly stronger antiproliferative properties. IC50 of both miransertib and rapamycin were comparable between control and *Pik3ca*^{H1047R} MLEC.

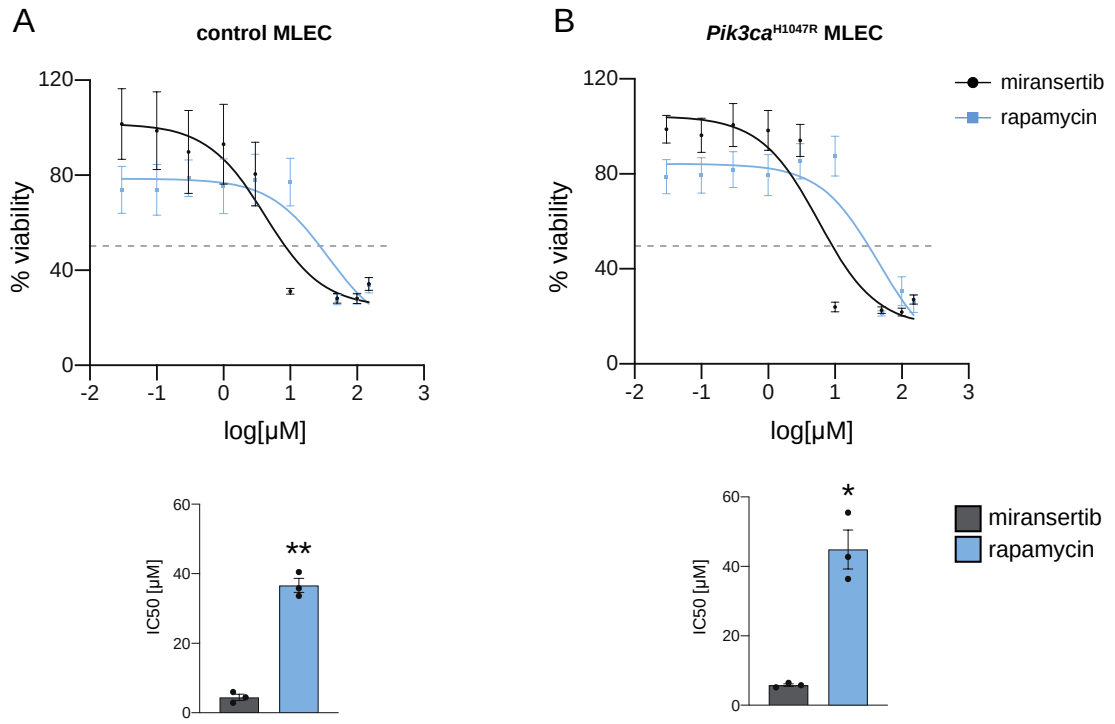

Figure 4. 1. 3. Miransertib reduces EC viability *in vitro*.
Cell viability of **(A)** control and **(B)** *Pik3ca*$^{H1047R/WT}$ MLEC was assessed by MTS assay. Nine doses of miransertib and rapamycin were tested: 0.03, 0.1, 0.3, 1, 3, 10, 50, 100 and 150 μM. DMSO-treated cells were used as controls to which data was normalised. Curves were fitted with nonlinear regression. Dashed line marks 50% cell viability. IC_{50} values for both inhibitors were calculated by non-linear regression (variable slope) and were presented as bar graphs (below each condition). n = 3. Data are presented as mean values. Error bars are s.e.m. Statistical analysis was performed by t-test with Welch's correction. *p < 0.05 and **p < 0.01 were considered statistically significant.

4.1.2. Miransertib prevents formation of vascular malformations

4.1.2.1. Preclinical mouse model of *Pik3ca*-driven vascular malformations

In humans, sporadic vascular malformations are present in a form of congenital isolated lesions that grow and progress with the child and oncogenic mutations in *PIK3CA* lead to the development of both venous and lymphatic malformations. In the previous studies using mouse retinas, high dose of 4-OHT evoked a massive hyperplasia, where it was no longer possible to distinguish the individual vessels and lesions [108]. Therefore, to model accurately the disease of *Pik3ca*-driven isolated vascular lesions in the mouse retinas, we decided to reduce a dose of 4-OHT needed to induce a phenotype. *Pdgfb*-Cre^{ERT2};*Pik3ca*$^{WT/WT}$ mice were used as a control in all *in vivo* experiments. Retinas were immunostained with isolectin-B4 (IB4), which binds to the plasma membrane on ECs. We determined that a single dose of 0.125 mg/kg 4-OHT given on postnatal day 1 (P1) was optimal to induce the formation of vascular lesions, of

both venous and capillary origin. We noted that no lesions were found within arterial compartment (**Figure 4.1.4. A**).

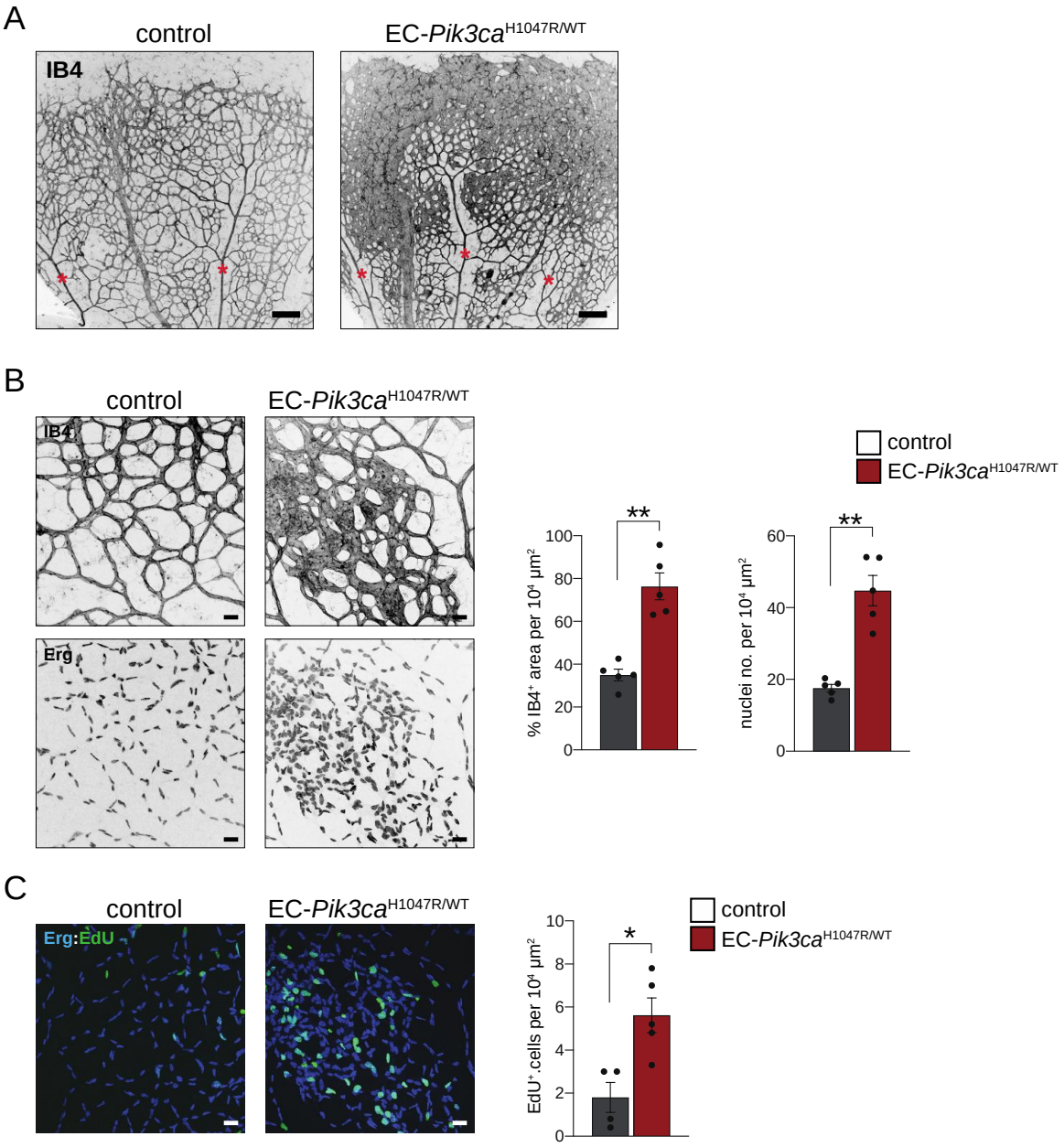

Figure 4. 1. 4. Modelling *Pik3ca*-driven vascular malformations in mouse retinas.
(A) P1 control and EC-*Pik3ca*$^{H1047R/WT}$ mice were injected with a single dose of 4-OHT (0.125 mg/kg), followed by retinas isolation on P6 and immunostaining for blood vessels (IB4). Representative confocal images are shown. Asterisks show arteries. Scale bar = 150 µm. n ≥ 3 retinas per genotype. **(B)** High magnification images of control and EC-*Pik3ca*$^{H1047R/WT}$ P6 retinas immunostained for blood vessels (IB4) and EC nuclei (Erg). Scale bar = 30 µm. Quantification of IB4-positive area and EC number per unit area are shown. n = 5. **(C)** High magnification images of control and EC-*Pik3ca*$^{H1047R/WT}$ P6 retinas immunostained for EC nuclei (Erg) and EdU proliferation marker. Scale bar = 30 µm. Quantification of EdU-positive ECs per unit area are shown. n ≥ 4. All data are presented as mean values. Error bars are s.e.m. Statistical analysis was performed by nonparametric Mann–Whitney test. *p < 0.05 and **p < 0.01 were considered statistically significant.

Moreover, despite a substantial decrease of 4-OHT dose we were able to reproduce already reported observations on increased tissue vascularity, EC number and their proliferation capacity as shown in **Figure 4.1.4 B-C**. To further characterise the model, we evaluated PI3K/AKT/mTOR signalling and PC coverage by immunostaining P6 retinas with p-S6- and NG2-specific antibodies, respectively. While vascular p-S6(240/244) levels were visibly increased upon *Pik3ca*^{H1047R} expression (**Figure 4.1.5. A**), we could not detect alterations in PC coverage in the mutant retinas as seen in the previous study (**Figure 4.1.5. B**).

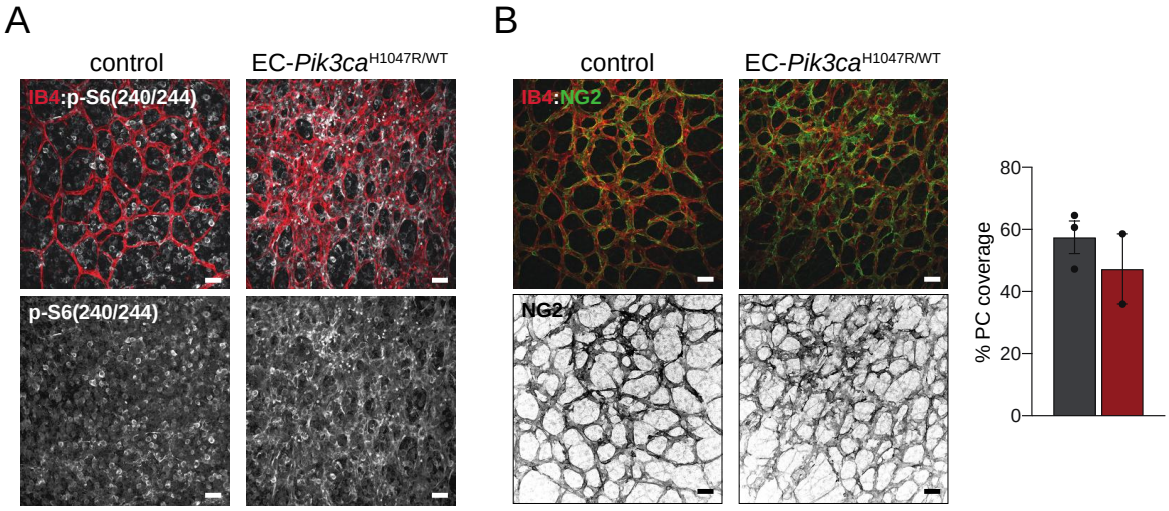

Figure 4. 1. 5. *Pik3ca*-driven vascular lesions exhibit elevated mTORC1 signalling.
(A) High magnification images of control and EC-*Pik3ca*$^{H1047R/WT}$ P6 retinas immunostained for blood vessels (IB4) and p-S6(240/244). Scale bar = 30 µm. n = 2. **(B)** High magnification images of control and EC-*Pik3ca*$^{H1047R/WT}$ P6 retinas immunostained for blood vessels (IB4) and pericyte marker (NG2). Scale bar = 30 µm. Quantification of the percentage of PC coverage per vessel area. n ≥ 2 retinas per genotype. Data are presented as mean values. Error bars are s.e.m.

4.1.2.2. High dose (75 mg/kg) of miransertib prevents *Pik3ca*-driven vascular malformations by blocking EC proliferation

First, we sought to evaluate the anti-angiogenic potential of miransertib in preventing the development of vascular malformations. Briefly, P1 pups were injected intraperitoneally with 0.125 mg/kg 4-OHT, followed by an immediate administration of miransertib at high dose (75 mg/kg). To maximise the therapeutic efficacy, the second dose of miransertib was administered the following day (P2). Vehicle-treated animals were used as a control (**Figure 4.1.6. A**). No toxicity or inhibitor-associated lethality was observed. Retinas were isolated on P6, followed by immunostaining for blood vessels (IB4) and EC nuclei (Erg). Confocal images showed that high dose of miransertib significantly prevented the formation of vascular lesions as seen in **Figure 4.1.6. B**.

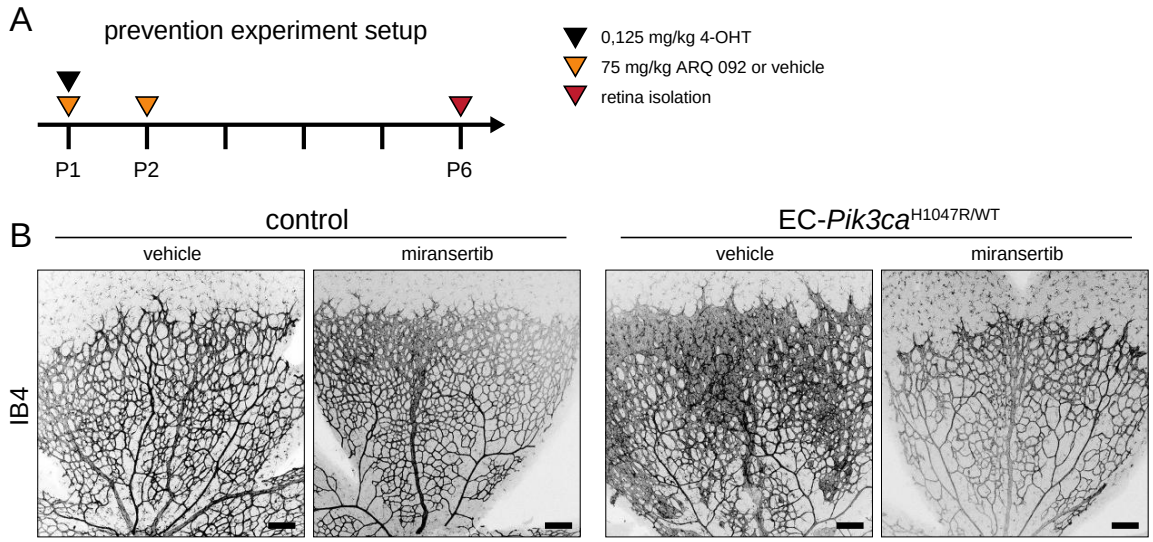

Figure 4. 1. 6. High dose of miransertib prevents *Pik3ca*-driven vascular malformation development.
(A) Dosing scheme for prevention experiments with a high dose (75 mg/kg/dose) of miransertib **(B)** Representative confocal images of whole-mount P6 retinas isolated from control and EC-*Pik3ca*$^{H1047R/WT}$ mouse littermates treated with vehicle or 75 mg/kg/dose of miransertib. Blood vessels visualised with IB4. Scale bar = 150 µm. n ≥ 3 retinas per genotype.

To measure the effect of miransertib on retinal vasculature, we took high magnification images and quantified the vascular area (IB4-positive) and the number of endothelial cells (Erg-positive) (**Figure 4.1.7. A**). As expected, endothelial *Pik3ca*^{H1047R} mutation clearly led to an increase in both vascularity and EC number. IB4-positive area and EC number were significantly reduced by miransertib treatment compared to vehicle-treated mice and these numbers were similar to those of wild-type retinas. Of note, miransertib did not reduce vascular growth nor EC number in wild-type mice, indicating that *Pik3ca*^{H1047R} mutant ECs are highly sensitive to AKT inhibition (**Figure 4.1.7. B and C**). High dose of miransertib also slightly (although insignificantly) decreased vessel area and EC number (**Figure 4.1.7. B and C**), which could be expected based on previously documented findings on the role of AKT during developmental angiogenesis [96].

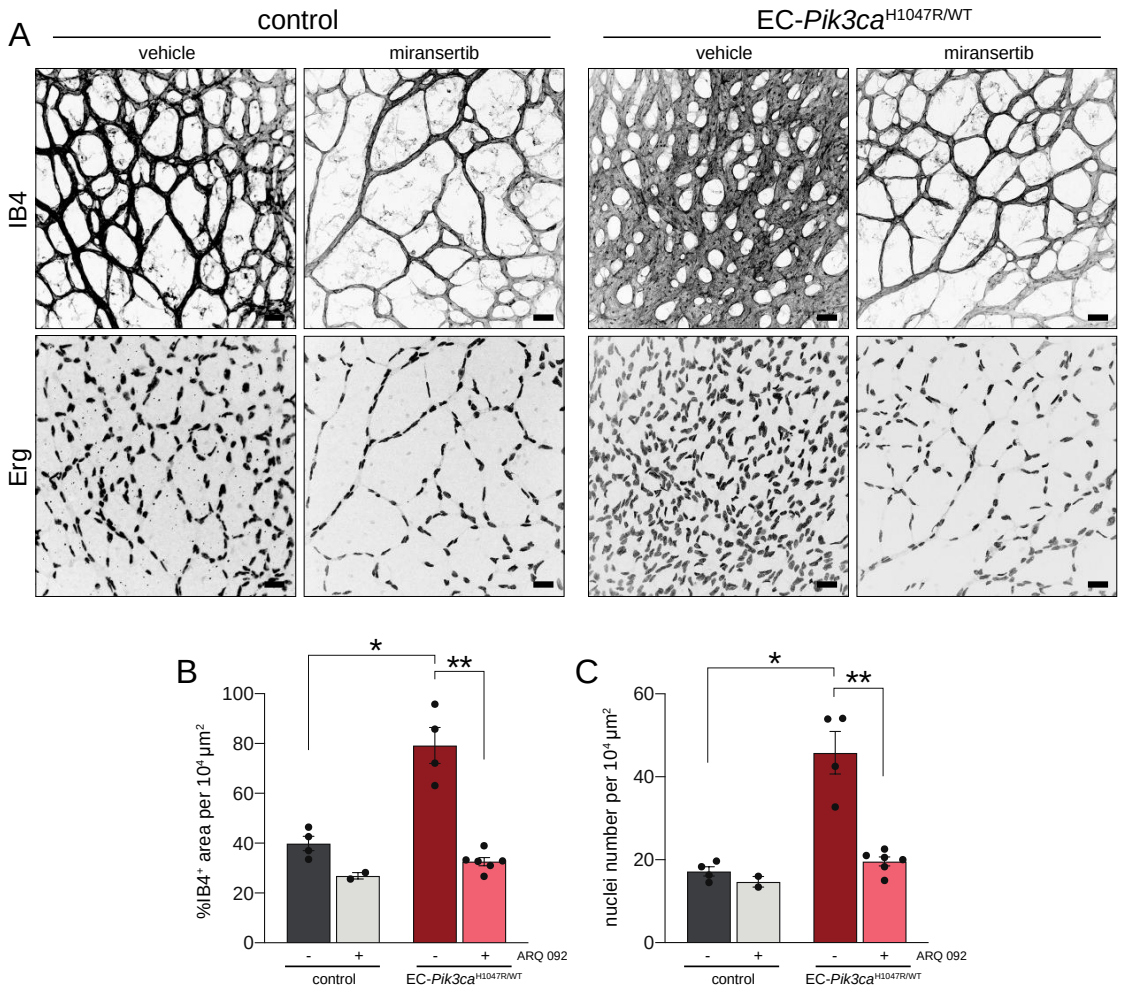

Figure 4. 1. 7. High dose of miransertib reduces vascular growth and EC number.
(A) High magnification confocal images of retinas isolated from control and EC-*Pik3ca*$^{H1047R/WT}$ mice treated with vehicle or 75 mg/kg/dose of miransertib and immunostained for blood vessels (IB4) and EC nuclei (Erg) Scale bar = 30 µm. **(B)** Quantification of IB4-positive area per unit area. **(C)** Quantification of EC number per unit area. n ≥ 4 retinas per genotype. Data are presented as mean values. Error bars are s.e.m. Statistical analysis was performed by nonparametric Mann–Whitney test. *p < 0.05 and **p < 0.01 were considered statistically significant.

In line with the *in vivo* data, our observations *in vitro* demonstrated that miransertib reduces cell viability and number. To test whether this is due to decreased EC proliferation capacity, we performed an *in vivo* EdU incorporation assay. During the S-phase of the cell cycle, EdU is actively incorporated into the nuclear DNA, indicating that cells positive for EdU are proliferative. Briefly, EdU was administered 2 hours prior to retinas isolation, followed by immunostaining for Erg and EdU. As shown in **Figure 4.1.8. A**, endothelial *Pik3ca*^{H1047R} led to a significant increase in proliferating ECs compared to WT littermates. We also observed slight reduction of EC proliferation in miransertib-treated WT animals. These data indicate that *in vivo* reduction in EC number upon high dose miransertib treatment is a result of EC proliferation arrest (**Figure 4.1.7. 8**).

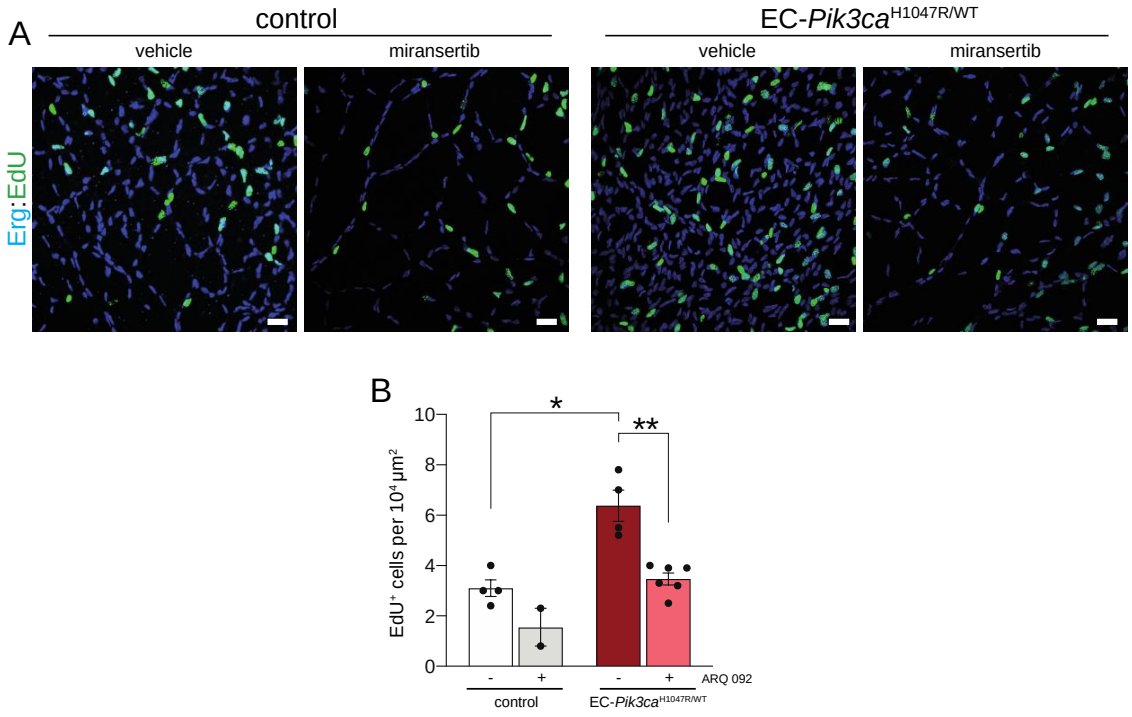

Figure 4. 1. 8. High dose of miransertib arrests EC proliferation *in vivo*.
(A) High magnification confocal images of retinas isolated from control and EC-*Pik3ca*$^{H1047R/WT}$ mice treated with vehicle or 75 mg/kg/dose of miransertib and immunostained for EC nuclei (Erg) and EdU. Scale bar = 30 µm. **(B)** Quantification of EdU-positive ECs per unit area. n ≥ 4 retinas per genotype. Data are presented as mean values. Error bars are s.e.m. Statistical analysis was performed by nonparametric Mann–Whitney test. *p < 0.05 and **p < 0.01 were considered statistically significant.

4.1.2.3. Low dose (35 mg/kg) of miransertib prevents *Pik3ca*-driven vascular malformations by inhibiting EC proliferation

Given the beneficial effects observed with a high, tolerable dose of the inhibitor, we wanted to test whether lower dose of 35 mg/kg would also prevent *Pik3ca*-driven vascular malformations. Therefore, as before, P1 mice were treated with 0.125 mg/kg of 4-OHT, followed by immediate administration of a lower dose of miransertib. The inhibitor was re-administered on P2 and the retinas were isolated on P6 (**Figure 4.1.9. A**). Confocal images of the retinas stained for blood vessels show that the lower dose of miransertib significantly hampers the development of vascular lesions (**Figure 4.1.9. B**). Quantification of the vascular area as well as EC number corroborated the therapeutic effect of the AKT inhibitor (**Figure 4.1.10. A-C**).

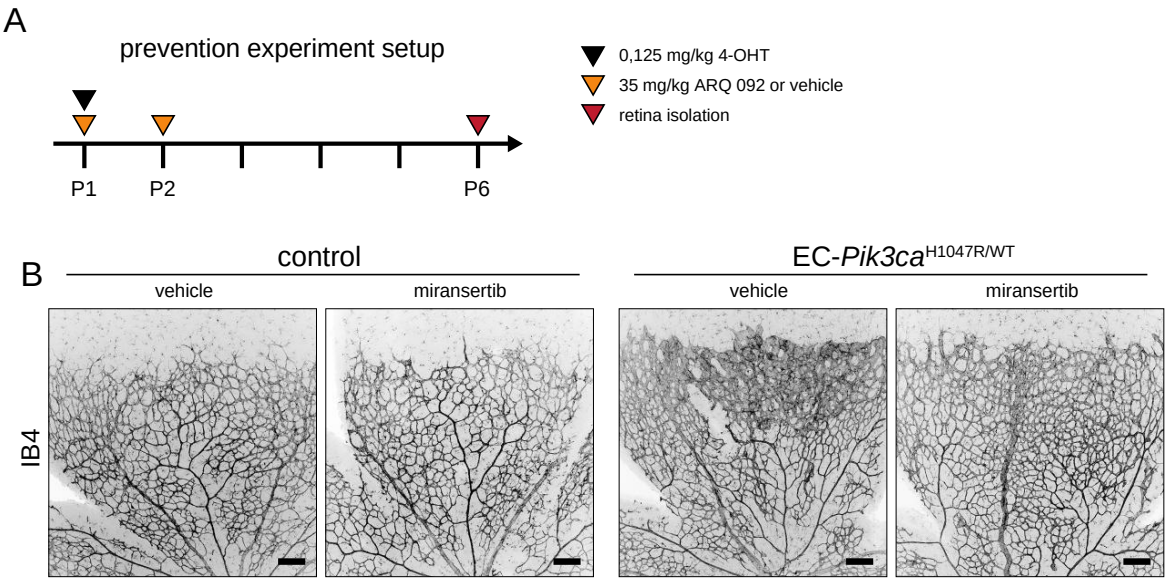

Figure 4. 1. 9. Lower dose of miransertib prevents *Pik3ca*-driven vascular malformation development.
(A) Dosing scheme for prevention experiments with a lower dose (35 mg/kg/dose) of miransertib **(B)** Representative confocal images of whole-mount P6 retinas isolated from control and EC-*Pik3ca*$^{H1047R/WT}$ mouse littermates treated with vehicle or 35 mg/kg/dose of miransertib. Blood vessels visualised with IB4. Scale bar = 150 µm. n ≥ 3 retinas per genotype.

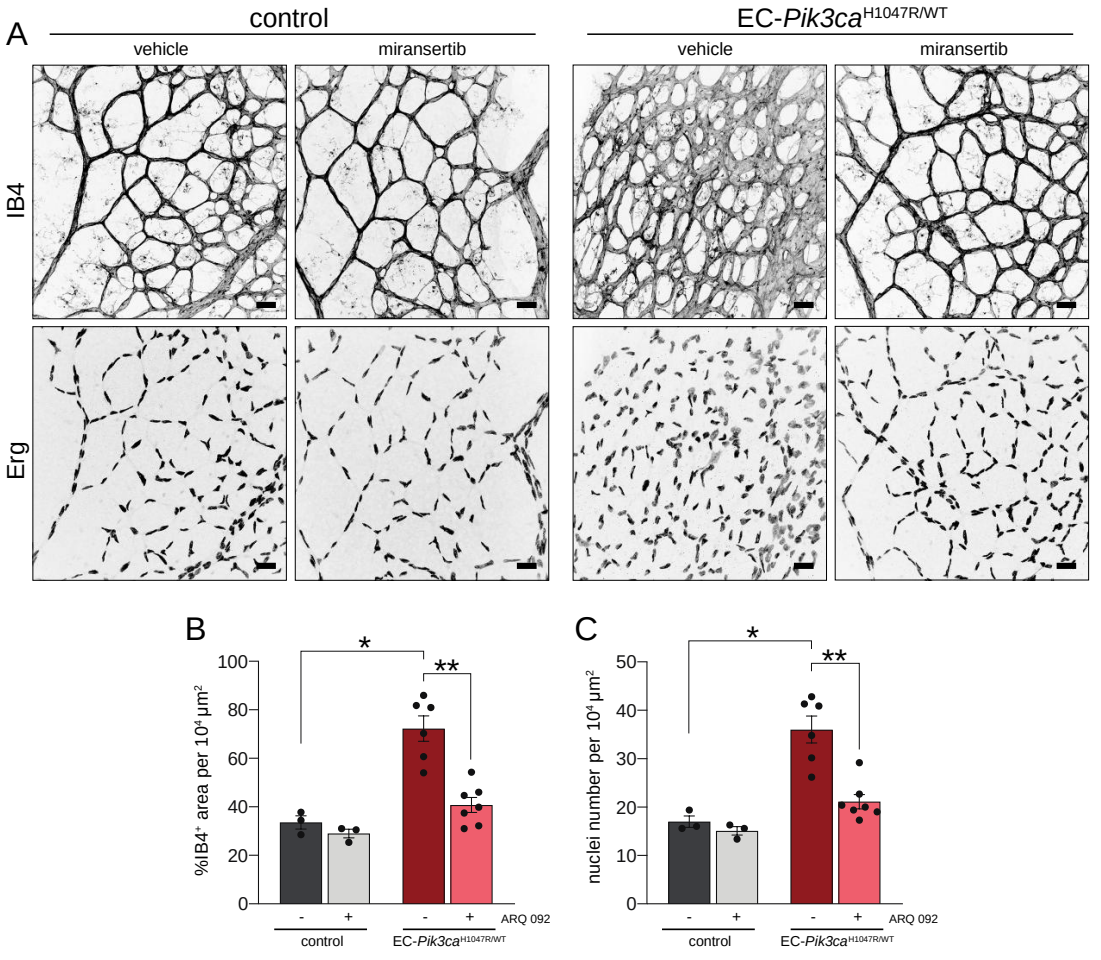

Figure 4. 1. 10. Lower dose of miransertib reduces vascular growth and EC number (previous page).
(A) High magnification confocal images of retinas isolated from control and EC-*Pik3ca*$^{H1047R/WT}$ mice treated with vehicle or 35 mg/kg/dose of miransertib and immunostained for blood vessels (IB4) and EC nuclei (Erg) Scale bar = 30 µm. **(B)** Quantification of IB4-positive area per unit area. **(C)** Quantification of EC number per unit area. n ≥ 3 retinas per genotype. Data are presented as mean values. Error bars are s.e.m. Statistical analysis was performed by nonparametric Mann–Whitney test. *p < 0.05 and **p < 0.01 were considered statistically significant.

EdU incorporation analysis revealed that 35 mg/kg miransertib treatment arrested cell proliferation compared to vehicle-treated mice, although the inhibitor treatment did not fully abrogated EC proliferation to wild-type levels as seen in high dose (**Figure 4.1.11.**). Taking together, we showed that miransertib significantly inhibits the growth of vascular lesions, through blocking EC proliferation, at both high (75 mg/kg) and lower (35 mg/kg) doses.

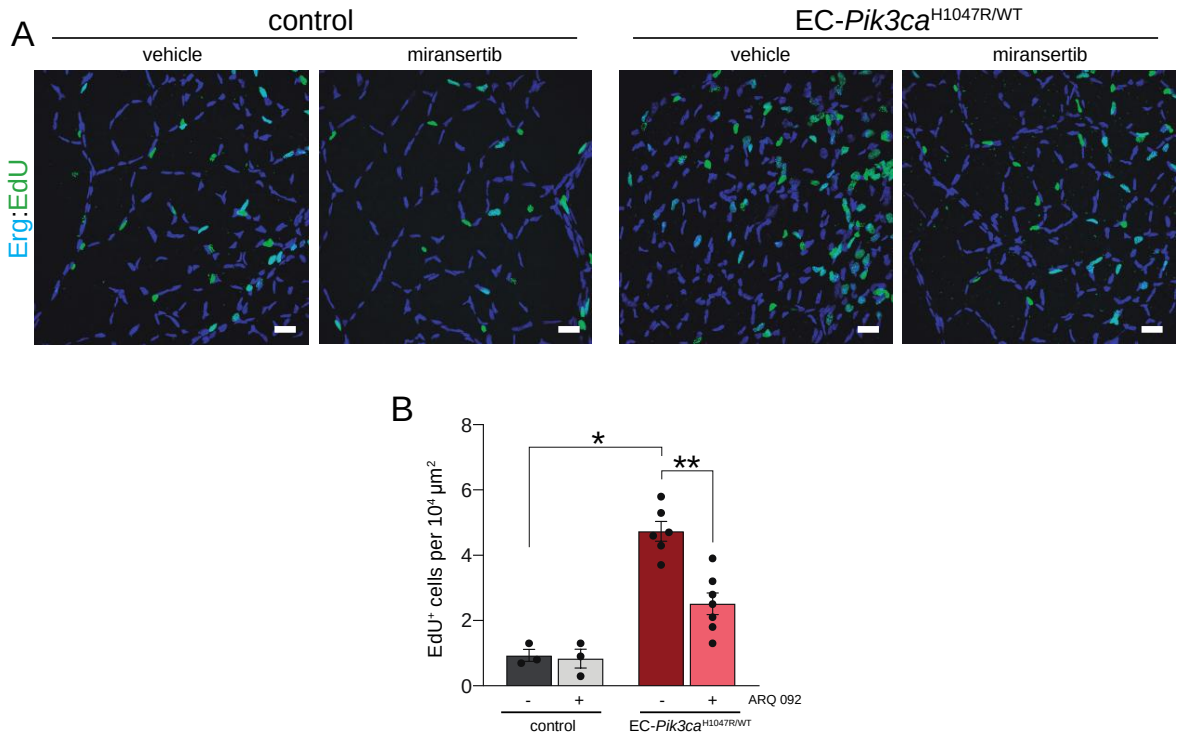

Figure 4. 1. 11. Lower dose of miransertib arrests EC proliferation *in vivo*.
(A) High magnification confocal images of retinas isolated from control and EC-*Pik3ca*$^{H1047R/WT}$ mice treated with vehicle or 35 mg/kg/dose of miransertib and immunostained for EC nuclei (Erg) and EdU. Scale bar = 30 µm. **(B)** Quantification of EdU-positive ECs per unit area. n ≥ 3 retinas per genotype. Data are presented as mean values. Error bars are s.e.m. Statistical analysis was performed by nonparametric Mann–Whitney test. *p < 0.05 and **p < 0.01 were considered statistically significant.

4.1.2.4. Inhibition of AKT by miransertib reverts *Pik3ca*-driven vascular malformations

Until now, there is no approved pharmacological therapy for vascular malformations patients. Recent preclinical and clinical works showed that PI3K signalling inhibitors are effective, and therefore many are currently being tested in clinical trials.

One of many critical factors regarding the inhibitors is their ability to revert the disease's symptoms and characteristics. In the case of vascular malformations, it would be of high importance to stop the growth of the lesions and reduce their size. To test whether miransertib is able to hamper the vascular growth and revert the phenotype of *Pik3ca*^{H1047}-vascular malformations, we proposed another curative experimental design using mouse retinas as a model. Briefly, *Pik3ca*^{H1047R} recombination was induced on P1, followed by inhibitor or vehicle treatment on P4 and P5 with a dose of 75 mg/kg. Retinas were isolated on P6 and immunostained for blood vessels (IB4) and EC nuclei (Erg) (**Figure 4.1.12. A**). Confocal images of the vasculature revealed that miransertib improves the regression of the vascular lesions (**Figure 4.1.12. B**)

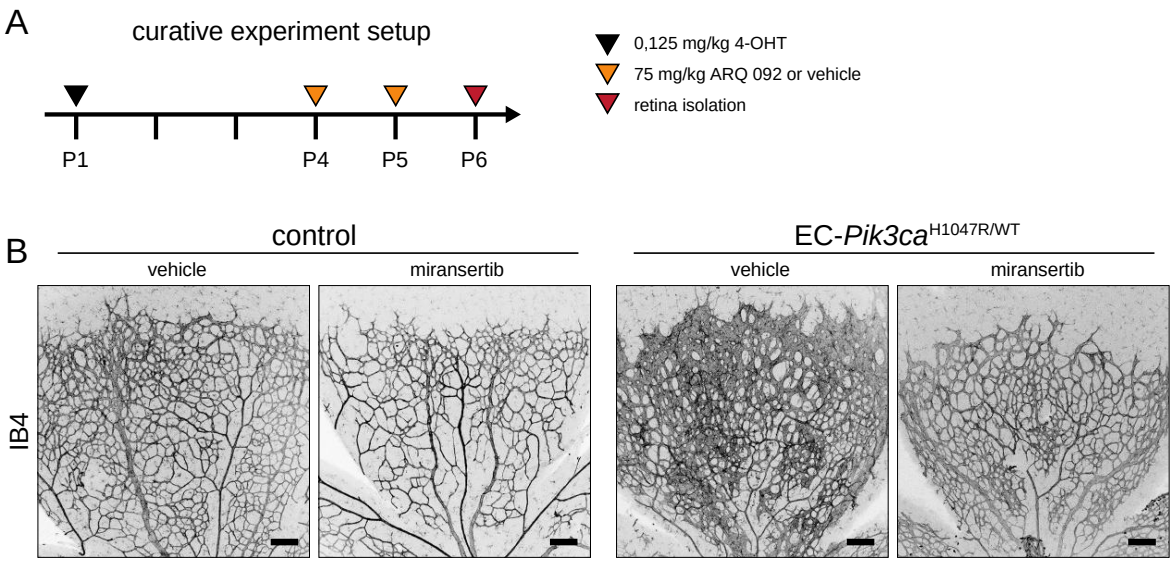

Figure 4. 1. 12. Miransertib reverts *Pik3ca*-driven vascular lesions.
(A) Dosing scheme for curative experiments with a high dose (75 mg/kg/dose) of miransertib **(B)** Representative confocal images of whole-mount P6 retinas isolated from control and EC-*Pik3ca*$^{H1047R/WT}$ mouse littermates treated with vehicle or 75 mg/kg/dose of miransertib. Blood vessels visualised with IB4. Scale bar = 150 µm. n ≥ 3 retinas per genotype.

To measure the therapeutic effect of the inhibitor, we quantified the vascular area (IB4-positive) in all conditions as well as the number of ECs (Erg-positive) using high magnification images. As seen before, both IB4-positive area and EC number are highly increased upon endothelial *Pik3ca*^{H1047R} allele expression. Treatment with 75 mg/kg of miransertib significantly normalised the vasculature and EC number, but had insignificant effect on the vessels of WT mice (**Figure 4.1.13. A-C**).

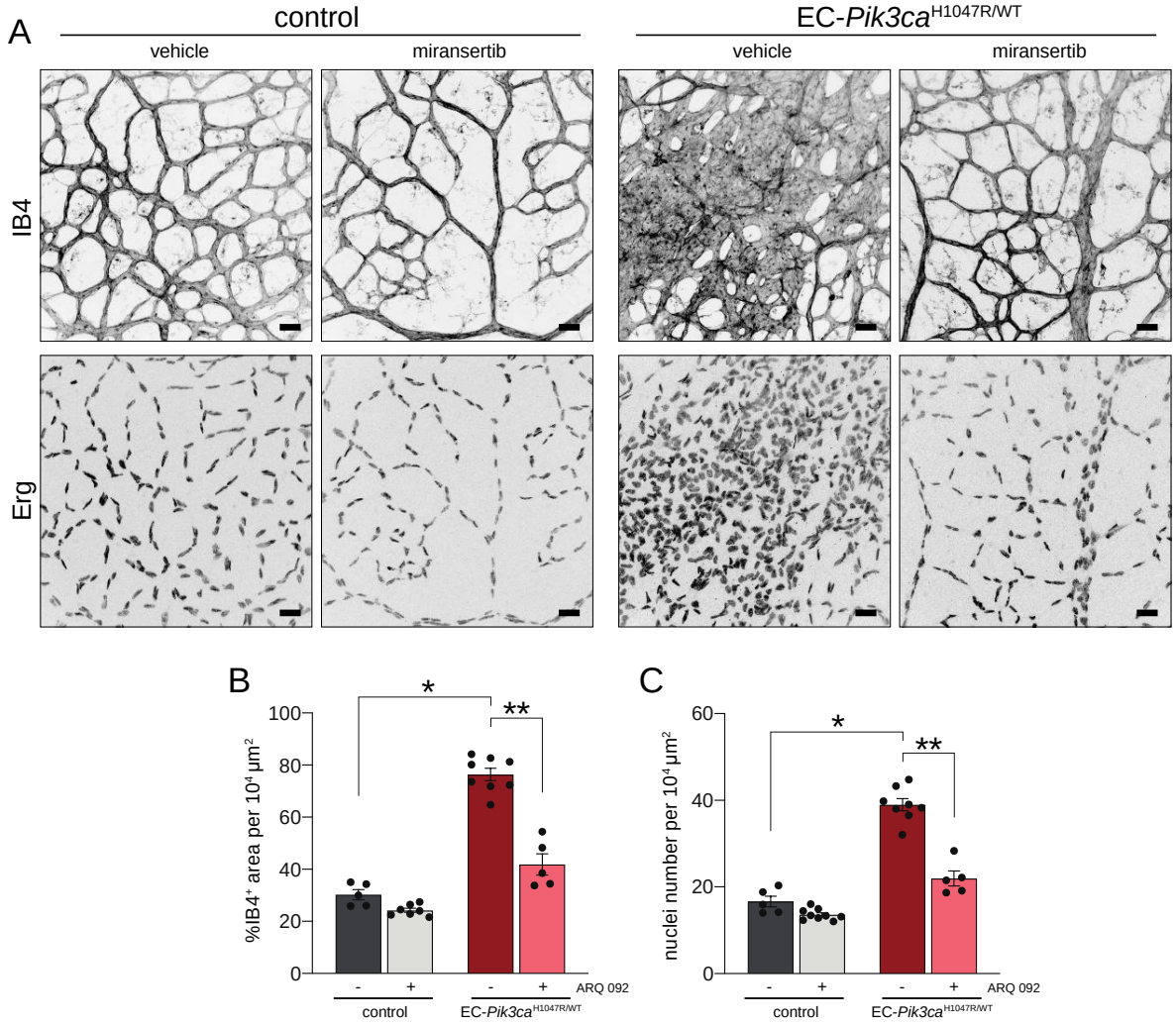

Figure 4. 1. 13. Miransertib regresses vascular lesions and reduces EC number.
(A) High magnification confocal images of retinas isolated from control and EC-*Pik3ca*$^{H1047R/WT}$ mice treated with vehicle or 75 mg/kg/dose of miransertib and immunostained for blood vessels (IB4) and EC nuclei (Erg) Scale bar = 30 µm. **(B)** Quantification of IB4-positive area per unit area. **(C)** Quantification of EC number per unit area. n ≥ 5 retinas per genotype. Data are presented as mean values. Error bars are s.e.m. Statistical analysis was performed by nonparametric Mann–Whitney test. *p < 0.05 and **p < 0.01 were considered statistically significant.

Next, we assessed EC proliferation capacity upon AKT inhibition using EdU incorporation assay. The quantification of proliferative ECs (Erg- and EdU-positive) showed that miransertib treatment arrests EC proliferation, and thus leading to vascular lesion regression (**Figure 4.1.14.**).

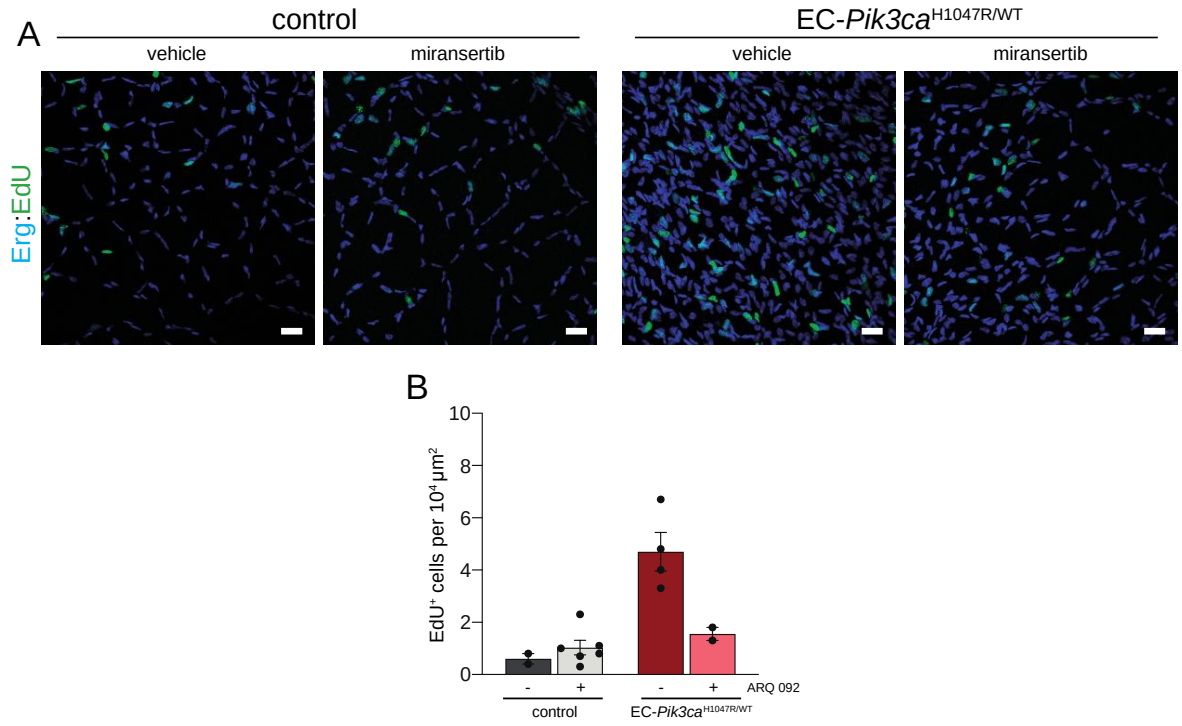

Figure 4. 1. 14. Miransertib arrests EC proliferation in curative experiment.
A) High magnification confocal images of retinas isolated from control and EC-*Pik3ca*$^{H1047R/WT}$ mice treated with vehicle or 75 mg/kg/dose of miransertib and immunostained for EC nuclei (Erg) and EdU. Scale

Here, we demonstrated that our preclinical mouse model of *Pik3ca*-driven vascular malformations constitutes a unique and convenient tool for preclinical drug testing. Moreover, using two different strategies (preventive and curative) we showed for the first time that targeting AKT, using pan-AKT inhibitor miransertib, has a high therapeutic potential in both prevention and treatment of vascular lesions exhibiting enhanced PI3K signalling.

4.2. Objective 2: The vascular function of PI3K-C2β

4.2.1. PI3K-C2β inactivation results in increased vascularity and vessel width at a later stage of angiogenesis

In order to address the vascular role of PI3K-C2β *in vivo*, we took advantage of the previously developed mouse model [75], in which PI3K-C2β catalytic activity is blocked as a result of a germline point mutation (D1212A) within a conserved ATP-binding DFG motif (Figure 4.2.1.). This knock-in strategy leads to the constitutive expression of the catalytically inactive protein without altering the expression of other members of the family. D212A/D1212A mice are viable, born at mendelian ratios, with no overt developmental and growth phenotype [75].

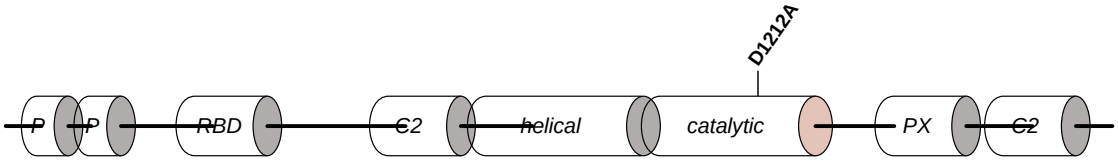

Figure 4. 2. 1. PI3K-C2β kinase-dead mouse model.
A germline point mutation D1212A was introduced within ATP-binding DFG motif in the catalytic domain to create a kinase-inactive variant of PI3K-C2β. No change in the gene expression was observed. Double mutant mice are viable with no overt developmental and growth alterations.

To assess the effects of PI3K-C2β kinase inactivation on angiogenic blood vessel growth, we decided to use a mouse retina model, a powerful *in vivo* system that allows a detailed characterisation of different stages of angiogenesis. Retinas from PI3K-C2β wild-type (PI3K-C2β$^{WT/WT}$) and PI3K-C2β double mutant (PI3K-C2β$^{D1212A/D1212A}$, hereafter referred to as PI3K-C2β$^{KI/KI}$) mice were isolated at different developmental time points: postnatal day 3 (P3) and P6, that correspond to early stages of sprouting angiogenesis, and P8 that refers to the later stage. Following the immunostaining using Isolectin B4 (IB4) that marks all blood vessels and high-resolution confocal imaging, we first compared the growth of the vascular tree between PI3K-C2β$^{WT/WT}$ and PI3K-C2β$^{KI/KI}$ (Figure 4.2.2. A). As expected, the vasculature expanded progressively from P3 to P8 in both measured groups. No statistical differences in radial expansion were observed between PI3K-C2β$^{WT/WT}$ and PI3K-C2β$^{KI/KI}$ mice (Figure 4.2.2. B). Curiously, the vascular expansion of the P6 PI3K-C2β$^{KI/KI}$ retinas appears to be slightly increased compared to the wild-type counterpart, but this mild phenotype is no longer visible on P8.

Next, we closely examined the density of the retinal vasculature in the sprouting front at each time points (P3, P6 and P8, respectively) (Figure 4.2.3. A). While no differences were observed in P3 and P6 retinas, we noticed a significant increase of IB4-positive vascular area on P8 in PI3K-C2β$^{KI/KI}$ retinas (Figure 4.2.3. B). Interestingly, the number of sprouts remained unchanged between the groups at all developmental stages (Figure 4.2.3. C), indicating that the observed vascular hyperplasia-like phenotype is unlikely the consequence of increased vessel sprouting. Furthermore, we measured the width of individual vessels within the sprouting front and detected that PI3K-C2β

inactivation results in the significant vessel enlargement on P8, but not on P3. A milder, although significant increase in vessel widening was also noticed on P6 (Figure 4.2.4.).

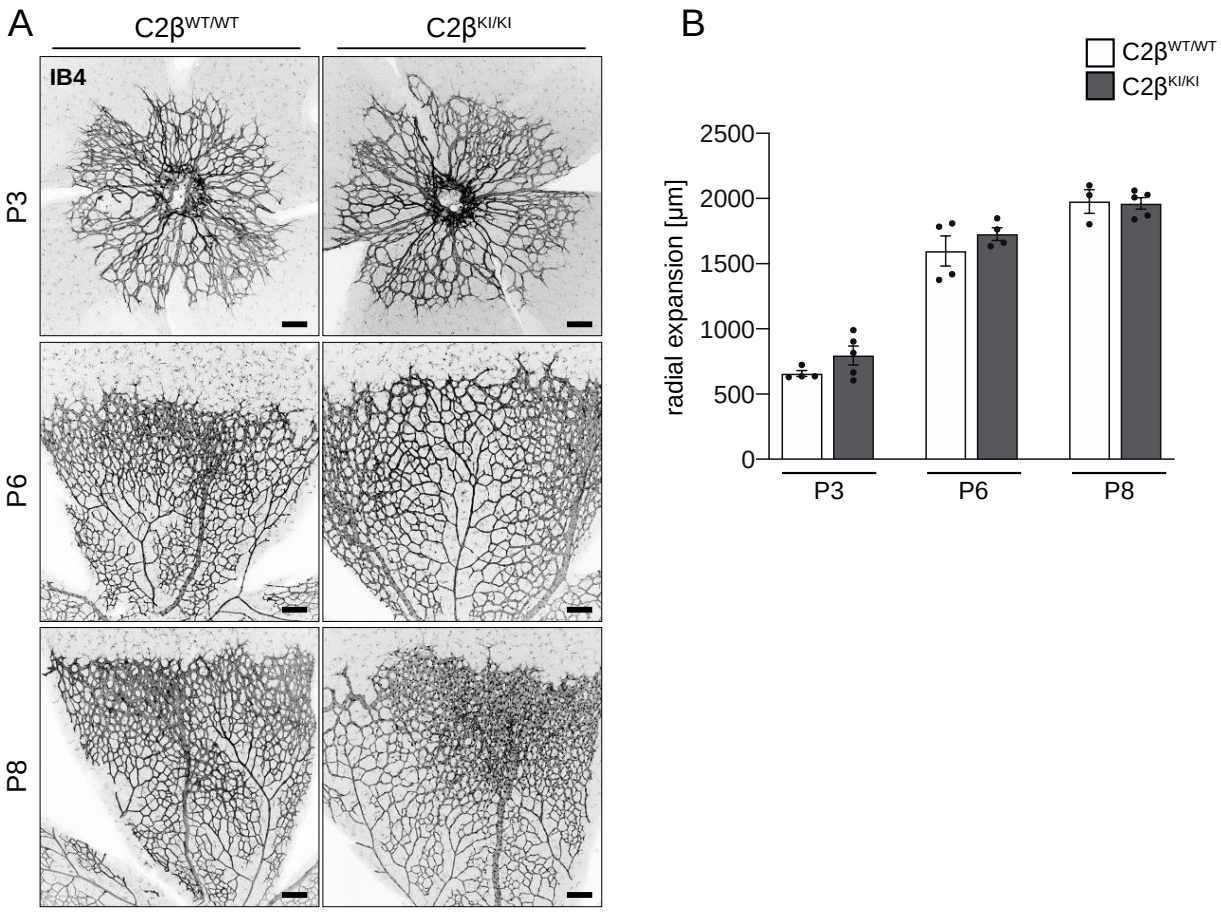

Figure 4. 2. 2. PI3K-C2β does not regulate radial expansion.
(A) Whole-mount visualisation of retinal blood vessels by Isolectin B4 (IB4) staining of PI3K-C2β$^{WT/WT}$ and PI3K-C2β$^{KI/KI}$ littermates at three developmental stages: P3, P6 and P8. Scale bar = 150 µm. (B) Quantification of radial expansion of retinal blood vessels on P3, P6 and P8. n ≥ 4 retinas per genotype. Data are presented as mean values. Error bars are s.e.m. Statistical analysis was performed by nonparametric Mann–Whitney test.

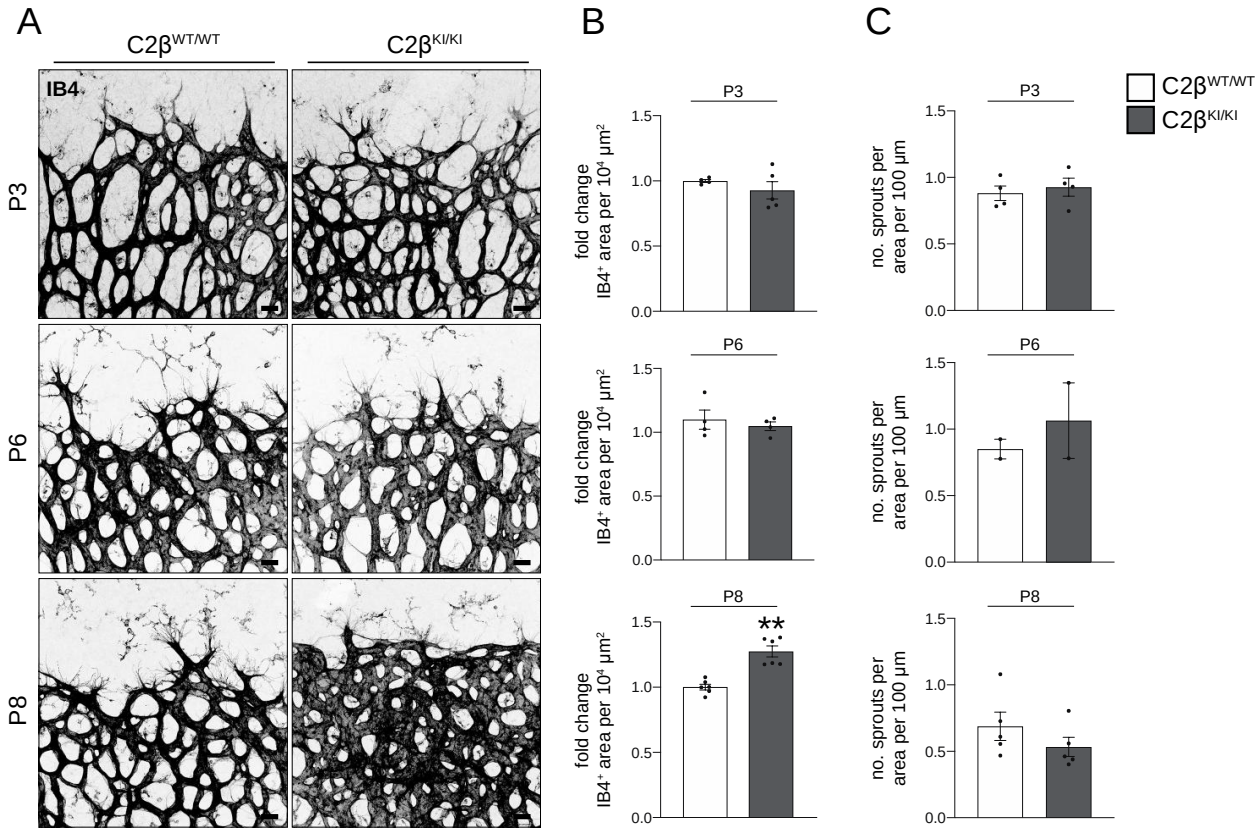

Figure 4. 2. 3. Inactivation PI3K-C2β results in increased retinal vascularity on P8.

(A) Confocal images of PI3K-C2β$^{WT/WT}$ and PI3K-C2β$^{KI/KI}$ retinal blood vessels of the sprouting front immunostained by IB4 at three developmental stages: P3, P6 and P8. Scale bar = 30 µm. (B) Quantification of the IB4-positive area in the sprouting front of the wild-type and PI3K-C2β$^{KI/KI}$ retinas. (C) Quantification of the number of sprouts per vascular front length of the wild-type and PI3K-C2β$^{KI/KI}$ retinas. n ≥ 4 retinas per genotype. Data are presented as mean values. Error bars are s.e.m. Statistical analysis was performed by nonparametric Mann–Whitney test. *p < 0.05 and **p < 0.01 were considered statistically significant.

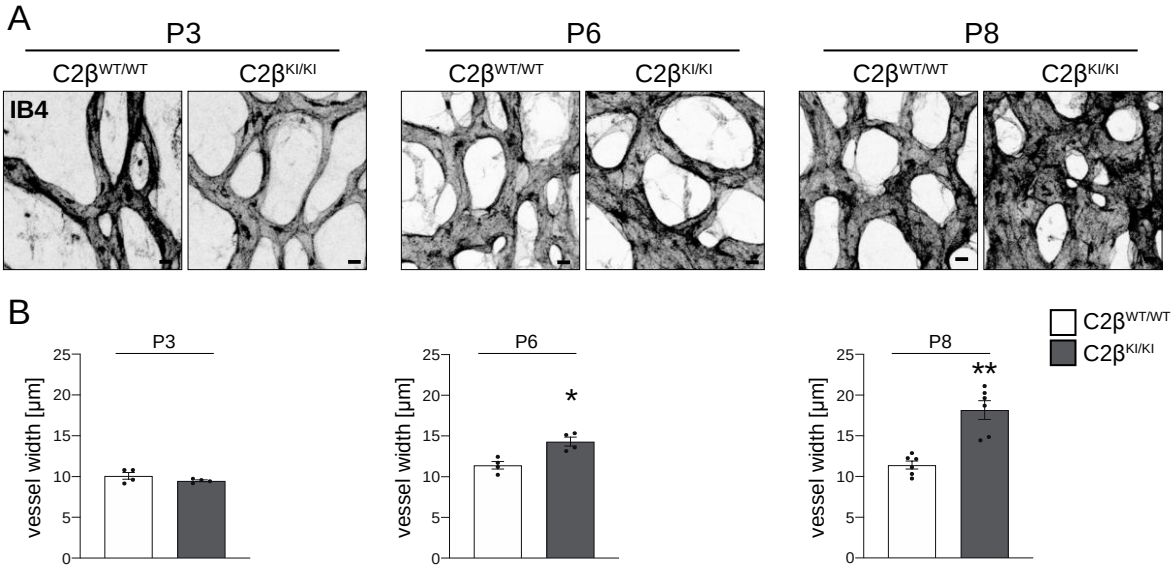

Figure 4. 2. 4. PI3K-C2β inactivation results in blood vessel enlargement.
(A) High magnification confocal images of PI3K-C2β$^{WT/WT}$ and PI3K-C2β$^{KI/KI}$ retinal blood vessels of the sprouting front immunostained by IB4 at three developmental stages: P3, P6 and P8. Scale bar = 10 µm. (B) Quantification of the vessel width in the sprouting front of the wild-type and PI3K-C2β$^{KI/KI}$ retinas. n ≥ 4 retinas per genotype. Data are presented as mean values. Error bars are s.e.m. Statistical analysis was performed by nonparametric Mann–Whitney test. *p < 0.05 and **p < 0.01 were considered statistically significant.

4.2.2. PI3K-C2β does not have an impact on EC number and proliferation

To test whether the observed increased vascularity in the front of the P8 PI3K-C2β$^{KI/KI}$ retinas was caused by the change in EC number, we decided to perform the immunostaining using Erg-recognising antibody that specifically decorates EC nuclei, following confocal imaging (Figure 4.2.5. A). Surprisingly, the subsequent quantification showed that PI3K-C2β does not impact on EC number at none of the analysed time points (Figure 4.2.5. B).

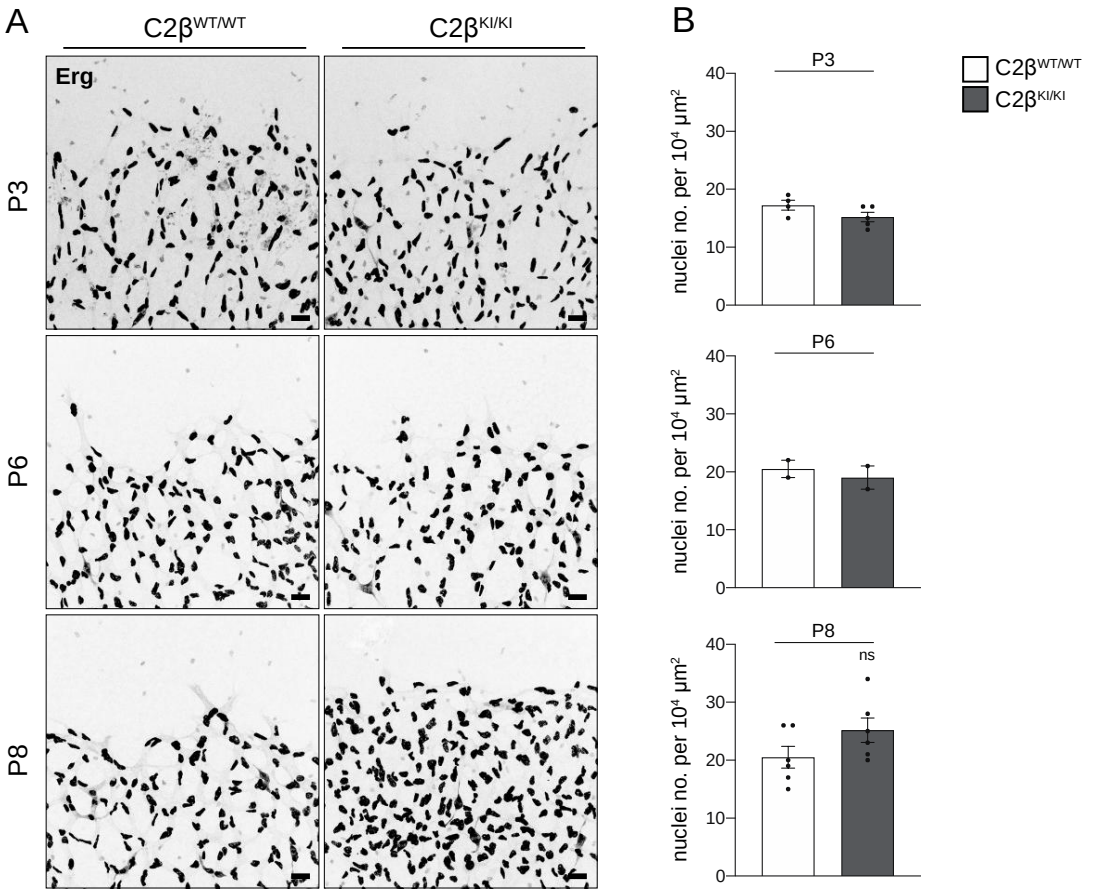

Figure 4. 2. 5. PI3K-C2β does not have an impact on EC number.
(A) Confocal images of the sprouting front of PI3K-C2β$^{WT/WT}$ and PI3K-C2β$^{KI/KI}$ retinas immunostained for EC-specific nuclear marker Erg on P3, P6 and P8. Scale bar = 30 µm. **(B)** Quantification of EC number per unit area. n ≥ 3 retinas per genotype. Data are presented as mean values. Error bars are s.e.m. Statistical analysis was performed by nonparametric Mann–Whitney test.

To finally rule out the possibility that the phenotype observed in P8 mutant retinas is a consequence of altered EC proliferation, we performed an *in vivo* EdU incorporation assay (Figure 4.2.6. A). Briefly, P8 pups were injected with EdU reagent two hours prior to retinas isolation, following the immunostaining for blood vessels (IB4), EC nuclei (Erg) and EdU. During S-phase of the cell cycle, EdU is incorporated into the newly synthesised DNA and the level of EdU incorporation is proportional to the level of cell proliferation. The number of EdU-positive ECs in the sprouting front did not changed upon PI3K-C2β inactivation, therefore indicating that PI3K-C2β does not regulate EC proliferation (Figure 4.2.6. B).

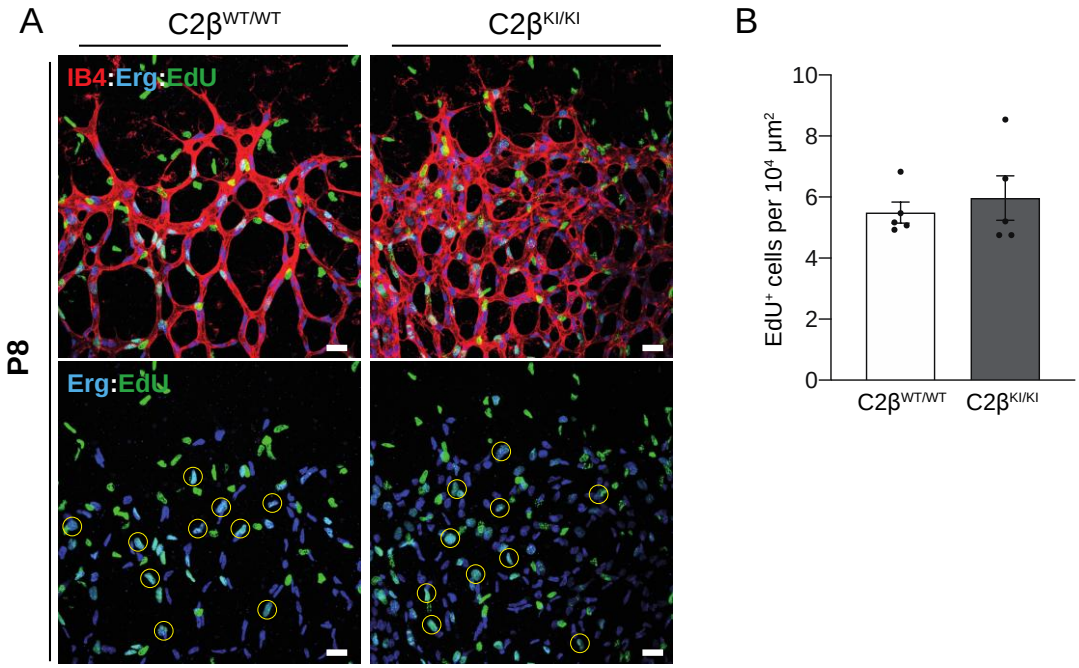

Figure 4. 2. 6. PI3K-C2β inactivation does not affect EC proliferation.
(A) Confocal images of the sprouting front of P8 PI3K-C2β$^{WT/WT}$ and PI3K-C2β$^{KI/KI}$ retinas immunostained for Erg and EdU. Blood vessels are visualised by IB4 staining. Scale bar = 30 µm. **(B)** Quantification of proliferative ECs (double positive for Erg and EdU) per unit area. n = 5 retinas per genotype. Data are presented as mean values. Error bars are s.e.m. Statistical analysis was performed by nonparametric Mann–Whitney test.

4.2.3. Enhanced collagen IV deposition upon PI3K-C2β inactivation

The retinal vasculature undergoes substantial remodelling of already formed EC connections. This process is partially regulated through collagen IV deposition, one of the main basement membrane proteins synthesised and secreted by ECs during maturation. During the remodelling, many unnecessary and blood flow-deprived vascular branches retract (vessel pruning). This process leaves a molecular footprint – an empty tube formed by collagen IV-enriched basement membrane, lacking living ECs. Therefore, we decided to assess the deposition of collagen IV and retraction events in P8 PI3K-C2β$^{WT/WT}$ and PI3K-C2β$^{KI/KI}$ retinas to compare their level of maturation. For this, we immunostained the retinas for collagen IV and blood vessels (IB4) and performed high-resolution microscopy of the sprouting front (**Figure 4.2.7. A**). We then measured the intensity of collagen IV staining within the vascular compartment (IB4-positive area) and noticed a significant increase in collagen IV deposition upon PI3K-C2β inactivation compared to the wild-type retinas (**Figure 4.2.7. B**). Moreover, the number of collagen IV-positive and IB4-negative branches (vessel retractions) was significantly reduced upon PI3K-C2β loss of function (**Figure 4.2.7. C**). Based on these observations, it is tempting to speculate that the loss of PI3K-C2β kinase activity might promote both vessel maturation and stability.

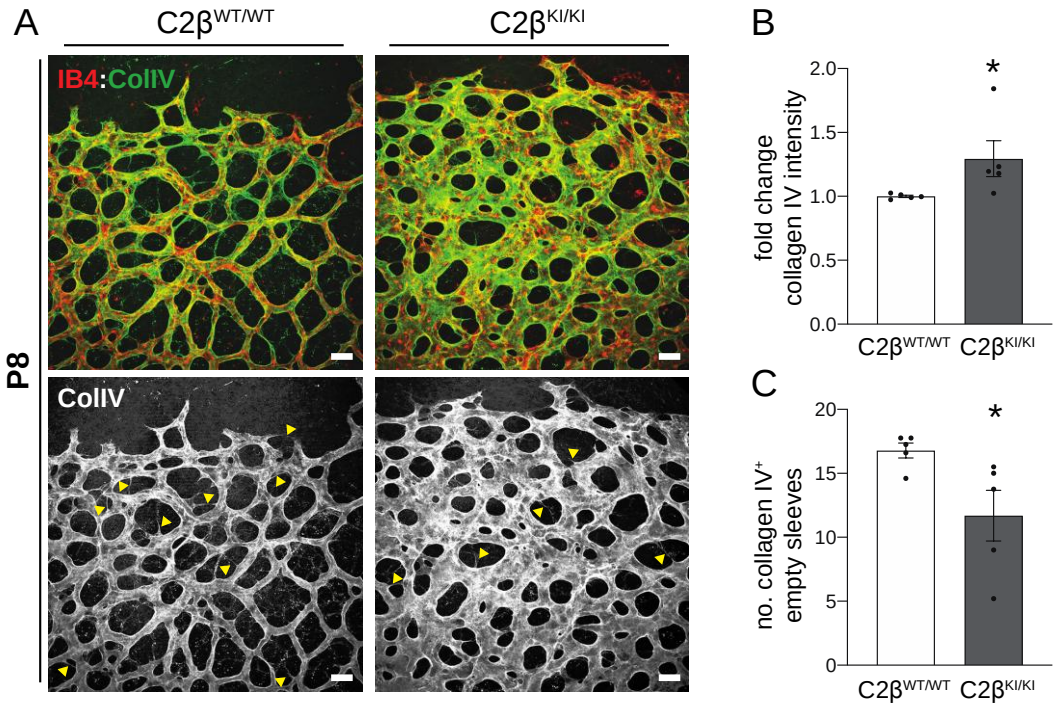

Figure 4. 2. 7. PI3K-C2β inactivation results in increased collagen IV deposition.
(A) Confocal images of the sprouting front of P8 PI3K-C2β$^{WT/WT}$ and PI3K-C2β$^{KI/KI}$ retinas immunostained for collagen IV (ColIV) and blood vessels (IB4). Scale bar = 30 µm. (B) Quantification of collagen IV intensity within the vascular area expressed as fold change. (C) Quantification of collagen IV-positive and IB4-negative empty sleeves (pointed by arrowheads). n = 5 retinas per genotype. Data are presented as mean values. Error bars are s.e.m. Statistical analysis was performed by nonparametric Mann–Whitney test. *p < 0.05 was considered statistically significant.

4.2.4. Loss of PI3K-C2β catalytic activity alters PC morphology

In PI3K-C2β$^{KI/KI}$ mouse model the, so-called, kinase-dead PI3K-C2β protein is expressed in a constitutive manner in all cells. This means that not only ECs are affected by the inactivation of the protein. Blood vessels are made of ECs surrounded by mural cells (both PCs and VSMCs) that significantly contribute to vascular development in all its stages. PCs play a role in vessel maturation and stability and they also participate in the response to environmental factors and stresses. Hence, to further characterise the model we immunostained P8 WT and mutant retinas for NG2, a PC-specific marker, followed by confocal imaging of the sprouting front. NG2 is expressed on PC cell membrane, thus it allows to visualise the cell morphology (Figure 4.2.8. A). We quantified the degree of PC coverage of the blood vessels and noticed no difference between PI3K-C2β$^{WT/WT}$ and PI3K-C2β$^{KI/KI}$ animals (Figure 4.2.8. B). Nevertheless, higher magnification images showed a peculiar change in PC morphology. While wild-type PCs appear flat and elongated, those in PI3K-C2β$^{KI/KI}$ retinas depict spiky, highly protruded morphology (Figure 4.2.8. C).

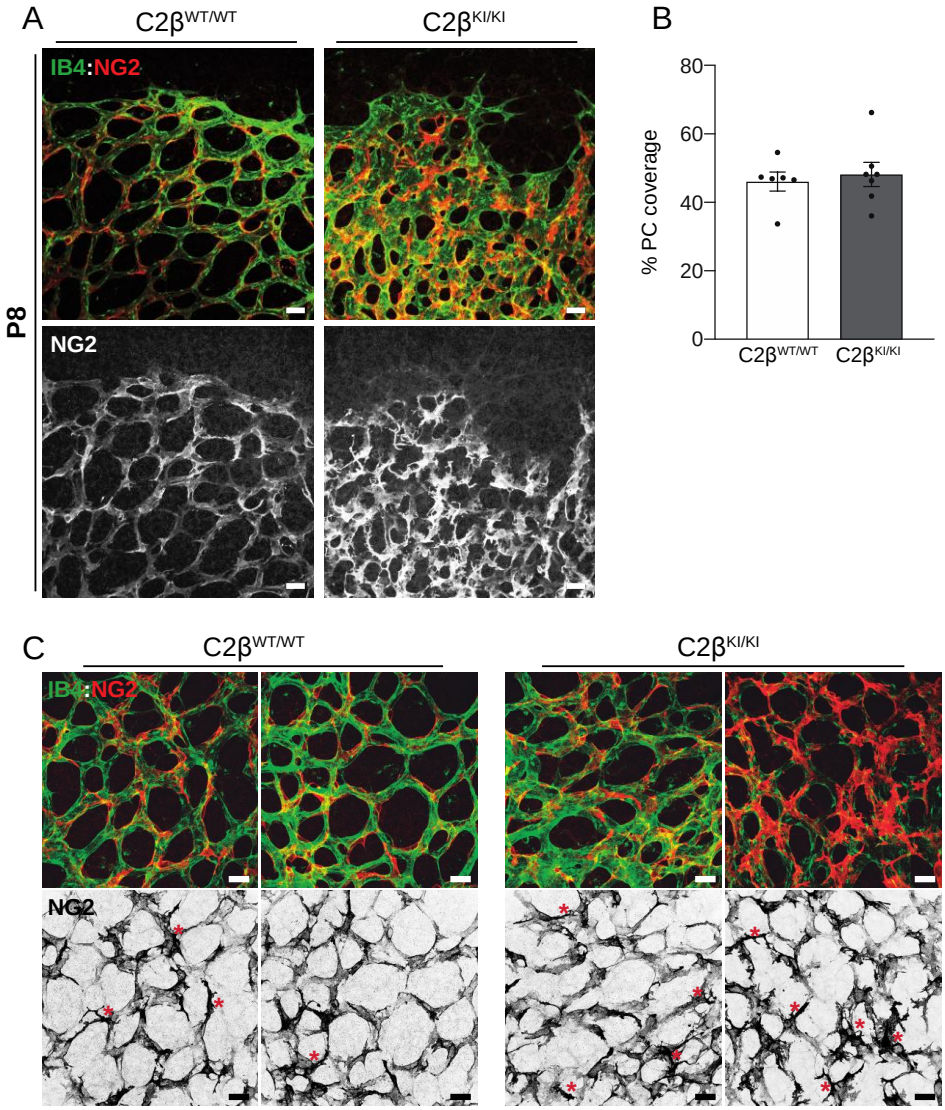

Figure 4. 2. 8. Inactivation of PI3K-C2β affects pericyte morphology but not coverage.
(A) Confocal images of the sprouting front of P8 PI3K-C2β$^{WT/WT}$ and PI3K-C2β$^{KI/KI}$ retinas immunostained for pericytes (NG2) and blood vessels (IB4). Scale bar = 30 µm. **(B)** Quantification of PC coverage per vessel area. **(C)** High magnification confocal images of NG2-positive PCs. Scale bar = 20 µm. n ≥ 6 retinas per genotype. Data are presented as mean values. Error bars are s.e.m. Statistical analysis was performed by nonparametric Mann–Whitney test.

This unexpected result prompted us to compare *Pik3c2b* level of expression between ECs and PCs. For this, wild-type primary mouse lung endothelial cells (MLEC) and mouse brain pericytes (MBPC) were isolated and cultured, followed by RNA

extraction, cDNA synthesis and quantitative PCR (QPCR) analysis. First, we measured the purity of both MLECs and MBPC cultures using EC- and PC-specific markers. As expected, MBPC showed no expression of EC-specific *Pecam1* marker, while PC-specific genes, namely *Pdgfrb*, *Cspg4* and *Cd248*, were highly expressed compared to MLEC. *Des*, a PC-specific gene, showed no enrichment in neither MLEC nor MBPC. Curiously, *Pik3c2b* gene expression was increased 30-fold in MBPC compared to MLEC. These data suggest that PI3K-C2β might play a key and unprecedented role in PCs which could be reflected in their morphology and function during angiogenesis (Figure 4.2.9.).

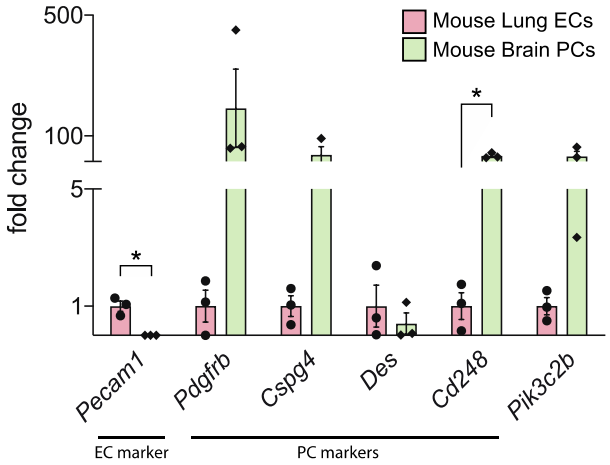

Figure 4. 2. 9. *Pik3c2b* expression is enriched in brain PCs.
Gene expression comparison of *Pecam1*, *Pdgfrb*, *Cspg4*, *Des*, *Cd248* and *Pik3c2b* in primary wild-type Mouse Lung Endothelial Cells (MLEC) and Mouse Brain Pericytes (MBPC) by quantitative PCR. Gene expression normalised to *Rpl32* housekeeping gene. Data presented as fold change relative to MLEC. n = 3. Error bars are s.e.m. Statistical analysis was performed by t-test with Welch's correction. *$p < 0.05$ and was considered statistically significant.

4.2.5. PI3K-C2β inactivation does not affect NO-mediated vasodilation

Given that EC proliferation remained unchanged upon PI3K-C2β genetic inactivation and the mutant PCs display morphological alterations, we postulated that the increased vessel width could be a result of enhanced vasodilation. Widening of blood vessels has a known physiological purpose – it improves blood flow to facilitate nutrients delivery. Vasodilation is controlled via contractile activity of VSMCs and there are some evidences showing that PCs may also control blood flow in small capillaries.

The increased blood flow results in a decline in blood pressure, therefore our first aim was to determine the systemic pressure. For technical reasons, the procedure was performed in adult mice. Both systolic and diastolic blood pressure was measured 10 times for 4 consecutive days for the animals to adapt. On the fifth and final day, the last measurement was taken and the average value was calculated. In addition, we measured heart rate. As shown in Figure 4.2.10. A, we did not observed differences in neither systolic nor diastolic blood pressure between PI3K-C2β$^{WT/WT}$ and PI3K-C2β$^{KI/KI}$ mice. Similarly, no alterations in heartbeat were noticed (Figure 4.2.10. B).

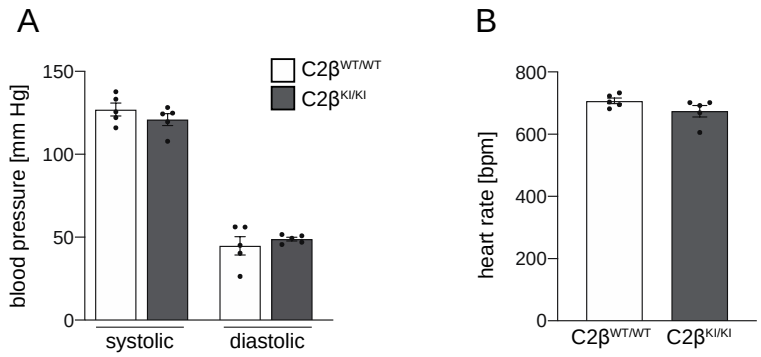

Figure 4. 2. 10. PI3K-C2β kinase loss of function has no impact on systemic blood pressure.
(A) Systolic and diastolic blood pressure in PI3K-C2β$^{WT/WT}$ and PI3K-C2β$^{KI/KI}$ mice were measured in ten technical replicates per mouse and the average value was calculated. (B) Heart rate measurement in PI3K-C2β$^{WT/WT}$ and PI3K-C2β$^{KI/KI}$ mice was performed in ten technical replicates per mouse and the average value was calculated. n = 5. Data are presented as mean values. Error bars are s.e.m. Statistical analysis was performed by nonparametric Mann–Whitney test.

Vasodilation may arise from increased endogenous production of vasodilating agents, such as nitric oxide (NO). Indeed, ECs locally produce and secrete NO to modulate the contractility of VSMCs. For this reason, we decided to block NO synthesis by targeting eNOS, the main enzyme of the pathway, using a competitive inhibitor N-methylarginine (L-NMMA). We hypothesised that if PI3K-C2β inactivation leads to NO-driven vasodilation on P8, we could rescue (at least partially) the phenotype by dampening NO production through eNOS inhibition. Therefore, P8 pups were injected intraperitoneally with a single dose of 50 mg/kg of L-NMMA 2 hours prior to retinas isolation. PBS-treated mice were used as a control. Following the immunostaining for blood vessels (IB4) and confocal imaging, we noticed that L-NMMA treatment led to narrowing of the vessels in PI3K-C2β$^{WT/WT}$, indicating that eNOS inhibition was efficient. However, we did not observe a phenotype rescue in PI3K-C2β$^{KI/KI}$ retinas upon inhibitor administration compared to PBS-treated counterpart (Figure 4.2.11).

Taken together, these results corroborate that increased vessel width and consequently vascularity are not a result of enhanced vasodilation as confirmed using two independent approaches – measuring blood pressure and blocking NO production.

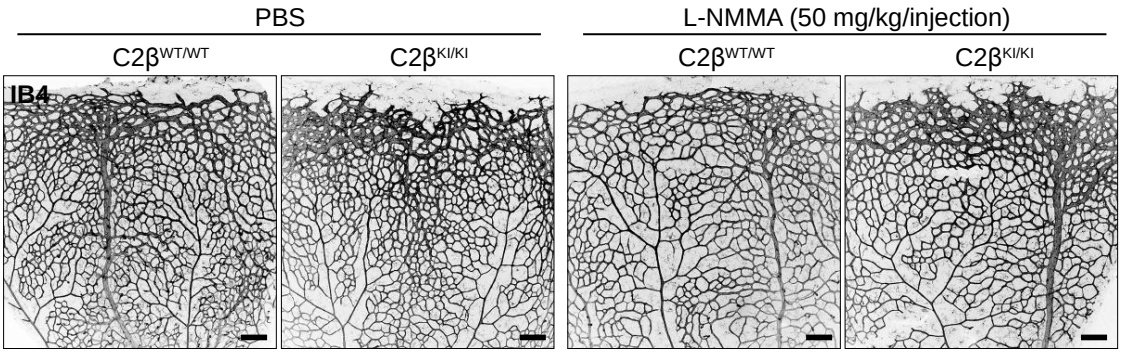

Figure 4. 2. 11. eNOS inhibition does not rescue PI3K-C2β$^{KI/KI}$ phenotype.
P8 PI3K-C2β$^{WT/WT}$ and PI3K-C2β$^{KI/KI}$ mice were injected with 50 mg/kg L-NMMA (eNOS-specific inhibitor) 2 hours prior to retinas isolation. PBS-treated mice were used as controls. Representative confocal images of retinas immunostained for blood vessels (IB4) are shown. Scale bar = 150 µm. n = 2.

4.2.6. Loss of PI3K-C2β activity does not impact on EC migration and proliferation *in vitro*

ECs are the main building blocks of blood vessels and so their ability to respond and maintain a proper function constitute a foundation of vascular development. Therefore, to better understand the *in vivo* phenotype observed in PI3K-C2β$^{KI/KI}$ mice, we decided to perform *in vitro* analyses of basic biological processes using cultured ECs. For this, we isolated primary Mouse Lung Endothelial Cells (MLEC) from adult PI3K-C2β$^{WT/WT}$ and PI3K-C2β$^{KI/KI}$ mice. Previous studies have reported that PI3K-C2β regulates HUVEC migration upon S1P- and HDL-induction *in vitro*. To test whether this phenotype is also observed under normal growth conditions, we performed a wound healing assay that allows us to study collective cell migration. Briefly, a single "scratch" was created on monolayer cells, followed by images acquisition at the beginning (T0), 7 and 24 hours later. Then, the wound area was measured and presented as a percentage of T0. Both PI3K-C2β$^{WT/WT}$ and PI3K-C2β$^{KI/KI}$ MLEC showed equal collective cell migration capacity under normal growth conditions (Figure 4.2.12. A). In addition, we analysed cell proliferation using BrdU incorporation assay. For this, BrdU reagent was added for 2 hours, followed by the immunostaining with BrdU-specific antibody and cell nuclei marker, DAPI. We quantified the percentage of BrdU-positive cells of all cells and, as expected from *in vivo* data, we have not detected any effects from PI3K-C2β loss of function on EC proliferation (Figure 4.2.12. B).

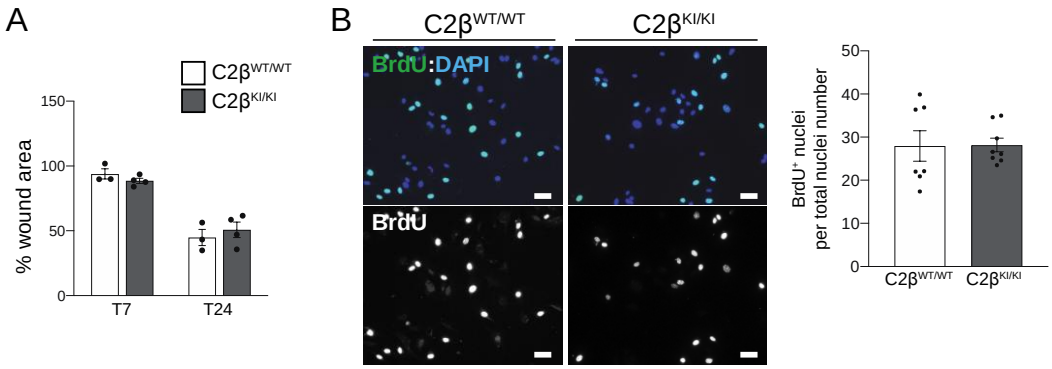

Figure 4. 2. 12. PI3K-C2β kinase inactivation does not regulate EC collective migration nor proliferation in vitro.

(A) Confluent PI3K-C2β$^{WT/WT}$ and PI3K-C2β$^{KI/KI}$ MLEC were subjected for a wound healing assay. Widefield microscopy images were taken at starting point (T0), 7 and 24 hours after. The percentage of the wound area was quantified relative to the starting point (T0) of the corresponding group. n ≥ 3. **(B)** PI3K-C2β$^{WT/WT}$ and PI3K-C2β$^{KI/KI}$ MLEC were used in BrdU-incorporation assay. The number of BrdU-positive nuclei was quantified by immunofluorescence and presented as the percentage of all nuclei. Scale bar = 100 µm. n ≥ 7. Data are presented as mean values. Error bars are s.e.m. Statistical analysis was performed by nonparametric Mann–Whitney test.

4.2.6.1. Endothelial focal adhesion assembly does not require PI3K-C2β catalytic activity

Unpublished data from our collaborators showed that PI3K-C2β participates in focal adhesion (FA) assembly and its knock-down in HeLa cells leads to an increase in FA number and size. We wondered whether PI3K-C2β kinase inactivation also promotes FA accumulation in ECs. WT and PI3K-C2β$^{KI/KI}$ MLEC were immunostained for paxillin, a FA-associated protein, and the quantification of FA number and size showed no difference between WT and mutant cells (Figure 4.2.13. A-C). This was indeed expected since PI3K-C2β$^{KI/KI}$ ECs showed no changes in migration.

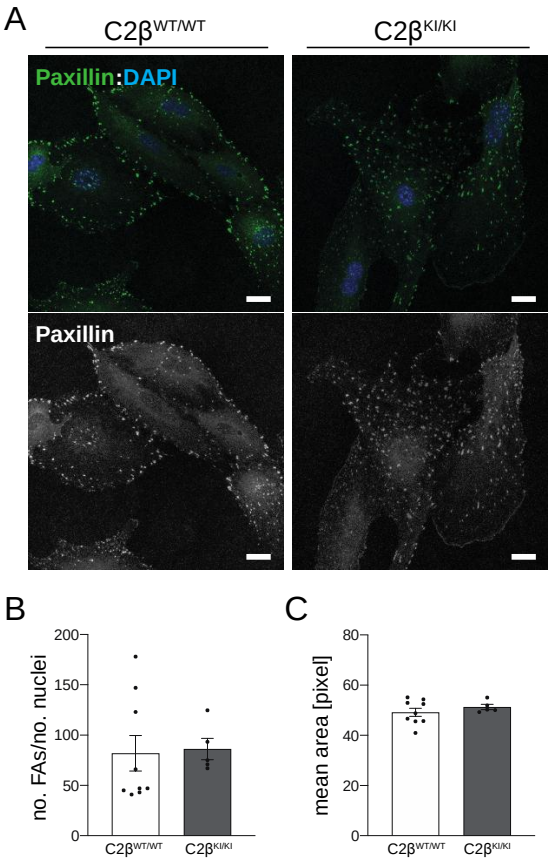

Figure 4. 2. 13. PI3K-C2β does not affect focal adhesion assembly.
(A) Confocal images of PI3K-C2β$^{WT/WT}$ and PI3K-C2β$^{KI/KI}$ MLEC immunostained for paxillin and nucleus (DAPI). Scale bar = 20 µm. **(B)** Quantification of the number and area of focal adhesions. n ≥ 5. Data are presented as mean values. Error bars are s.e.m. Statistical analysis was performed by nonparametric Mann–Whitney test.

4.2.7. PI3K-C2β kinase inactivation results in increased EC size

Next, we wanted to check whether there are any alterations in the morphology of the cells upon loss of PI3K-C2β kinase activity. We used the immunostaining for β-catenin, a protein associating with adherent junctions, to visualise cellular outlines. We then measured the area of individual cells. Quite surprisingly, we found out that PI3K-C2β$^{KI/KI}$ MLEC are significantly bigger compared to their WT counterparts (**Figure 4.2.14.**), suggesting that PI3K-C2β-generated phospholipids control the size of the cell.

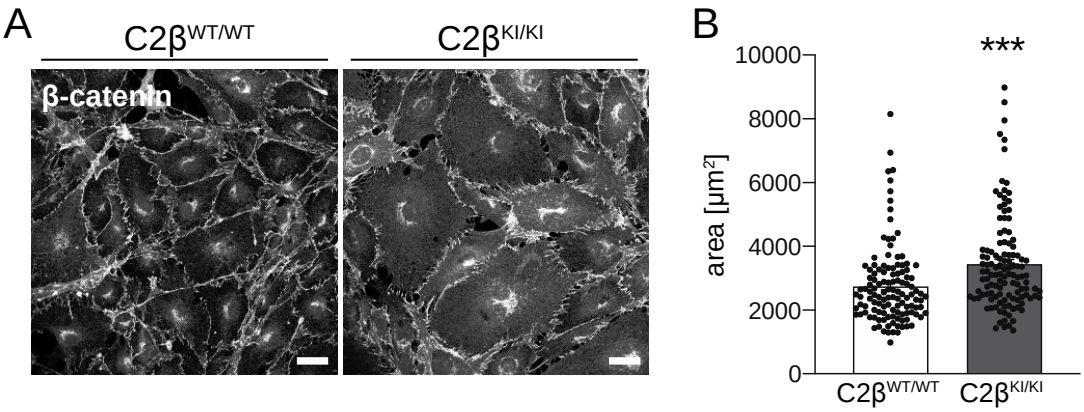

Figure 4. 2. 14. Inactivation of PI3K-C2β results in increased endothelial cell area
(A) PI3K-C2β$^{WT/WT}$ and PI3K-C2β$^{KI/KI}$ MLEC were immunostained for β-catenin, followed by high magnification confocal imaging. Scale bar = 20 µm. **(B)** Quantification of the cell area. n = 3. Data are presented as mean values. Error bars are s.e.m. Statistical analysis was performed by nonparametric Mann–Whitney test. *p < 0.05, **p < 0.01 and ***p < 0,0001 were considered statistically significant.

4.2.8. The effect of PI3K-C2β kinase inactivation on EC signalling

This led us to speculate that perhaps loss of PI3K-C2β function affects signalling pathways that control cell growth. One of the key molecules that governs cell size is mTOR (associated with complex 1). In fact, PI3K-C2β-produced PI(3,4)P_2 was shown to negatively regulate the activity of mTORC1. Therefore, we sought to determine the molecular signalling, in particular the effects on canonical class I PI3K signalling. For this, subconfluent PI3K-C2β$^{WT/WT}$ and PI3K-C2β$^{KI/KI}$ MLEC were serum starved for 5 hours, followed by a stimulation with mouse recombinant VEGF-A (100 ng/ml) and 1% FBS for 15 minutes. These factors are known to activate the class I PI3K signalling. Then, the cells were lysed and total cell proteins were separated by SDS-PAGE, following immunoblotting. Using phosphoprotein-specific antibodies, we detected a slight increase in p-S6 (S235/236) level in PI3K-C2β$^{KI/KI}$ MLEC in all tested conditions compared to the WT cells. No changes in p-AKT (S473) levels were observed (Figure 4.2.15.). Unfortunately, we experienced technical difficulties when using MLEC for cell signalling studies, since they appeared to be particularly resistant to serum starvation. Consequently, results were not always reproducible, limiting their applicability.

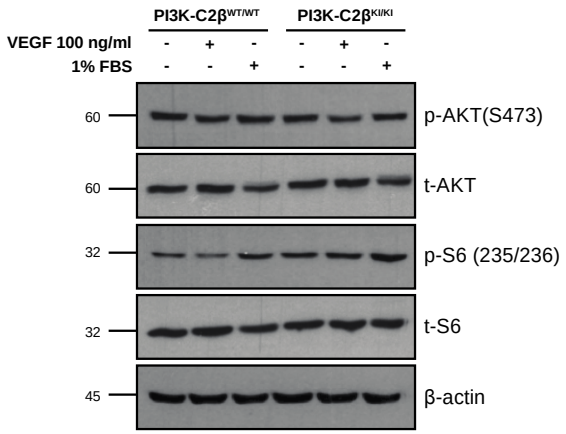

Figure 4. 2. 15. PI3K signalling comparison in MLEC upon PI3K-C2β kinase inactivation.
PI3K-C2β$^{WT/WT}$ and PI3K-C2β$^{KI/KI}$ MLEC were serum starved, followed by 100 ng/ml VEGF-A or 1% FBS stimulation for 15 minutes. AKT and S6 phosphorylation was assessed by immunoblotting. Non-stimulated cells were used as a control. A representative immunoblot from three (n = 3) independent experiments is shown.

4.2.9. PI3K-C2β knock-down results in enhanced mTORC1 signalling in ECs

To check whether loss of PI3K-C2β may indeed affect class I PI3K signalling, as reported elsewhere, we decided to implement RNA interference strategy to knock-down PI3K-C2β in Human Umbilical Vein Endothelial Cells (HUVEC). This *in vitro* system was shown to be highly reproducible and applicable for cell signalling studies. For this reason, primary HUVEC were transfected with two different siRNA oligonucleotide sequences against PI3K-C2β (siRNA #1 and #2, respectively) and scrambled-transfected HUVEC were used as a control. We first aimed to determine the efficiency of the knock-down by immunoblotting and we confirmed that both siRNA sequences significantly reduced the expression of PI3K-C2β, although siRNA #1 appeared more efficient (**Figure 4.2.16.**). Therefore, all subsequent *in vitro* assays were performed using siRNA #1.

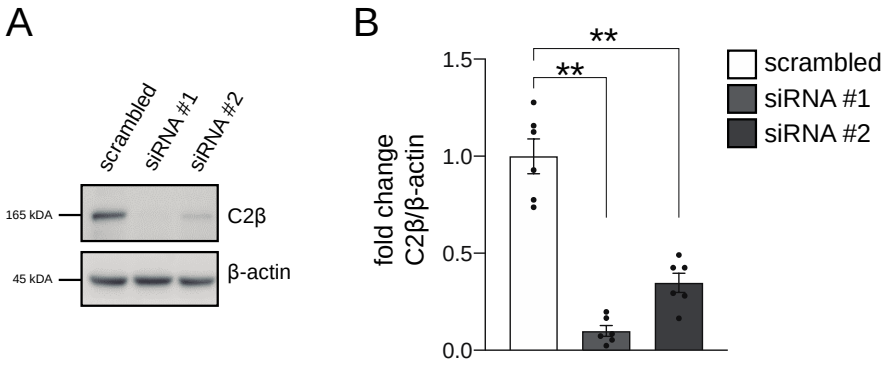

Figure 4. 2. 16. PI3K-C2β knock-down efficiency in HUVEC upon siRNA-transfection.
(A) HUVEC were transfected with two different PI3K-C2β-specific siRNA oligonucleotides. Scrambled-transfected cells were used as a control. Knock-down efficiency was assessed by immunoblotting. **(B)** Quantification of relative protein expression. Data were normalised to β-actin. n = 6. Data are presented as fold change. Error bars are s.e.m. Statistical analysis was performed by nonparametric Mann–Whitney test. *p < 0.05 and **p < 0.01 were considered statistically significant.

Next, we aimed to decipher the signalling changes upon silencing of PI3K-C2β as performed before on MLEC. Briefly, scrambled- and siRNA-transfected HUVEC were serum starved, followed by stimulation with either human recombinant VEGF-A (100 ng/ml) or 1% FBS. Non-stimulated cells were used as controls. Total cell lysates were subjected for SDS-PAGE and separated proteins were transferred onto the membrane. Upon incubation with phosphoprotein-specific antibodies, we detected an increase in p-S6 levels (both S235/236 and S240/244 residues) under starved condition in PI3K-C2β-depleted cells compared to the scrambled. The phosphorylation of S6 is further increased upon VEGF-A and FBS stimulation, with the higher difference in p-S6 235/236. Interestingly, silencing PI3K-C2β elevated to a lesser degree p-AKT levels, both S473 and T308 upon FBS stimulation (Figure 4.2.17.). Based on these observations and given that S6 signals downstream of mTORC1, it is tempting to speculate that PI3K-C2β negatively controls mTORC1 activity in ECs.

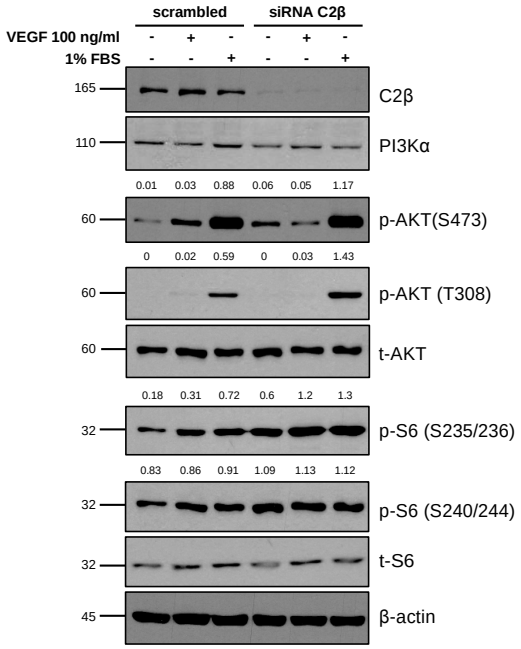

Figure 4. 2. 17. PI3K-C2β knock-down impacts on mTORC1 signalling in ECs.
Serum-starved scrambled and siRNA-C2β-depleted HUVEC were stimulated with 100 ng/ml VEGF-A or 1% FBS for 15 minutes, followed by protein extraction and immunoblotting. Non-treated cells were used as a control. The quantification of the relative phosphorylation of each protein was normalised to corresponding total proteins. Data are presented as the mean of three independent experiments (n = 3).

4.2.10. PI3K-C2β silencing does not affect EC migration and proliferation *in vitro*

To further corroborate previous findings in MLEC, we performed similar *in vitro* assays using HUVEC instead. Unlike in previous settings, where the loss of PI3K-C2β kinase activity was tested, here we additionally – although not specifically – address a putative kinase-independent function of the protein (so far not reported).

To analyse the effects of PI3K-C2β knock-down on collective cell migration, we performed the wound healing assay. As seen in MLEC, collective cell migration, was not affected by the loss of the expression of PI3K-C2β (Figure 4.2.18. A). Likewise, no differences were observed in EC proliferation capacity in BrdU incorporation assay (Figure 4.2.18. B), ultimately demonstrating that neither kinase-dependent nor kinase-independent functions of PI3K-C2β are important in the regulation of cell collective migration and proliferation.

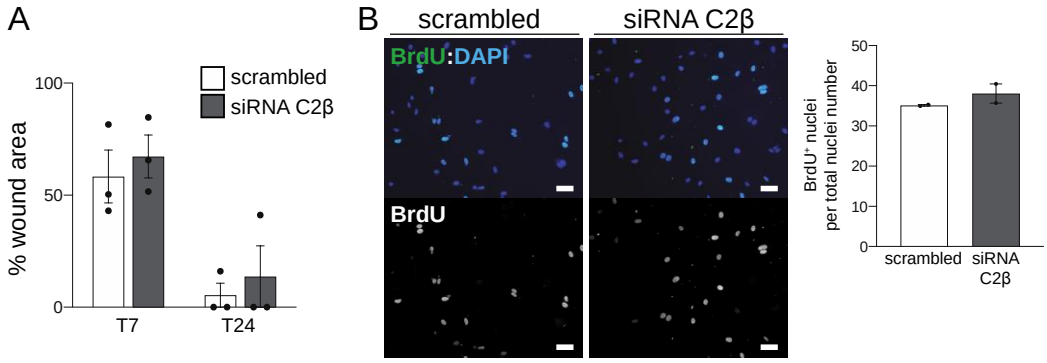

Figure 4. 2. 18. Knocking down PI3K-C2β does not alter EC collective migration nor proliferation *in vitro*.
(A) Confluent scrambled- and siRNA-C2β-transfected HUVEC were subjected for a wound healing assay. Widefield microscopy images were taken at starting point (T0), 7 and 24 hours after. The percentage of the wound area was quantified relative to the starting point (T0) of the corresponding group. n ≥ 3. (B) Scrambled and PI3K-C2β-knocked down HUVEC were used in BrdU-incorporation assay. The number of BrdU-positive nuclei was quantified by immunofluorescence and presented as the percentage of all nuclei. Scale bar = 100 µm. n ≥ 7. Data are presented as mean values. Error bars are s.e.m. Statistical analysis was performed by nonparametric Mann–Whitney test.

4.2.10.1. Knocking down PI3K-C2β in ECs does not alter focal adhesion assembly

Similar to MLEC, we immunostained PI3K-C2β-depleted HUVEC for FA-associated protein – paxillin. While, lipid kinase inactivation in MLEC did not indicate a role of the protein in FA assembly, we wondered if a putative PI3K-C2β scaffolding property might participate in the process. Microscopy-based quantitative analysis revealed that neither FA number nor size change upon PI3K-C2β knock-down, further indicating that FA assembly in ECs does not require PI3K-C2β (Figure 4.2.19. A-C).

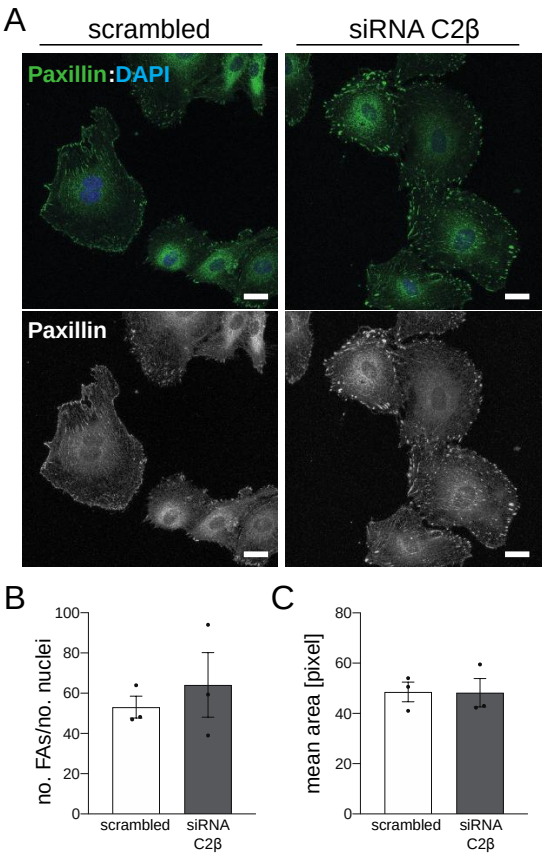

Figure 4. 2. 19. PI3K-C2β knock-down does not affect focal adhesion assembly.
(A) Confocal images of scrambled- and siRNA-C2β-transfected HUVEC immunostained for paxillin and nucleus (DAPI). Scale bar = 20 µm. (B) Quantification of the number and area of focal adhesions. n ≥ 5. Data are presented as mean values. Error bars are s.e.m. Statistical analysis was performed by nonparametric Mann–Whitney test.

4.2.11. Loss of PI3K-C2β expression results in EC enlargement *in vitro*

Intrigued by the previous findings in MLEC on cell size, we wondered whether this could be reproduced in HUVEC upon PI3K-C2β silencing. Indeed, β-catenin immunostaining showed that PI3K-C2β-depleted HUVEC were significantly enlarged compared to scrambled control (Figure 4.2.20. A-B).

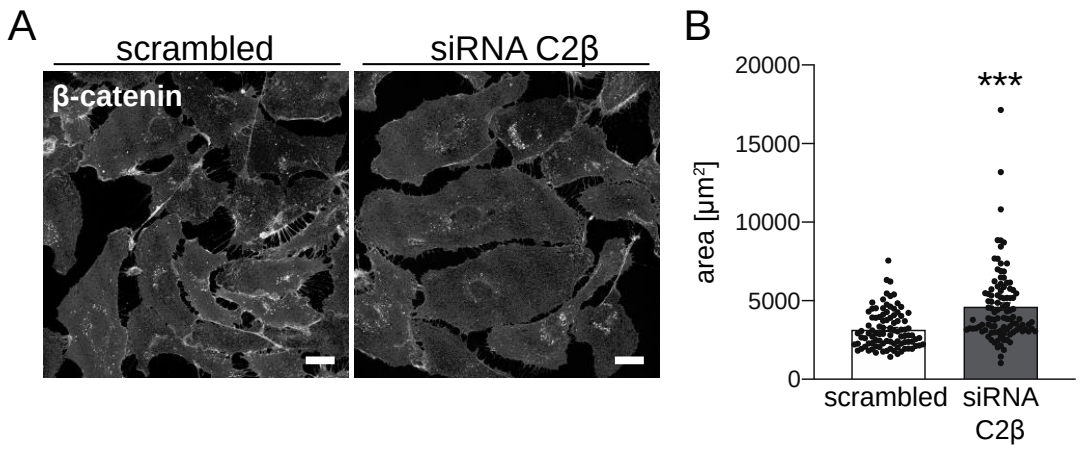

Figure 4. 2. 20. Silencing PI3K-C2β increases endothelial cell area.
(A) Scambled and siRNA-C2β-transfected HUVEC were immunostained for β-catenin, followed by high magnification confocal imaging. Scale bar = 20 µm. (B) Quantification of the cell area. n = 3. Data are presented as mean values. Error bars are s.e.m. Statistical analysis was performed by nonparametric Mann–Whitney test. *p < 0.05, **p < 0.01 and ***p < 0,0001 were considered statistically significant.

4.2.12. Elevated mTORC1 signalling upon PI3K-C2β inactivation during sprouting angiogenesis

These observations together with an elevated phosphorylation of S6 protein upon PI3K-C2β loss of function imply an enhanced mTORC1 activity in ECs. Encouraged by *in vitro* data on signalling and size, we decided to compare p-S6 (both S235/236 and S240/244) between PI3K-C2β$^{WT/WT}$ and PI3K-C2β$^{KI/KI}$ in the *in vivo* retina model. Here, we isolated the retinas on P6 as, based on our previous experience, this time point exhibits the highest peak of PI3K/AKT/mTORC1 activity. Following immunostaining using p-S6-specific antibodies and IB4 staining, we measured the intensity levels of p-S6 within blood vessels in the front of the retinas. We were able to demonstrate, for the first time, that loss of PI3K-C2β activity enhances mTORC1-dependent signalling *in vivo*. S6, the downstream target of mTORC1, showed a significant increase of both phosphorylation sites (Figure 4.2.21. A-D).

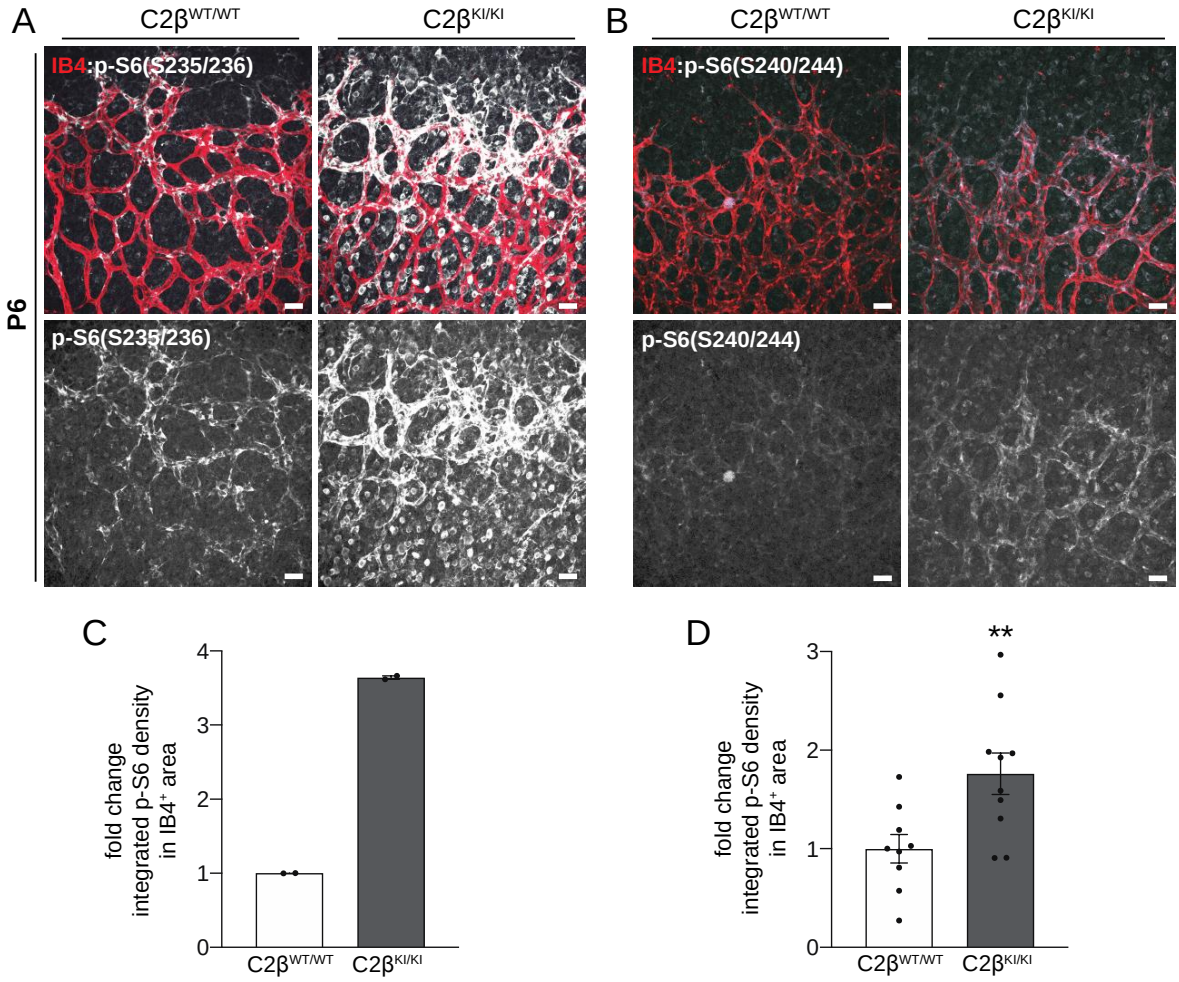

Figure 4. 2. 21. PI3K-C2β controls mTORC1 signalling during angiogenesis.
(A) P6 retinas were isolated from PI3K-C2β$^{WT/WT}$ and PI3K-C2β$^{KI/KI\ mice,}$ followed by immunostaining for p-S6 (S240/244) and p-S6 (S235/236). Blood vessels were visualised by IB4. Scale bar = 30 µm. **(B)** Quantification of p-S6 intensity within the vascular area IB4-positive. n = 2 for p-S6(235/236) and n ≥ 9 for p-S6(240/244). Data are presented as mean values. Error bars are s.e.m. Statistical analysis was performed by nonparametric Mann–Whitney test. *p < 0.05 and **p < 0.01 were considered statistically significant.

4.2.13. Loss of PI3K-C2β kinase activity does not impact on pathological vessel growth in oxygen-induced retinopathy mouse model

Many studies have shown that exposing a mouse model to exogenous stress allows to identify a new, putative role of the protein of interest. Given the phenotype observed in P8 PI3K-C2β$^{KI/KI}$ retinas, we wondered whether PI3K-C2β might participate in either onset and progression or prevention of vascular diseases. For this, we took advantage of the disease model of retinopathy of prematurity (ROP), well established in our laboratory. Although recent advances in the control of oxygen delivery to preterm infants have reduced the number of severe ROP cases, this disease still poses a threat especially in underdeveloped and developing countries. High extrauterine concentration of oxygen leads to cessation of retinal blood vessel growth (vasoregression). This causes an elevation of VEGF-A expression that, consequently,

induces pathological vascular growth (neoangiogenesis), that is characterised by an abnormal, hyperplastic vasculature with neovascular tufts. To recapitulate the disease in mice, we implemented an accelerated oxygen-induced retinopathy (OIR) model. Briefly, P8 pups were exposed to 85% oxygen for 4 days (vasoregression phase), followed by 6 days in normoxia conditions (neovascularisation phase) (Figure 4.2.22. A). Isolated P17 retinas were then immunostained for blood vessels (IB4) and confocal tile-scanning imaging of the whole retina was performed (Figure 4.2.22. B). We quantified two parameters: avascular (IB4-negative) and neovascular area. Our analysis showed that PI3K-C2β kinase inactivation has no impact on retinal vasculature during pathological growth as both measured parameters were unaltered (Figure 4.2.22. C and D).

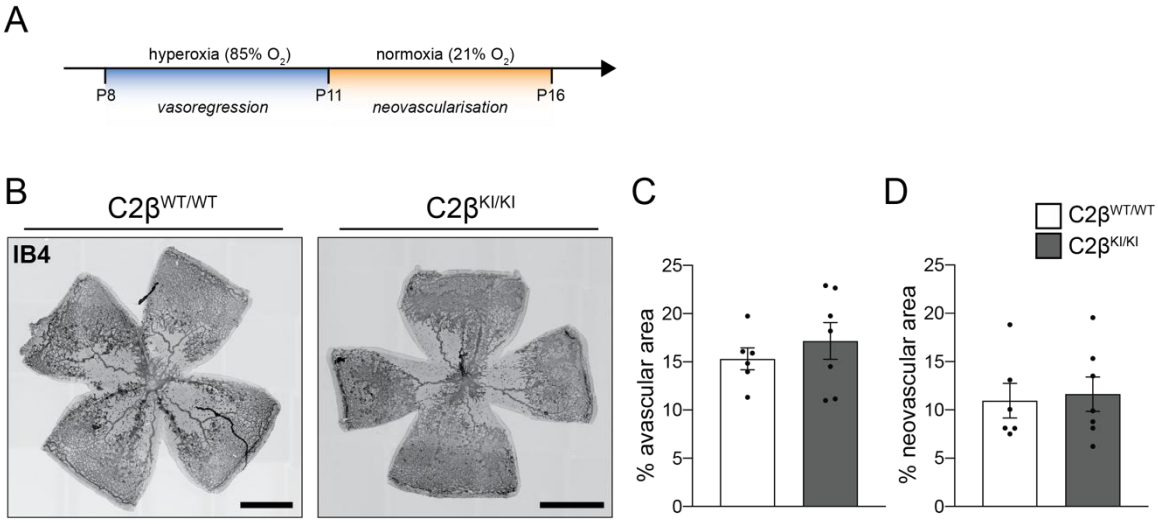

Figure 4. 2. 22. Inactivation of PI3K-C2β does not impact on neovascularisation in the mouse model of retinopathy of prematurity.

(A) Oxygen-induced retinopathy experimental setup. **(B)** P17 retinas from PI3K-C2β$^{WT/WT}$ and PI3K-C2β$^{KI/KI}$ mice were isolated and immunostained with IB4, followed by confocal imaging of the whole retina. Scale bar = 1 mm. **(C)** Quantification of the avascular area per whole retina. **(D)** Quantification of the neovascular area per whole retina. n = 7. Data are presented as mean values. Error bars are s.e.m. Statistical analysis was performed by nonparametric Mann–Whitney test.

CHAPTER 5
Discussion

PI3K signalling has been broadly studied for the last 30 years since it became clear that the pathway plays an important part in pathophysiology of many human diseases. During this exciting discovery period, our knowledge on PI3K signalling has notably extended: from identifying different PI3K isoforms and key components of the signalling pathway to understanding of their basic contribution to tissue development and physiology as well as their role in pathologies. This prompted a rapid advancement in the development of PI3K signalling inhibitors, with many currently being under clinical evaluation. Despite this tremendous progress, we still do not fully understand the organismal importance of certain PI3K isoforms (in particular class II PI3Ks) along with cell-, tissue- and context-specific outcomes of the pathway activation [49].

Previous studies have cemented the crucial position of PI3K signalling in controlling EC behaviour during blood vessel growth. Among eight PI3K isoforms, only two are essential for proper cardiovascular development: class I PI3Kα and class II PI3K-C2α. EC-specific depletion of either of them results in lethality during early-stage mouse embryonic development as a consequence of severe defects in blood vessel growth.

Recently, cancer-associated mutations in PI3Kα-encoding gene have been detected in ECs and are responsible for the onset of vascular lesions such as VMs and LMs. These mutations were also detected in vascular malformations associated with some overgrowth syndromes (CLOVES or Klippel–Trenaunay), collectively known as *PIK3CA*-Related Overgrowth Spectrum (PROS). While researchers have identified, to some extent, the genetic cause of these pathologies, there is still a lack of extensive knowledge on the mechanism of action. In particular, when and how activation of PI3K signalling in the endothelium leads to vascular lesion formation and what are the phenotypic consequences of different somatic mutations in *PIK3CA* gene. Despite the progress in the field, there are no approved pharmacological therapies for these diseases to date, and the existing treatment is insufficient or not applicable in most cases. Moreover, the complexity of vascular overgrowth diseases makes it difficult to model in laboratories, therefore hampering clinical research.

Here, we develop an *in vivo* system, through genetic activation of *Pik3ca* gene in a cell- and a dose-specific (limited number of targeted ECs) manner and we show that it

could serve as a tool in preclinical drug testing. Moreover, we demonstrate for the first time that AKT constitutes a promising drug target for prevention and treatment of *Pik3ca*-driven vascular malformations. We will further discuss the advantages and limitations of the mouse model as well as clinical benefits and restrictions to consider when targeting AKT in the treatment of vascular lesions (see section 5.1).

Both PI3Kα and PI3K-C2α generate distinct pool of phospholipids that regulate EC response through different molecular mechanisms. While some of the remaining isoforms are not expressed in ECs (PI3Kγ and PI3K-C2γ), the role of the others emerges upon specific stress factors as shown for PI3Kβ [139] and PI3Kδ [140]. The endothelial functions of class II PI3K-C2β and class III Vps34 remain elusive and call for further investigation.

In this study, we sought to determine the physiological role of PI3K-C2β during angiogenic growth, with a particular focus on endothelial cell compartment. We demonstrate for the first time that PI3K-C2β regulates retinal vascularity and vessel width, most likely through mTORC1. Moreover, we show that PI3K-C2β is highly expressed in pericytes, therefore shedding light on these cells as putative key players in PI3K-C2β-regulated vessel growth. We will discuss these and other observations in section 5.2.

5.1. Objective 1: Antiangiogenic properties of miransertib

5.1.1. Modelling *Pik3ca*-driven vascular malformations in mice

Since the discovery that somatic activating mutations (E542K, E545K, H1047R and H1047L) in *PIK3CA* gene occur in ECs and give rise to vascular lesions of lymphatic and venous origin, several mouse models were developed in order to study the mechanisms behind these pathologies [109]. These models were also shown to be useful for preclinical drug testing. In our studies, we took advantage of the previously developed Cre^{ERT2}-dependent conditional mouse model in which a single $Pik3ca^{H1047R}$ allele is specifically expressed in ECs [108]. Previous study showed that a single high dose of 4-OHT promoted EC hyperproliferation that led to a massive vascular hyperplasia in the retina, resulting in loss of vascular architecture and both arterial and venous markers expression. The phenotype does not fully reflect *PIK3CA*-driven vascular malformation features since they lack their "isolated" character. VMs, when not associated with overgrowth syndromes, arise as isolated lesions that can present in any part of the body. To better model the disease, we decided to use a 20-fold lower dose of 4-OHT to induce Cre-mediated recombination. This allowed us to target fewer ECs that give rise to isolated lesions within veins and venules as well as capillaries. The lack of vascular lesions in arteries and arterioles was consistent with previous findings in humans [107-108]. This model offers a number of advantages over existing mouse systems.

First, it captures the genetic etiology of those diseases, in which hotspot *PIK3CA* mutations occur somatically in a single cell lineage (mesoderm- ECs derived) and display clonality. Importantly, in our model the $Pik3ca^{H1047R}$ allele is expressed under its

endogenous promoter, therefore is regulated by intrinsically. This is in contrast to the other mouse model in which *Pik3ca*^{H1047R} allele was expressed in a mosaic fashion under the embryonic T promoter [108]. This promoter is highly active in the primitive streak and bud tail of the embryo that together can generate all three germ layers [141]. Although these mice mostly develop vascular malformations (of venous origin) of different severity and location, the overall robustness of this model appears questionable. This is due to high heterogeneity of the phenotype together with increased mortality events that affect both reproducibility and application for preclinical studies. Second, in comparison to our system, other common mouse models of vascular malformations were created by either the introduction of viral oncogenes (such as polyomavirus middle T antigen) [142] or xenotransplantation of immortalised or patient-derived ECs expressing a mutated variant of the gene (e.g. *PIK3CA* and *TIE2*) [143]. However, both models do not mirror the genetic origin of vascular lesions and the impact of mutated genes on natural disease progression. Moreover, the xenograft models are oversimplified and the laborious multistep process (including cell isolation and manipulation, implantation into mice and *in vivo* growth) demands advanced technical experience and time, both of which can affect research reproducibility.

We chose the postnatal retina model, a unique system for studying mammalian blood vessel development and vessel pathology [144]. Indeed, mouse retinas are being widely used in the field, mostly due to their simplicity, high reproducibility and research reliability. Our model allows to study the impact of endothelial *Pik3ca* hyperactivation on lesion initiation, disease dynamism and progression as well as clonality. It also constitutes a convenient tool for rapid testing of potentially anti-angiogenic drugs and offers an alternative to other *in vivo* systems that well model the disease [128,145].

Like with many research models, also our presents certain limitations. First, it does not properly mirror the tissue complexity and heterogeneity of the disease as we only analyse retinal vasculature. Although *PIK3CA* mutations are present in ECs, the role of other cells (e.g. adipocytes, mural and immune cells) in the development and progression of vascular malformations is yet to be determined. ECs indeed were shown to control the physiology of other tissues and organs, such as muscles, brain or liver [146-148]. It is likely then that they contribute to the disease through different ways, including modulation of inflammation and tissue remodelling. Second, vascular lesions (either isolated or associated with syndromes) rarely occur in the retina. Although our studies mainly address the impact of EC-specific *Pik3ca*^{H1047R} expression on developmental retinal angiogenesis, we cannot ignore the fact that most of the vascular lesions appear in other tissues (skin, adipose and muscular tissue).

5.1.2. Aiming at AKT – a novel target in a therapy of vascular malformations

Hyperactivation of the three AKT isoforms has long been seen in malignant diseases such as cancer. This could either result from direct *AKT* genes alterations (such as mutations or amplifications) or modifications of upstream AKT regulators, including PI3K gain of function mutations, loss of PTEN activity as well as activating mutations in cell

receptors (RTKs, GPCR or integrins) and Ras kinase [132]. Overactive AKT has also been shown in some non-malignant diseases: *TIE2*- and *PIK3CA*-driven vascular lesions, PROS and PHTS syndromes [149]. Moreover, somatic activating mutation in *AKT1* gene is the leading cause of Proteus syndrome, a rare overgrowth disease [113]. Therefore, it appears clear that targeting AKT could potentially bring clinical benefits in the treatment of these diseases.

While anticancer properties of AKT inhibitors received a lot of attention in the last decade, their anti-angiogenic potential in the context of vascular lesions has never been studied before. Using the mouse retina model of *Pik3ca*^{H1047R}-driven vascular malformations, we show for the first time that blocking AKT with an allosteric pan-AKT inhibitor miransertib successfully prevents and treats vascular anomalies. This is very important from the clinical perspective since none of the previously reported inhibitors (against mTORC1 and PI3Kα) has been approved for the treatment so far. Previous preclinical studies showed that formation of *Pik3ca*-driven vascular lesions could be prevented by rapamycin, but upon treatment cessation the lesion growth recurrence was observed [108,145]. Similar conclusions were drawn from phase I and II clinical trials in patients with venous malformations of different types: daily low doses of rapamycin improved the quality of life by reducing pain and bleeding events, but unfortunately were unable to fully eradicate the lesions [150]. Moreover, rapamycin and its analogues are known immunosuppressants, therefore their continuous applications pose a risk of secondary infections and unexpected toxicity. In parallel, PI3Kα-specific inhibitor alpelisib showed impressive efficacy in the treatment of overgrowth-related vascular abnormalities in preclinical and clinical studies, with relatively few side effects observed [128]. This is most likely due to low doses applied in the study, compared to relatively high doses used in the treatment of cancer [151-152]. Despite these promising preliminary results, more preclinical and clinical studies on a bigger cohort of patients are needed. Our *in vitro* data in *Pik3ca*$^{H1047R/WT}$ ECs demonstrated an enhanced antiproliferative capacity of miransertib compared to rapamycin, thus indicating that AKT inhibition might have stronger therapeutic potential in the treatment of vascular lesions. It would be interesting to juxtapose miransertib with other PI3K signalling inhibitors, such as alpelisib, to compare their impact on *Pik3ca*$^{H1047R/WT}$ EC signalling and proliferation.

Activation of AKT in some diseases might be used as a predictor of response to AKT inhibitors and render their application a first-line therapy. Proteus syndrome, a highly mortal disease primarily caused by somatic gain-of-function mutation in *AKT1*, constitutes a good example of such personalised approach. Initial trials with diseased individuals corroborated that miransertib efficiently inhibited AKT hyperactivation by reducing its phosphorylation and, in consequence, led to significant overall improvement of patients' health and everyday life [137-138,153-154]. It would be important to test the impact of AKT inhibition on vascular lesions often associated with the syndrome. Based on our data, it is tempting to speculate that miransertib could help in the treatment of vascular anomalies. Currently, a larger cohort of Proteus patients is being enrolled in a phase I miransertib dose finding trial (NCT02594215).

A big challenge for clinicians is to establish optimal dosing schemes that show maximal clinical benefits with minimal toxicity and adverse effects. It is even more problematic as vascular malformations and related diseases occur both in children and adults that differ in tolerance and response to therapy. In our studies we used two different doses of miransertib, referred to as high (75 mg/kg) and low (35 mg/kg). Although previous reports demonstrated good tolerability and relatively low toxicity of the high dose in endometrial cancer mouse model [155], it is crucial to investigate the safety of miransertib in patients. Moreover, comparative studies using different types of AKT inhibitors in distinct disease contexts (including vascular lesions) are needed to select those of high efficiency and safety.

The heterogeneity of a genetic landscape of vascular malformations questions the use of a single agent for the treatment of these diseases. Moreover, an emerging problem of drug resistance requires constant search for new therapeutics and/or drug combinations. Although no studies on vascular malformation resistance to treatment have been performed yet, combination of rapamycin with the ABL kinase inhibitor ponatinib was shown to improve the therapeutic benefit in a preclinical mouse model of venous malformations [156]. Testing possible combinations of inhibitors and other available treatment options, especially in difficult and rare cases, could significantly improve the clinical management of these diseases. Our *in vivo* data suggest that miransertib could be used postsurgically as a preventive measure in order to block regrowth of the vascular lesions.

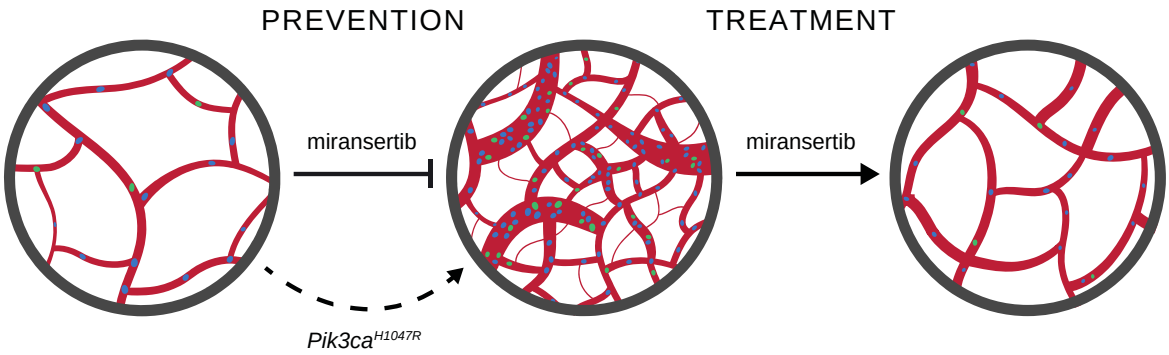

Figure 5. 1. Schematic representation of anti-angiogenic activity of miransertib in *Pik3ca*-driven vascular malformations mouse model.

Our study demonstrated that miransertib at high (75 mg/kg) and low (35 mg/kg) doses effectively prevents the formation of *Pik3ca*^{H1047R}-driven vascular malformation in the mouse retina model. Furthermore, miransertib showed high efficacy in regression of already developed vascular lesions, thus provided an explicit rationale for the therapeutic application of miransertib in the treatment of vascular malformations. Blue dots represent EC nuclei. Green dots represent proliferative ECs.

5.1.3. Future studies

There are certain remaining and open questions that, due to time limitations, could not be studied within this work. Here, we would like to discuss the most important

ones. It would be critical to further explore the proposed *Pik3ca*-driven vascular malformation mouse model. In particular, transcriptional and signalling alterations could provide missing and crucial information. Indeed, transcriptome screening allowed identification of specific gene signatures in both HHT and vascular Ehlers-Danlos syndrome mouse models [157-158]. The outcomes of these studies might provide a rationale for therapeutic application of certain combinations of inhibitors. Moreover, signalling changes in fixed tissues are difficult to detect by immunohistochemistry and require a number of reliable phosphoprotein-specific antibodies. So far, there are no functional p-AKT-specific antibodies available for immunofluorescence, thus we could not analyse AKT activity in the retina model. These limitations could be largely omitted with the help of genomics and proteomics, such as RNA sequencing and phosphoproteomic analyses, respectively. Although such studies still require high financial expenses, the annual drop of sequencing and mass-spectrometry costs makes this type of analyses more and more feasible to perform.

Despite promising data on miransertib in the retina model, we have not tested the impact of low dose (35 mg/kg) in vascular regression experimental settings. Moreover, we would like to investigate whether withdrawal of the inhibitor leads to vascular lesion regrowth at a later time point as it was observed in the case of rapamycin [108]. In addition, it would be critical to assess miransertib treatment efficacy at later developmental stages (when developmental angiogenesis does not take place anymore), that could partially mirror the disease in adults.

Last but not least, incorporating human samples would strengthen the clinical applicability of miransertib. For this, we would like to use freshly isolated ECs derived from vascular lesions of patients carrying *PIK3CA* and *TEK* hotspot mutations and study the impact of miransertib on viability and signalling of these cells.

5.2. Objective 2: Deciphering the vascular function of PI3K-C2β

5.2.1. The crosstalk between PI3K-C2β and mTORC1

3-phosphoinositides play a vital role in the regulation of EC function during vessel growth. They control EC migration and rearrangement, proliferation and vessel stability, but also the metabolic adaptation to environmental changes. Although ECs express most of the PI3K isoforms, they are strictly dependent on two: class I PI3Kα and class II PI3K-C2α. It remains unknown what stands behind PI3K isoform selectivity, but recent findings provide evidence that other isoforms notably contribute to blood vessel growth in a context-dependent and an EC-extrinsic manner [91].

The vascular function of class II PI3K-C2β is still unexplored, although it is ubiquitously expressed. Unlike PI3K-C2α, loss of PI3K-C2β does not result in an overt vascular phenotype during development [159]. Moreover, it remains elusive why ECs show preference to PI3K-C2α over PI3K-C2β despite the fact that both isoforms generate the same lipidic product. Here, we have used the retina model to address whether PI3K-C2β play any role in angiogenesis. The rational of our choice is that mouse

retina is a highly sensitive angiogenesis model that allows to investigate in a spatiotemporal manner whether a specific gene expression product is relevant for vascular development. The main caveat of the model is that a putative phenotype tends to resolve over time as a result of compensation mechanisms. However, the fact that it is easy to work with and to study cell behaviour at high resolution makes it an ideal system for this purpose. By using mouse retina, we identified previously unspotted vascular role of PI3K-C2β. Its global kinase inactivation results in hyperplasia in frontal retina vasculature, most likely as a consequence of vessel enlargement. Critically, blood vessels exhibit higher p-S6 levels upon loss of PI3K-C2β catalytic function, suggesting an upregulated mTORC1 activity. Criticaly, this is the first *in vivo* evidence PI3K-C2β regulates mTORC1 activity. This result was reproduced in *in vitro* signalling assays in primary mouse and human ECs. Interestingly, loss of PI3K-C2β resulted in an increased size of ECs *in vitro*, which is consistent with elevated mTORC1 signalling in these cells. Our observations are in agreement with previously identified effects of PI3K-C2β on mTORC1 activity. Studies in HeLa and HEK293T cells showed that starvation-induced local (late endosome/lysosome) synthesis of $PI(3,4)P_2$ by PI3K-C2β represses mTORC1 signalling by facilitating association of Raptor with inhibitory 14-3-3 proteins. Conversely, both PI3K-C2β knockout or kinase inactivation hyperactivate mTORC1. PI3K-C2β-depleted cells were also significantly enlarged as measured by fluorescence-activated cell sorting (FACS), further supporting our results [74]. Interestingly, under normal conditions PI3K-C2β was shown to be phosphorylated and suppressed by PKN2 kinase downstream of mTORC2 [160]. We postulate that the vascular hyperplasia and the vessel enlargement in the sprouting front of PI3K-C2β$^{KI/KI}$ retinas (with no differences in EC proliferation) are the consequences of elevated mTORC1 signalling. In order to prove it, it would be essential to perform a rescue experiment using mTORC1-specific inhibitor such as rapamycin. Moreover, the *in vitro* data suggest that there is a correlation between mTORC1 activity and EC size, but this phenomenon has never been studied *in vivo*. To investigate this in more details, EC shape and size analyses are necessary. This could be achieved by using a double fluorescent (mTmG) Cre-mediated reporter mouse model with EC-specific Cre^{ERT2} expression [88,161]. These data are interesting as they would suggest that cell growth precedes cell proliferation during sprouting angiogenesis. This is known in other physiological systems such as in germinal centre during B cell selection and clonal expansion: mTORC1 signalling first promotes cell growth, followed by cell proliferation only after these cells have reached a certain size [162]. How does mTORC1 coordinate endothelial cells growth and proliferation remains unknown. Further investigation will quite likely require life imaging.

It is important to highlight that the observed phenotype is temporal and resolves in time. This suggests that perhaps PI3K-C2β regulates mTORC1 activity under specific conditions. Given that mTORC1 can be activated by nutrients [163], it would be interesting to study how nutrient-deprivation affects vessel growth in PI3K-C2β$^{KI/KI}$ mice. Moreover, although we have only examined retina tissues, it is likely that other vascular beds behave differently. For this reason, the role of PI3K-C2β in the vasculature of other organs should be analysed to draw more general conclusions. To recapitulate, our observations in ECs and the retina model corroborate previously characterised role of

PI3K-C2β in mTORC1 regulation, but also identify for the first time a consequence of PI3K-C2β inactivation on the vascular system development.

Angiogenesis is a metabolically demanding process and it requires a proper fine-tuning of EC metabolism. During blood vessel growth, ECs need energy and nutrients for migration and biomass synthesis [164]. mTOR (associated with complexes I and II), one of the key metabolites sensors, integrates hypoxia, nutrient and cellular energy status to control cell growth and angiogenesis [165]. Curiously, the specific function of mTORC1 during developmental angiogenesis has been rather poorly addressed. EC-specific Tsc1 loss of function in mice results in mTORC1 hyperactivation and is embryonic lethal due to multiple and severe vascular defects [166]. Interestingly, studies in postnatal mouse retinas revealed that EC-specific Tsc1 deletion promotes retina vascularity and EC proliferation [167]. These findings are in line with the observations in PI3K-C2β$^{KI/KI}$ retinas, although in our studies this phenotype appears to be EC proliferation-independent. mTORC1 hyperactivation was also observed in EC-specific DEPTOR-deficient mice but, on the contrary, was not fatal. Instead, overexpression of VEGF-A and HIF-1α and consequent accelerated angiogenesis in different organs were observed [99]. Despite its crucial vascular role, the physiological functions of mTOR (in particular mTORC1) during vessel growth have not been well studied. Specifically, the degree of mTORC1 activity during angiogenesis and its correlation with EC behaviour and morphology remains ambiguous.

5.2.2. PI3K-C2β beyond ECs

One of the limitations of the presented work is that the mouse model used to study PI3K-C2β function *in vivo* lacks cell-specificity. Kinase-deficient PI3K-C2β, generated by introducing a germline point mutation (D1212A) in the protein's kinase domain, is expressed in all body cells. Although the model showed an advantage in identifying novel systemic role of PI3K-C2β [75], it still remains challenging to determine its cell-autonomous functions. On the other hand, a global inactivation of PI3K-C2β allows to address the role of this isoform beyond one cell type. Blood vessels encompass not only ECs, but also closely attached mural cells (vSMCs and PCs) that play a key role in vessel growth, maturation and function. In our studies, we found that P8 PI3K-C2β$^{KI/KI}$ retinas exhibit altered PC morphology, despite no overt differences in blood vessel coverage. While in wild-type mice PCs are mostly elongated with only few protrusions, PI3K-C2β-inactive PCs appear spiky, with many more protrusions standing out from the cell body. Moreover, we showed that cultured primary brain PCs express higher levels of *Pik3c2b* mRNA compared to lung ECs. Together, this promted us to speculate that PI3K-C2β is quite likely required for PC function and its inactivation might result in temporarily altered vasculature. Previous studies showed that class I PI3K isoforms regulate angiogenesis in a cell-selective manner. Whereas PI3Kα is indispensable for ECs, it does not regulate PC biology. On the contrary, PI3Kβ functionally dominates in PCs while it is not required for ECs during angiogenesis [87,91]. Based on the maturation stage, two distinct subtypes of PCs were identified that correlated with their morphology and

PI3K/AKT/mTORC1 activity – immature (stellated and high PI3K signalling) and mature (elongated and low PI3K signalling) wild-type PCs [91]. Curiously, PI3K-C2β$^{KI/KI}$ spiky PCs morphologically resemble immature wild-type PCs. This hypothesis is further strengthened by elevated mTORC1 activity (as measured by p-S6 levels) in the frontal vasculature of PI3K-C2β$^{KI/KI}$ retinas. However, more detailed experiments are needed in order to verify whether enhanced mTORC1 signalling is related to ECs or PCs (or both). Moreover, to confirm our findings it would be necessary to measure PC morphological alterations in PI3K-C2β$^{WT/WT}$ and PI3K-C2β$^{KI/KI}$ retina preparations by using PC-specific mTmG reporter mouse model [91,168].

Furthermore, using publicly available RNA sequencing dataset obtained from immature (P3) and mature (P9) pericytes [91], we have found that the expression of *Pik3c2b* drops significantly on P9 compared to P3 (data not shown). Interestingly, we did not find any changes in *Pik3c2a* gene expression (encoding PI3K-C2α). It is still not very clear to us what the differences *Pik3c2b* expression pattern in immature vs. mature PCs mean. Based on the notion that PI3K/AKT/mTORC1 signalling is higher in immature pericytes and that PI3K-C2β inhibits mTORC1, we expected to identify reduced levels of *Pik3c2b* mRNA at P3. The observation that the levels are higher at P3 might simply indicate that a fine regulation of mTORC1 activity is required and this is achieved, at least partially, through PI3K-C2β. This allows us to speculate that perhaps PI3K-C2β is more important in PC biology and function than we previously anticipated.

Nevertheless, it remains unclear how PI3K-C2β would regulate PCs and thus the vasculature. One possible way is through modulation of PC contractility. Indeed, many factors, including vasodilating and vasoconstricting agents (e.g. NO and endothelin-1, respectively) were shown to stimulate and induce PC responses *in vitro* [169]. It has also been demonstrated that contractile PCs regulate blood flow and vessel diameter in brain [170] and pancreatic capillaries [171]. Although the rescue experiment with eNOS inhibitor ruled out enhanced NO-mediated vasodilation in PI3K-C2β$^{KI/KI}$ retinal vasculature, we cannot exclude other possible mechanisms of vessel enlargement. Studies using primary PCs isolated from PI3K-C2β$^{WT/WT}$ and PI3K-C2β$^{KI/KI}$ mice are needed to corroborate the putative function of this isoform in PC biology. Since class II PI3Ks participate in vesicle traffic and exocytosis [172], it would be interesting to perform an unbiased analysis of cell secretome of cultured ECs and PCs and its possible regulation by PI3K-C2β. This would help in identifying new molecular players that could explain the phenotype observed in mouse retinas. Additionally, *in vivo* blood flow assessment using two-photon microscopy would be useful in verifying whether alteration in PC morphology translates into blood vessel functions.

5.2.3. PI3K-C2β and cell migration

PI3K-C2β has already been reported to control cellular migration in some cell types, although the molecular mechanism behind this regulation and its significance at organismal level remain unexplored. The picture gets more complicated when taking into account kinase-dependent and kinase-independent functions of PI3K-C2β. Indeed,

while some studies pointed at lipid-mediated regulation of cell migration, others showed that PI3K-C2β can also associate with other protein complexes and effect actin cytoskeleton, cell morphology and in consequence migration [77-79, 105]. Moreover, PI3K-C2β isoform was shown to mediate EC migration upon stimulation with S1P and HDL [104]. Curiously, another class II PI3K isoform – PI3K-C2α – is also required for S1P-induced EC migration and FA formation [80]. These observations suggest overlapping functions of both class II PI3Ks, which could arise from the fact that both isoforms generate the same phospholipid products – PI(3)P and PI(3,4)P_2. Within this work, we aimed to identify the impact of PI3K-C2β kinase-dependent as well kinase-independent functions on collective EC migration and FA assembly using PI3K-C2β kinase-deficient MLEC and PI3K-C2β-depleted HUVEC, respectively. In both cases, PI3K-C2β did not affect collective cell migration, which was in contrary to previous observations in other cell lines. Similarly, we did not notice differences in focal adhesion assembly as suggested by others (unpublished data). One possible explanation, which at the same time constitutes an omission in our studies, is that we examined the cell behavior only under basal conditions. Given that in PI3K-C2β-depleted HUVEC we observed starvation- and VEGF-A-induced elevated mTORC1 signalling, it is tempting to speculate that perhaps under such conditions these cells exhibit a certain migratory advantage. Indeed, studies in different cell lines demonstrated that genetic and pharmacological inhibition of mTORC1 hampers actin cytoskeleton reorganisation and cell migration in a RhoA-dependent manner [173]. Interestingly, PI3K-C2β interaction with Dbl was shown to modulate RhoA activity, and consequently cell morphology and actin rearrangement [174]. Independently, hyperactivation of mTORC1 through EC-specific Tsc1 loss of function led to accelerated EC collective migration, proliferation and tubulogenesis *in vitro*, thus clearly suggesting that enhanced mTORC1 signalling results in an activation of ECs [162]. Although our data seem to contradict previous observations, we cannot exclude the important role of the cellular context. Perhaps, starving and/or challenging the cells with different stimuli would lead to identification of a particular condition under which PI3K-C2β influence EC collective migration and FA assembly, both essential during angiogenesis. On the other hand, we have not observed clear migration defects in the retina model, which could be noticed if the process was significantly altered in a mutant mouse (as in the case of PI3Kα). This could imply that perhaps PI3K-C2β is not essential for EC migration during sprouting angiogenesis and its temporary impact on mTORC1 signalling might be compensated by PI3K-C2α.

5.2.4. PI3K-C2β in vascular diseases

Unlike class I PI3Ks, class II isoforms have not been yet confirmed to contribute to human diseases. Moreover, despite the indispensable role of PI3K-C2α in blood vessel development, there are no associations between PI3K-C2α and vascular-related diseases. Interestingly, recent studies on PI3K-C2β in mice showed that its loss of function effectively protects from high-fat-diet-induced liver steatosis [75] and myotubular myopathy [175]. Furthermore, downregulation of PI3K-C2β reduced cell

invasion *in vitro* in prostate and breast cancer cells as well as breast cancer metastasis *in vivo* [176-177]. These results offer new therapeutic opportunities and explore the possibility of targeting PI3K-C2β in human diseases. Nevertheless, the clinical significance of these findings remains to be determined.

In this study, we aimed to identify a vascular pathological condition in which PI3K-C2β could be involved. For this, we chose a well-established oxygen-induced retinopathy (OIR) model that resembles retinopathy of prematurity (ROP). ECs response to VEGF-A is critical for the progression of pathological neoangiogenesis and reduced response to VEGF-A was shown to inhibit aberrant blood vessel formation associated with ROP [178]. Our previous results in both retinas and cells led us to hypothesise that PI3K-C2β loss of function could impact the pathological vessel growth during a VEGF-A-dependent phase of neovascularisation. Although our results do not support that hypothesis, we cannot completely rule out the possibility that perhaps an incorrect mouse model has been used in the study. Neoangiogenesis in OIR model occurs from P11 onwards [179] and we observed that the phenotype of PI3K-C2β$^{KI/KI}$ resolves in time and is not present on P14 (**data not shown**). Perhaps, inactivating PI3K-C2β at the onset of neoangiogenesis could help to better understand the putative role of PI3K-C2β in ROP. Unfortunately, such an approach could only be feasible with an inducible knock-out/knock-in mouse model.

Molecular dissection of many vascular-associated diseases constitutes a great challenge. Given the potential role of PI3K-C2β during physiological angiogenesis, it would be interesting to investigate the role of PI3K-C2β in development of other vascular-related pathologies. The association of vascular PI3K-C2β with mTORC1 activity as well as the putative function in PC biology let us speculate that perhaps PI3K-C2β could be involved (at least partially) in the development and progression of atherosclerosis. Indeed, studies in preclinical animal models showed preventative properties of mTORC1 inhibitors in atherosclerotic plaque formation, highlighting the importance of mTORC1-dependent signalling in pathoetiology of atherosclerosis [180]. Moreover, pathological neoangiogenesis and altered mural cell functions can favor the progression and the negative outcomes of the disease [181-182]. An existing ApoE-deficient mouse model, prone to development of atherosclerosis upon high-cholesterol diet, could be therefore crossed with PI3K-C2β kinase-dead mouse to verify the impact of class II PI3K-C2β isoform on this vascular disease. Previous studies showed that such approach can identify a novel, previously undescribed role of a particular protein in disease's pathogenesis [183].

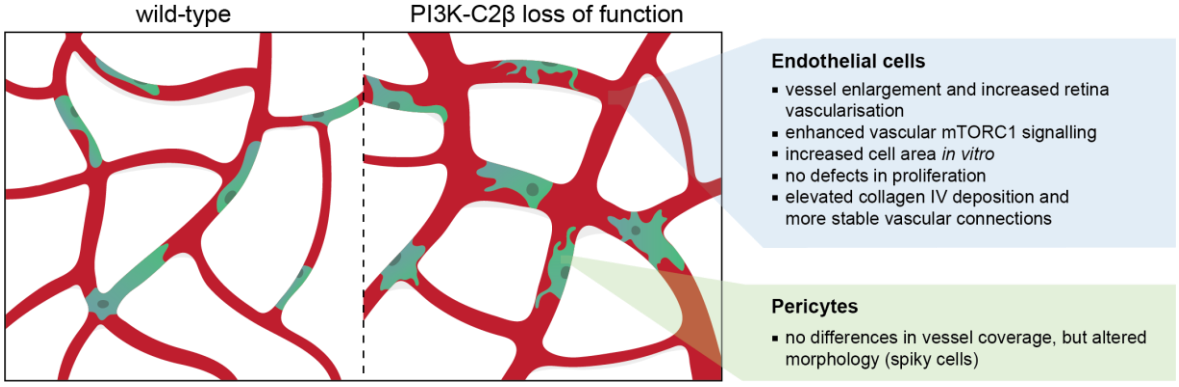

Figure 5. 2. Schematic summary of the findings on the vascular role of PI3K-C2β.
A list of phenotypic alterations found in the retinal vasculature (both in endothelium and pericytes) upon PI3K-C2β loss of function.

5.2.5. Concluding remarks

Vascular development during a process of angiogenesis requires tight regulation on many levels, both molecular and cellular. Over the past years we learnt that during this process ECs dynamically adapt to fluctuations in phosphoinositides generated by PI3K isoforms. In this study we identify a new molecular player, namely class II PI3K-C2β, that impacts on EC growth and thus blood vessel formation. Using mouse retina model, we provide the first *in vivo* evidence that PI3K-C2β negatively regulates vascular mTORC1 signalling, which could explain a consequent vascular enlargement and hyperplasia. This also highlights that endothelial mTORC1 activity might be regulated at multiple levels during sprouting angiogenesis. Although our studies primarily focus on ECs, we cannot rule out the possibility that the observed vascular phenotype is, at least partially, a result of morphological (and thus functional) changes in mural cells such as PCs. Our observations in developmental role of PI3K-C2β open a new path in the vascular research field that could be further explored in pathological contexts.

CHAPTER 6
Conclusions

Objective 1

1. Lowering the dose of 4-hydroxytamoxifen allowed to better model the etiology of *Pik3ca*^{H1047R}-driven vascular malformations in mice.
2. Miransertib exhibits stronger cytotoxic effects on *Pik3ca*^{H1047R} ECs compared to rapamycin.
3. Miransertib prevents the formation and regresses *Pik3ca*^{H1047R}-driven vascular malformations in the preclinical mouse retina model.

Objective 2

1. Loss of PI3K-C2β kinase activity results in vascular hyperplasia during angiogenesis as a consequence of vessel enlargement.
2. PI3K-C2β does not regulate EC proliferation nor migration, but its loss of function results in increased cell size *in vitro*.
3. PI3K-C2β negatively regulates mTORC1 signalling in endothelial cells *in vitro* and *in vivo*.
4. Vascular response upon hyperoxia in the retina is not affected by loss of PI3K-C2β activity.

References

[1] P. Carmeliet, "Angiogenesis in health and disease," *Nat. Med.*, vol. 9, no. 6, pp. 653–660, 2003, doi: 10.1016/S0306-3623(01)00111-2.

[2] M. Potente and T. Mäkinen, "Vascular heterogeneity and specialization in development and disease," *Nature Reviews Molecular Cell Biology*, vol. 18, no. 8. Nature Publishing Group, pp. 477–494, 01-Aug-2017, doi: 10.1038/nrm.2017.36.

[3] A. Plein, A. Fantin, L. Denti, J. W. Pollard, and C. Ruhrberg, "Erythro-myeloid progenitors contribute endothelial cells to blood vessels," *Nature*, vol. 562, no. 7726, pp. 223–228, Oct. 2018, doi: 10.1038/s41586-018-0552-x.

[4] W. De Spiegelaere *et al.*, "Intussusceptive angiogenesis: A biologically relevant form of angiogenesis," *J. Vasc. Res.*, vol. 49, no. 5, pp. 390–404, 2012, doi: 10.1159/000338278.

[5] S. J. Mentzer and M. A. Konerding, "Intussusceptive angiogenesis: Expansion and remodeling of microvascular networks," *Angiogenesis*, vol. 17, no. 3, pp. 499–509, 2014, doi: 10.1007/s10456-014-9428-3.

[6] M. Potente, H. Gerhardt, and P. Carmeliet, "Basic and therapeutic aspects of angiogenesis," *Cell*, vol. 146, 2011, doi: 10.1016/j.cell.2011.08.039.

[7] S. P. Herbert and D. Y. R. Stainier, "Molecular control of endothelial cell behaviour during blood vessel morphogenesis," *Nat. Rev. Mol. Cell Biol.*, vol. 12, no. 9, pp. 551–564, 2011, doi: 10.1038/nrm3176.

[8] L. K. Phng and H. Gerhardt, "Angiogenesis: A Team Effort Coordinated by Notch," *Dev. Cell*, vol. 16, no. 2, pp. 196–208, 2009, doi: 10.1016/j.devcel.2009.01.015.

[9] R. Blanco and H. Gerhardt, "VEGF and Notch in tip and stalk cell selection.," *Cold Spring Harb. Perspect. Med.*, vol. 3, no. 1, p. a006569, Jan. 2013, doi: 10.1101/cshperspect.a006569.

[10] J. D. Leslie, L. Ariza-McNaughton, A. L. Bermange, R. McAdow, S. L. Johnson, and J. Lewis, "Endothelial signalling by the Notch ligand Delta-like 4 restricts angiogenesis," *Development*, vol. 134, no. 5, pp. 839–844, 2007, doi: 10.1242/dev.003244.

[11] M. Hellström *et al.*, "Dll4 signalling through Notch1 regulates formation of tip cells during angiogenesis," *Nature*, vol. 445, no. 7129, pp. 776–780, 2007, doi: 10.1038/nature05571.

[12] S. Suchting *et al.*, "The Notch ligand Delta-like 4 negatively regulates endothelial tip cell formation and vessel branching," *Proc. Natl. Acad. Sci. U. S. A.*, vol. 104, no. 9, pp. 3225–3230, 2007.

[13] L. Jakobsson *et al.*, "Endothelial cells dynamically compete for the tip cell position during angiogenic sprouting," *Nat. Cell Biol.*, vol. 12, no. 10, pp. 943–953, 2010, doi: 10.1038/ncb2103.

[14] L. K. Phng *et al.*, "Nrarp Coordinates Endothelial Notch and Wnt Signaling to Control Vessel Density in Angiogenesis," *Dev. Cell*, vol. 16, no. 1, pp. 70–82, 2009, doi: 10.1016/j.devcel.2008.12.009.

[15] K. Bentley *et al.*, "The role of differential VE-cadherin dynamics in cell rearrangement during angiogenesis," *Nat. Cell Biol.*, vol. 16, no. 4, pp. 309–321, 2014, doi: 10.1038/ncb2926.

[16] A. Lenard *et al.*, "Endothelial Cell Self-fusion during Vascular Pruning," *PLoS Biol.*, vol. 13, no. 4, pp. 1–25, 2015, doi: 10.1371/journal.pbio.1002126.

[17] A. Fantin *et al.*, "Tissue macrophages act as cellular chaperones for vascular anastomosis downstream of VEGF-mediated endothelial tip cell induction," *Blood*, vol. 116, no. 5, pp. 829–840, 2010, doi: 10.1182/blood-2009-12-257832.

[18] M. S. Charpentier and F. L. Conlon,

"Cellular and molecular mechanisms underlying blood vessel lumen formation," *BioEssays*, vol. 36, pp. 251–259, 2013, doi: 10.1002/bies.201300133.

[19] M. L. Iruela-Arispe and G. E. Davis, "Cellular and Molecular Mechanisms of Vascular Lumen Formation," *Dev. Cell*, vol. 16, no. 2, pp. 222–231, 2009, doi: 10.1016/j.devcel.2009.01.013.

[20] M. Potente, H. Gerhardt, and P. Carmeliet, "Basic and therapeutic aspects of angiogenesis," *Cell*, vol. 146, no. 6. pp. 873–887, 16-Sep-2011, doi: 10.1016/j.cell.2011.08.039.

[21] E. Dejana, "Endothelial cell-cell junctions: Happy together," *Nat. Rev. Mol. Cell Biol.*, vol. 5, no. 4, pp. 261–270, 2004, doi: 10.1038/nrm1357.

[22] M. G. Lampugnani, "Endothelial cell-to-cell junctions: Adhesion and signaling in physiology and pathology," *Cold Spring Harb. Perspect. Med.*, vol. 2, no. 10, pp. 1–14, 2012, doi: 10.1101/cshperspect.a006528.

[23] S. Gory-Fauré *et al.*, "Role of vascular endothelial-cadherin in vascular morphogenesis," *Development*, vol. 126, no. 10, pp. 2093–2102, 1999.

[24] P. Carmeliet *et al.*, "Targeted deficiency or cytosolic truncation of the VE-cadherin gene in mice impairs VEGF-mediated endothelial survival and angiogenesis," *Cell*, vol. 98, no. 2, pp. 147–157, 1999, doi: 10.1016/S0092-8674(00)81010-7.

[25] M. Giannotta, M. Trani, and E. Dejana, "VE-cadherin and endothelial adherens junctions: Active guardians of vascular integrity," *Dev. Cell*, vol. 26, no. 5, pp. 441–454, 2013, doi: 10.1016/j.devcel.2013.08.020.

[26] M. Marchand, C. Monnot, L. Muller, and S. Germain, "Extracellular matrix scaffolding in angiogenesis and capillary homeostasis," *Semin. Cell Dev. Biol.*, vol. 89, no. August, pp. 147–156, 2019, doi: 10.1016/j.semcdb.2018.08.007.

[27] C. Korn and H. G. Augustin, "Mechanisms of Vessel Pruning and Regression," *Dev. Cell*, vol. 34, no. 1, pp. 5–17, 2015, doi: 10.1016/j.devcel.2015.06.004.

[28] T. Alon, I. Hemo, A. Itin, J. Pe'er, J. Stone, and E. Keshet, "Vascular endothelial growth factor acts as a survival factor for newly formed retinal vessels and has implications for retinopathy of prematurity," *Nat. Med.*, vol. 1, no. 10, pp. 1024–1028, 1995, doi: 10.1038/nm1095-1024.

[29] C. A. Franco *et al.*, "Dynamic Endothelial Cell Rearrangements Drive Developmental Vessel Regression," *PLoS Biol.*, vol. 13, no. 4, pp. 1–19, 2015, doi: 10.1371/journal.pbio.1002125.

[30] C. K. Domigan *et al.*, "Autocrine VEGF maintains endothelial survival through regulation of metabolism and autophagy," *J. Cell Sci.*, vol. 128, no. 12, pp. 2236–2248, 2015, doi: 10.1242/jcs.163774.

[31] H. G. Augustin, G. Young Koh, G. Thurston, and K. Alitalo, "Control of vascular morphogenesis and homeostasis through the Angiopoietin-Tie system," *Nat. Rev. Mol. Cell Biol.*, vol. 10, no. 3, pp. 165–177, 2009, doi: 10.1038/nrm2639.

[32] G. Zarkada, K. Heinolainen, T. Makinen, Y. Kubota, and K. Alitalo, "VEGFR3 does not sustain retinal angiogenesis without VEGFR2," *Proc. Natl. Acad. Sci. U. S. A.*, vol. 112, no. 3, pp. 761–766, 2015, doi: 10.1073/pnas.1423278112.

[33] T. Yamazaki and Y. Mukouyama, "Tissue Specific Origin, Development, and Pathological Perspectives of Pericytes," *Front. Cardiovasc. Med.*, vol. 5, no. June, pp. 1–6, 2018, doi: 10.3389/fcvm.2018.00078.

[34] R. H. Adams and K. Alitalo, "Molecular regulation of angiogenesis and lymphangiogenesis," *Nat. Rev. Mol. Cell Biol.*, vol. 8, pp. 464–478, 2007, doi: 10.1038/nrm2183.

[35] P. Carmeliet *et al.*, "Abnormal blood vessel development and lethality in embryos lacking a single VEGF allele," *Nature*, vol. 380, no. 6573. pp. 435–439, 1996, doi: 10.1038/380435a0.

[36] S. Karaman, V. M. Leppänen, and K. Alitalo, “Vascular endothelial growth factor signaling in development and disease,” *Development*, vol. 145, no. 14, pp. 1–8, 2018, doi: 10.1242/dev.151019.

[37] F. Shalaby *et al.*, “Failure of blood-island formation and vasculogenesis in Flk-1-deficient mice,” *Nature*, vol. 376, no. 6535. pp. 62–66, 1995, doi: 10.1038/376062a0.

[38] R. Benedito *et al.*, “Notch-dependent VEGFR3 upregulation allows angiogenesis without VEGF-VEGFR2 signalling,” *Nature*, vol. 484, no. 7392, pp. 110–114, 2012, doi: 10.1038/nature10908.

[39] G. H. Fong, J. Rossant, M. Gertsenstein, and M. L. Breitman, “Role of the Flt-1 receptor tyrosine kinase in regulating the assembly of vascular endothelium,” *Nature*, vol. 376, no. 6535. pp. 66–70, 1995, doi: 10.1038/376066a0.

[40] V. C. Ho, L. J. Duan, C. Cronin, B. T. Liang, and G. H. Fong, “Elevated vascular endothelial growth factor receptor-2 abundance contributes to increased angiogenesis in vascular endothelial growth factor receptor-1-deficient mice,” *Circulation*, vol. 126, no. 6, pp. 741–752, 2012, doi: 10.1161/CIRCULATIONAHA.112.091603.

[41] T. Tammela *et al.*, “Blocking VEGFR-3 suppresses angiogenic sprouting and vascular network formation,” *Nature*, vol. 454, no. 7204, pp. 656–660, 2008, doi: 10.1038/nature07083.

[42] T. Tammela *et al.*, “VEGFR-3 controls tip to stalk conversion at vessel fusion sites by reinforcing Notch signalling,” *Nat. Cell Biol.*, vol. 13, no. 10, pp. 1202–1213, 2011, doi: 10.1038/ncb2331.

[43] K. Heinolainen *et al.*, “VEGFR3 Modulates Vascular Permeability by Controlling VEGF/VEGFR2 Signaling,” *Circ. Res.*, vol. 120, no. 9, pp. 1414–1425, 2017, doi: 10.1161/CIRCRESAHA.116.310477.

[44] K. Hori, A. Sen, and S. Artavanis-Tsakonas, “Notch signaling at a glance,” *J. Cell Sci.*, vol. 126, no. 10, pp. 2135–2140, 2013, doi: 10.1242/jcs.127308.

[45] S. Suchting *et al.*, “The Notch ligand Delta-like 4 negatively regulates endothelial tip cell formation and vessel branching,” *Proc. Natl. Acad. Sci. U. S. A.*, vol. 104, no. 9, pp. 3225–3230, 2007, doi: 10.1073/pnas.0611177104.

[46] A. R. Pedrosa *et al.*, “Endothelial Jagged1 antagonizes Dll4 regulation of endothelial branching and promotes vascular maturation downstream of Dll4/Notch1,” *Arterioscler. Thromb. Vasc. Biol.*, vol. 35, no. 5, pp. 1134–1146, 2015, doi: 10.1161/ATVBAHA.114.304741.

[47] A. Quillien *et al.*, “Distinct Notch signaling outputs pattern the developing arterial system,” *Dev.*, vol. 141, no. 7, pp. 1544–1552, 2014, doi: 10.1242/dev.099986.

[48] M. Ehling, S. Adams, R. Benedito, and R. H. Adams, “Notch controls retinal blood vessel maturation and quiescence,” *Dev.*, vol. 140, no. 14, pp. 3051–3061, 2013, doi: 10.1242/dev.093351.

[49] D. A. Fruman, H. Chiu, B. D. Hopkins, S. Bagrodia, L. C. Cantley, and R. T. Abraham, “The PI3K Pathway in Human Disease,” *Cell*, vol. 170, no. 8, pp. 605–635, 2017, doi: 10.1016/j.cell.2017.07.029.

[50] L. C. Cantley and D. Ph, “Phosphatidylinositol 3-Kinase, Growth Disorders, and Cancer,” *N. Engl. J. Med.*, vol. 379, pp. 2052–2062, 2018, doi: 10.1056/NEJMra1704560.

[51] B. Vanhaesebroeck, J. Guillermet-Guibert, M. Graupera, and B. Bilanges, “The emerging mechanisms of isoform-specific PI3K signalling,” *Nat. Rev. Mol. Cell Biol.*, vol. 11, pp. 329–341, 2010, doi: 10.1038/nrm2882.

[52] B. Bilanges, Y. Posor, and B. Vanhaesebroeck, “PI3K isoforms in cell signalling and vesicle trafficking,” *Nat. Rev. Mol. Cell Biol.*, vol. 20, no. 5, pp. 515–534, 2019, doi: 10.1038/s41580-019-0129-z.

[53] B. D. Manning and L. C. Cantley, “AKT/PKB Signaling: Navigating Downstream,” *Cell*, vol. 129, no. 7, pp.

1261–1274, 2007, doi: 10.1016/j.cell.2007.06.009.

[54] B. D. Manning and A. Toker, “AKT/PKB Signaling: Navigating the Network,” *Cell*, vol. 169, no. 3, pp. 381–405, 2017, doi: 10.1016/j.cell.2017.04.001.

[55] S. L. Cai *et al.*, “Activity of TSC2 is inhibited by AKT-mediated phosphorylation and membrane partitioning,” *J. Cell Biol.*, vol. 173, no. 2, pp. 279–289, 2006, doi: 10.1083/jcb.200507119.

[56] K. S. Kovacina *et al.*, “Identification of a proline-rich Akt substrate as a 14-3-3 binding partner,” *J. Biol. Chem.*, vol. 278, no. 12, pp. 10189–10194, 2003, doi: 10.1074/jbc.M210837200.

[57] E. Vander Haar, S. il Lee, S. Bandhakavi, T. J. Griffin, and D. H. Kim, “Insulin signalling to mTOR mediated by the Akt/PKB substrate PRAS40,” *Nat. Cell Biol.*, vol. 9, no. 3, pp. 316–323, 2007, doi: 10.1038/ncb1547.

[58] S. R. Datta *et al.*, “Akt phosphorylation of BAD couples survival signals to the cell- intrinsic death machinery,” *Cell*, vol. 91, no. 2, pp. 231–241, 1997, doi: 10.1016/S0092-8674(00)80405-5.

[59] L. del Peso, M. González-García, C. Page, R. Herrera, and G. Nuñez, “Interleukin-3-induced phosphorylation of BAD through the protein kinase Akt,” *Science (80-.).*, vol. 278, no. 5338, pp. 687–689, 1997, doi: 10.1126/science.278.5338.687.

[60] P. F. Dijkers *et al.*, “FKHR-L1 can act as a critical effector of cell death induced by cytokine withdrawal: Protein kinase B-enhanced cell survival through maintenance of mitochondrial integrity,” *J. Cell Biol.*, vol. 156, no. 3, pp. 531–542, 2002, doi: 10.1083/jcb.200108084.

[61] B. P. Zhou, Y. Liao, W. Xia, Y. Zou, B. Spohn, and M. C. Hung, “HER-2/neu induces p53 ubiquitination via Akt-mediated MDM2 phosphorylation,” *Nat. Cell Biol.*, vol. 3, no. 11, pp. 973–982, 2001, doi: 10.1038/ncb1101-973.

[62] C. L. A. Incheol Shin, F Michael Yakes, Federico Rojo, Nah-Young Shin, Andrei V Bakin, Jose Baselga, “PKB/Akt Mediates Cell-Cycle Progression by Phosphorylation of p27(Kip1) at Threonine 157 and Modulation of Its Cellular Localization,” *Nat Med*, vol. 1, no. 10, pp. 1145–1152, 2002, doi: 10.1038/nm.

[63] T. Sekimoto, M. Fukumoto, and Y. Yoneda, “14-3-3 Suppresses the nuclear localization of threonine 157-phosphorylated p27Kip1,” *EMBO J.*, vol. 23, no. 9, pp. 1934–1942, 2004, doi: 10.1038/sj.emboj.7600198.

[64] B. P. Zhou, Y. Liao, W. Xia, B. Spohn, M. H. Lee, and M. C. Hung, “Cytoplasmic localization of p21 CIP1/WAF1 by Akt-induced phosphorylation in HER-2/neu-overexpressing cells,” *Nat. Cell Biol.*, vol. 3, no. 3, pp. 245–252, 2001, doi: 10.1038/35060032.

[65] M. Welcker *et al.*, “Multisite phosphorylation by Cdk2 and GSK3 controls cyclin E degradation,” *Mol. Cell*, vol. 12, no. 2, pp. 381–392, 2003, doi: 10.1016/S1097-2765(03)00287-9.

[66] E. Yeh *et al.*, “A signalling pathway controlling c-Myc degradation that impacts oncogenic transformation of human cells,” *Nat. Cell Biol.*, vol. 6, no. 4, pp. 308–318, 2004, doi: 10.1038/ncb1110.

[67] H. Sano *et al.*, “Insulin-stimulated phosphorylation of a Rab GTPase-activating protein regulates GLUT4 translocation,” *J. Biol. Chem.*, vol. 278, no. 17, pp. 14599–14602, 2003, doi: 10.1074/jbc.C300063200.

[68] L. Eguez *et al.*, “Full intracellular retention of GLUT4 requires AS160 Rab GTPase activating protein,” *Cell Metab.*, vol. 2, no. 4, pp. 263–272, 2005, doi: 10.1016/j.cmet.2005.09.005.

[69] R. L. Elstrom *et al.*, “Akt stimulates aerobic glycolysis in cancer cells,” *Cancer Res.*, vol. 64, no. 11, pp. 3892–3899, 2004, doi: 10.1158/0008-5472.CAN-03-2904.

[70] R. A. Saxton and D. M. Sabatini, “mTOR Signaling in Growth, Metabolism, and Disease,” *Cell*, vol. 168, no. 9, pp. 960–976, 2017.

[71] J. Kim and K. Guan, “mTOR as a central hub of nutrient signalling and cell growth,” *Nat. Cell Biol.*, vol. 21, no. January, 2019, doi: 10.1038/s41556-018-0205-1.

[72] C. M. Taniguchi, B. Emanuelli, and C. R. Kahn, “Critical nodes in signalling pathways: insights into insulin action,” *Nat. Rev. Mol. Cell Biol.*, vol. 7, no. February, pp. 85–96, 2006, doi: 10.1038/nrm1837.

[73] C. C. Campa, I. Franco, and E. Hirsch, “PI3K-C2α : One enzyme for two products coupling vesicle trafficking and signal transduction,” *FEBS Lett.*, vol. 589, no. 14, pp. 1552–1558, 2015, doi: 10.1016/j.febslet.2015.05.001.

[74] A. L. Marat *et al.*, “mTORC1 activity repression by late endosomal phosphatidylinositol 3,4-bisphosphate,” *Science (80-.).*, vol. 356, no. 365, pp. 968–972, 2017.

[75] S. Alliouachene *et al.*, “Inactivation of the Class II PI3K-C2β Potentiates Insulin Signaling and Sensitivity,” *Cell Rep.*, vol. 13, no. 9, pp. 1881–1894, Dec. 2015, doi: 10.1016/j.celrep.2015.10.052.

[76] L. Braccini *et al.*, “PI3K-C2γ 3 is a Rab5 effector selectively controlling endosomal Akt2 activation downstream of insulin signalling,” *Nat. Commun.*, vol. 6, no. May, 2015, doi: 10.1038/ncomms8400.

[77] J. Domin *et al.*, “The class II phosphoinositide 3-kinase PI3K-C2β regulates cell migration by a PtdIns(3)P dependent mechanism,” *J. Cell. Physiol.*, vol. 205, no. 6, pp. 452–462, 2005, doi: 10.1002/jcp.20478.

[78] T. Maffucci, F. T. Cooke, F. M. Foster, C. J. Traer, M. J. Fry, and M. Falasca, “Class II phosphoinositide 3-kinase defines a novel signaling pathway in cell migration,” *J. Cell Biol.*, vol. 169, no. 5, pp. 789–799, 2005, doi: 10.1083/jcb.200408005.

[79] R. M. Katso *et al.*, “Phosphoinositide 3-Kinase C2β Regulates Cytoskeletal Organization and Cell Migration via Rac-dependent Mechanisms,” *Mol. Biol. Cell*, vol. 17, no. 9, pp. 3729–3744, 2006, doi: 10.1091/mbc.E05.

[80] K. Biswas *et al.*, “Essential Role of Class II Phosphatidylinositol-3-kinase-C2α in Sphingosine 1-Phosphate Receptor-1-mediated Signaling and Migration in Endothelial Cells,” *J. Biol. Chem.*, vol. 288, pp. 2325–2339, 2013, doi: 10.1074/jbc.M112.409656.

[81] F. Gulluni *et al.*, “Mitotic Spindle Assembly and Genomic Stability in Breast Cancer Require PI3K-C2α Scaffolding Function,” *Cancer Cell*, vol. 32, no. 4, pp. 444–459, 2017, doi: 10.1016/j.ccell.2017.09.002.

[82] N. Jaber *et al.*, “Class III PI3K Vps34 plays an essential role in autophagy and in heart and liver function,” *Proc. Natl. Acad. Sci. U. S. A.*, vol. 109, no. 6, pp. 2003–2008, 2012, doi: 10.1073/pnas.1112848109.

[83] B. Bilanges *et al.*, “Vps34 PI 3-kinase inactivation enhances insulin sensitivity through reprogramming of mitochondrial metabolism,” *Nat. Commun.*, vol. 8, no. 1, pp. 1–14, 2017, doi: 10.1038/s41467-017-01969-4.

[84] R. Bago *et al.*, “ The hVps34- SGK 3 pathway alleviates sustained PI3K/Akt inhibition by stimulating mTORC 1 and tumour growth ,” *EMBO J.*, vol. 35, no. 17, pp. 1902–1922, 2016, doi: 10.15252/embj.201693929.

[85] F. O’Farrell *et al.*, “Class III phosphatidylinositol-3-OH kinase controls epithelial integrity through endosomal LKB1 regulation,” *Nat. Cell Biol.*, vol. 19, no. 12, pp. 1412–1423, 2017, doi: 10.1038/ncb3631.

[86] M. Graupera and M. Potente, “Regulation of angiogenesis by PI3K signaling networks,” *Experimental Cell Research*, vol. 319, no. 9. Academic Press Inc., pp. 1348–1355, 15-May-2013, doi: 10.1016/j.yexcr.2013.02.021.

[87] M. Graupera *et al.*, “Angiogenesis selectively requires the p110 a isoform of PI3K to control endothelial cell migration,” *Nature*, vol. 453, no. May, 2008, doi: 10.1038/nature06892.

[88] A. Angulo-Urarte *et al.*, “Endothelial cell rearrangements during vascular patterning require PI3-kinase-mediated inhibition of actomyosin contractility,”

Nat. Commun., vol. 9, no. 4826, pp. 1–16, 2018, doi: 10.1038/s41467-018-07172-3.

[89] S. P. Herbert *et al.*, "Arterial-venous segregation by selective cell sprouting: an alternative mode of blood vessel formation," *Science (80-.).*, vol. 326, no. 5950, pp. 294–298, 2009, doi: 10.1126/science.1178577.

[90] B. Ren *et al.*, "ERK1/2-Akt1 crosstalk regulates arteriogenesis in mice and zebrafish," *J. Clin. Invest.*, vol. 120, no. 4, pp. 1217–1228, 2010, doi: 10.1172/JCI39837.

[91] A. M. Figueiredo *et al.*, "PI3Kβ-Regulated Pericyte Maturation Governs Vascular Remodeling," *Circulation*, no. 5, pp. 1–40, 2020, doi: 10.1161/CIRCULATIONAHA.119.042354.

[92] K. Hamada *et al.*, "The PTEN / PI3K pathway governs normal vascular development and tumor angiogenesis," *Genes Dev.*, vol. 19, pp. 2054–2065, 2005, doi: 10.1101/gad.1308805.12.

[93] S. Choorapoikayil, B. Weijts, R. Kers, A. De Bruin, and J. Den Hertog, "Loss of Pten promotes angiogenesis and enhanced vegfaa expression in zebrafish," *DMM Dis. Model. Mech.*, vol. 6, no. 5, pp. 1159–1166, 2013, doi: 10.1242/dmm.012377.

[94] M. Stumpf and J. Den Hertog, "Differential requirement for pten lipid and protein phosphatase activity during zebrafish embryonic development," *PLoS One*, vol. 11, no. 2, pp. 1–16, 2016, doi: 10.1371/journal.pone.0148508.

[95] H. Serra *et al.*, "PTEN mediates Notch-dependent stalk cell arrest in angiogenesis," *Nat. Commun.*, vol. 6, no. 7, p. 7935, 2015, doi: 10.1038/ncomms8935.

[96] M. Y. Lee, A. K. Luciano, E. Ackah, J. Rodriguez-vita, T. A. Bancroft, and A. Eichmann, "Endothelial Akt1 mediates angiogenesis by phosphorylating multiple angiogenic substrates," *Proc. Natl. Acad. Sci.*, vol. 35, pp. 12865–12870, 2014, doi: 10.1073/pnas.1408472111.

[97] W. S. Chen *et al.*, "Growth retardation and increased apoptosis in mice with homozygous disruption of the akt1 gene," *Genes Dev.*, vol. 15, no. 312, pp. 2203–2208, 2001, doi: 10.1101/gad.913901.GENES.

[98] O. Dormond, J. C. Madsen, and D. M. Briscoe, "The effects of mTOR-Akt interactions on anti-apoptotic signaling in vascular endothelial cells," *J. Biol. Chem.*, vol. 282, no. 32, pp. 23679–23686, 2007, doi: 10.1074/jbc.M700563200.

[99] "DEPTOR Deficiency-Mediated mTORC1 Hyperactivation in Vascular Endothelial Cells Promotes Angiogenesis," *Cell Physiol. Biochem.*, vol. 46, pp. 520–531, 2018, doi: 10.1159/000488619.

[100] M. A. Farhan, K. Carmine-simmen, J. D. Lewis, R. B. Moore, and G. Murray, "Endothelial Cell mTOR Complex-2 Regulates Sprouting Angiogenesis," *PLoS One*, pp. 1–20, 2015, doi: 10.1371/journal.pone.0135245.

[101] K. Wilhelm *et al.*, "FOXO1 couples metabolic activity and growth state in the vascular endothelium," *Nature*, pp. 1–18, 2016, doi: 10.1038/nature16498.

[102] M. Potente *et al.*, "Involvement of Foxo transcription factors in angiogenesis and postnatal neovascularization," *J. Clin. Invest.*, vol. 115, pp. 2382–2392, 2005, doi: 10.1172/JCI23126DS1.

[103] K. Yoshioka *et al.*, "Endothelial PI3K-C2α, a class II PI3K, has an essential role in angiogenesis and vascular barrier function," *Nat. Med.*, vol. 18, no. 10, pp. 1560–1569, 2012, doi: 10.1038/nm.2928.

[104] D. Chiozzotto *et al.*, "Class II Phosphoinositide 3-Kinases Contribute to Endothelial Cells Morphogenesis," *PLoS One*, vol. 8, no. 1, pp. 3–7, 2013, doi: 10.1371/journal.pone.0053808.

[105] A. Dompmartin, M. Vikkula, and L. M. Boon, "Venous malformation: Update on aetiopathogenesis, diagnosis and management," *Phlebology*, vol. 25, no. 5, pp. 224–235, 2010, doi: 10.1258/phleb.2009.009041.

[106] V. L. Luks *et al.*, "Lymphatic and other

vascular malformative/overgrowth disorders are caused by somatic mutations in PIK3CA," *J. Pediatr.*, vol. 166, no. 4, pp. 1048-1054.e5, 2015, doi: 10.1016/j.jpeds.2014.12.069.

[107] P. Castel *et al.*, "Somatic PIK3CA mutations as a driver of sporadic venous malformations," *Sci. Transl. Med.*, vol. 8, pp. 332–342, Mar. 2016, doi: 10.1126/scitranslmed.aaf1164.

[108] S. D. Castillo *et al.*, "Somatic activating mutations in Pik3ca cause sporadic venous malformations in mice and humans," *Sci. Transl. Med.*, vol. 8, pp. 332–343, 2016, doi: 10.1126/scitranslmed.aad9982.

[109] S. D. Castillo, E. Baselga, and M. Graupera, "PIK3CA mutations in vascular malformations," *Curr. Opin. Hematol.*, vol. 26, no. 3, pp. 170–178, 2019, doi: 10.1097/MOH.0000000000000496.

[110] L. M. Hare *et al.*, "Heterozygous expression of the oncogenic Pik3caH1047R mutation during murine development results in fatal embryonic and extraembryonic defects," *Dev. Biol.*, vol. 404, no. 1, pp. 14–26, Aug. 2015, doi: 10.1016/j.ydbio.2015.04.022.

[111] R. R. Madsen, B. Vanhaesebroeck, and R. K. Semple, "Cancer-Associated PIK3CA Mutations in Overgrowth Disorders," *Trends in Molecular Medicine*, vol. 24, no. 10. Elsevier Ltd, pp. 856–870, 01-Oct-2018, doi: 10.1016/j.molmed.2018.08.003.

[112] I. M. Berenjeno *et al.*, "Oncogenic PIK3CA induces centrosome amplification and tolerance to genome doubling," *Nat. Commun.*, vol. 8, no. 1, Dec. 2017, doi: 10.1038/s41467-017-02002-4.

[113] M. J. Lindhurst *et al.*, "A mosaic activating mutation in AKT1 associated with the Proteus syndrome," *N. Engl. J. Med.*, vol. 365, no. 7, pp. 611–619, 2011, doi: 10.1056/NEJMoa1104017.

[114] W. H. Tan *et al.*, "The spectrum of vascular anomalies in patients with PTEN mutations: Implications for diagnosis and management," *J. Med. Genet.*, vol. 44, no. 9, pp. 594–602, 2007, doi: 10.1136/jmg.2007.048934.

[115] C. J. Gallione *et al.*, "Mutation and expression analysis of the endoglin gene in Hereditary Hemorrhagic Telangiectasia reveals null alleles," *Hum. Mutat.*, vol. 11, no. 4, pp. 286–294, 1998, doi: 10.1002/(SICI)1098-1004(1998)11:4<286::AID-HUMU6>3.0.CO;2-B.

[116] M. E. M. P. & D. A. M. D.W. Johnson, J.N. Berg, M.A. Baldwin, C.J. Gallione, I. Marondel, S.-J. Yoon, T.T. Stenzel, M. Speer, M.A. Pericak-Vance, A. Diamond, A.E. Guttmacher, C.E. Jackson, L. Attisano, R. Kucherlapati, "Mutations in the activin receptor–like kinase 1 gene in hereditary haemorrhagic telangiectasia type 2," *Nat. Genet.*, vol. 13, no. 6, pp. 189–195, 1996, doi: https://doi.org/10.1038/ng0696-189.

[117] P. Hillmann and D. Fabbro, "PI3K/mTOR pathway inhibition: Opportunities in oncology and rare genetic diseases," *Int. J. Mol. Sci.*, vol. 20, no. 11, pp. 1–12, 2019, doi: 10.3390/ijms20225792.

[118] K. Okkenhaug, M. Graupera, and B. Vanhaesebroeck, "Targeting PI3K in cancer: Impact on tumor cells, their protective stroma, angiogenesis, and immunotherapy," *Cancer Discov.*, vol. 6, no. 10, pp. 1090–1105, 2016, doi: 10.1158/2159-8290.CD-16-0716.

[119] F. André *et al.*, "Alpelisib for PIK3CA-mutated, hormone receptor-positive advanced breast cancer," *N. Engl. J. Med.*, vol. 380, no. 20, pp. 1929–1940, 2019, doi: 10.1056/NEJMoa1813904.

[120] J. P. Sharman *et al.*, "Final results of a randomized, phase III study of rituximab with or without idelalisib followed by open-label idelalisib in patients with relapsed chronic lymphocytic leukemia," *J. Clin. Oncol.*, vol. 37, no. 16, pp. 1391–1402, 2019, doi: 10.1200/JCO.18.01460.

[121] T. L. Yuan *et al.*, "Class 1A PI3K regulates vessel integrity during development and tumorigenesis," *Proc. Natl. Acad. Sci.*, vol. 105, no. 28, pp. 9739–9744, 2008.

[122] C. R. Schnell *et al.*, "Effects of the dual phosphatidylinositol 3-

kinase/mammalian target of rapamycin inhibitor NVP-BEZ235 on the tumor vasculature: Implications for clinical imaging," *Cancer Res.*, vol. 68, no. 16, pp. 6598–6607, 2008, doi: 10.1158/0008-5472.CAN-08-1044.

[123] A. Soler *et al.*, "Inhibition of the p110α isoform of PI 3-kinase stimulates nonfunctional tumor angiogenesis," *J. Exp. Med.*, vol. 210, no. 10, pp. 1937–1945, 2013, doi: 10.1084/jem.20121571.

[124] A. Soler *et al.*, "Therapeutic benefit of selective inhibition of p110a PI3-kinase in pancreatic neuroendocrine tumors," *Clin. Cancer Res.*, vol. 22, no. 23, pp. 5805–5817, 2016, doi: 10.1158/1078-0432.CCR-15-3051.

[125] N. Qayum *et al.*, "Tumor vascular changes mediated by inhibition of oncogenic signaling," *Cancer Res.*, vol. 69, no. 15, pp. 6347–6354, 2009, doi: 10.1158/0008-5472.CAN-09-0657.

[126] E. Fokas *et al.*, "Dual inhibition of the PI3K/mTOR pathway increases tumor radiosensitivity by normalizing tumor vasculature," *Cancer Res.*, vol. 72, no. 1, pp. 239–248, 2012, doi: 10.1158/0008-5472.CAN-11-2263.

[127] M. Lee *et al.*, "PI3 kinase inhibition improves vascular malformations in mouse models of hereditary haemorrhagic telangiectasia," *Nat. Commun.*, vol. 7, 2016, doi: 10.1038/ncomms13650.

[128] Q. Venot *et al.*, "Targeted therapy in patients with PIK3CA-related overgrowth syndrome," *Nature*, vol. 558, no. 7711, pp. 540–546, Jun. 2018, doi: 10.1038/s41586-018-0217-9.

[129] E. Boscolo *et al.*, "Rapamycin improves TIE2-mutated venous malformation in murine model and human subjects," *J. Clin. Invest.*, vol. 125, no. 9, pp. 3491–3504, 2015, doi: 10.1172/JCI76004.

[130] R. G. A. Denise M. Adams, MD, Cameron C. Trenor III, MD, PhD, Adrienne M. Hammill, MD, PhD, Alexander A. Vinks, PhD, Manish N. Patel, DO, Gulraiz Chaudry, MBChB, Mary Sue Wentzel, MSN, Paula S. Mobberley-Schuman, MS, Lisa M. Campbell, MS, Christine Brookbank, MEd, "Efficacy and Safety of Sirolimus in the Treatment of Complicated Vascular Anomalies," *J. Vasc. Surg.*, vol. 137, no. 1, p. 10, 2016, doi: 10.1016/j.jvs.2019.06.217.

[131] J. Hammer *et al.*, "Sirolimus is efficacious in treatment for extensive and/or complex slow-flow vascular malformations: A monocentric prospective phase II study," *Orphanet J. Rare Dis.*, vol. 13, no. 1, pp. 1–13, 2018, doi: 10.1186/s13023-018-0934-z.

[132] M. Song, A. M. Bode, Z. Dong, and M. H. Lee, "AKt as a therapeutic target for cancer," *Cancer Res.*, vol. 79, no. 6, pp. 1019–1031, 2019, doi: 10.1158/0008-5472.CAN-18-2738.

[133] Y. Yu *et al.*, "Targeting AKT1-E17K and the PI3K/AKT pathway with an allosteric AKT inhibitor, ARQ 092," *PLoS One*, vol. 10, no. 10, pp. 1–26, 2015, doi: 10.1371/journal.pone.0140479.

[134] Y. Yu *et al.*, "In vitro and in vivo anti-tumor activity of ARQ 092, a potent and selective pan-AKT inhibitor.," *Eur. J. Cancer*, vol. 50, no. 11, pp. 172–173, 2014, doi: 10.1016/s0959-8049(14)70657-4.

[135] G. S. Roth *et al.*, "Efficacy of AKT inhibitor ARQ 092 compared with sorafenib in a cirrhotic rat model with hepatocellular carcinoma," *Mol. Cancer Ther.*, vol. 16, no. 10, pp. 2157–2165, 2017, doi: 10.1158/1535-7163.MCT-16-0602-T.

[136] C. Ranieri *et al.*, "In vitro efficacy of ARQ 092, an allosteric AKT inhibitor, on primary fibroblast cells derived from patients with PIK3CA-related overgrowth spectrum (PROS)," *Neurogenetics*, vol. 19, no. 2, pp. 77–91, 2018, doi: 10.1007/s10048-018-0540-1.

[137] M. J. Lindhurst, M. R. Yourick, Y. Yu, R. E. Savage, D. Ferrari, and L. G. Biesecker, "Repression of AKT signaling by ARQ 092 in cells and tissues from patients with Proteus syndrome," *Sci. Rep.*, vol. 5, no. 12, pp. 1–12, 2015, doi: 10.1038/srep17162.

[138] C. Leoni *et al.*, "First evidence of a

therapeutic effect of miransertib in a teenager with Proteus syndrome and ovarian carcinoma," *Am. J. Med. Genet. Part A*, vol. 179, no. 7, pp. 1319–1324, 2019, doi: 10.1002/ajmg.a.61160.

[139] X. Chen *et al.*, "Endothelial and cardiomyocyte PI3Kβ divergently regulate cardiac remodelling in response to ischaemic injury," *Cardiovasc. Res.*, vol. 115, no. 8, pp. 1343–1356, 2019, doi: 10.1093/cvr/cvy298.

[140] M. A. Whitehead, M. Bombardieri, C. Pitzalis, and B. Vanhaesebroeck, "Isoform-selective induction of human p110δ PI3K expression by TNFα: Identification of a new and inducible PIK3CD promoter," *Biochem. J.*, vol. 443, no. 3, pp. 857–867, 2012, doi: 10.1042/BJ20112214.

[141] M. J. Anderson, L. A. Naiche, C. P. Wilson, C. Elder, D. A. Swing, and M. Lewandoski, "TCreERT2, a Transgenic Mouse Line for Temporal Control of Cre-Mediated Recombination in Lineages Emerging from the Primitive Streak or Tail Bud," *PLoS One*, vol. 8, no. 4, pp. 1–7, 2013, doi: 10.1371/journal.pone.0062479.

[142] Y. A. Wang *et al.*, "A novel transgenic mice model for venous malformation," *Transgenic Res.*, vol. 18, no. 2, pp. 193–201, 2009, doi: 10.1007/s11248-008-9224-1.

[143] J. Goines *et al.*, "A xenograft model for venous malformation," *Angiogenesis*, vol. 21, no. 4, pp. 725–735, 2018, doi: 10.1007/s10456-018-9624-7.

[144] M. E. Pitulescu, I. Schmidt, R. Benedito, and R. H. Adams, "Inducible gene targeting in the neonatal vasculature and analysis of retinal angiogenesis in mice," *Nat. Protoc.*, vol. 5, no. 9, pp. 1518–1534, 2010, doi: 10.1038/nprot.2010.113.

[145] L. di Blasio *et al.*, "PI3K/mTOR inhibition promotes the regression of experimental vascular malformations driven by PIK3CA-activating mutations article," *Cell Death Dis.*, vol. 9, no. 2, Feb. 2018, doi: 10.1038/s41419-017-0064-x.

[146] S. Rafii, J. M. Butler, and B. Sen Ding, "Angiocrine functions of organ-specific endothelial cells," *Nature*, vol. 529, no. 7586, pp. 316–325, 2016, doi: 10.1038/nature17040.

[147] A. Al-Soudi, M. H. Kaaij, and S. W. Tas, "Endothelial cells: From innocent bystanders to active participants in immune responses," *Autoimmun. Rev.*, vol. 16, no. 9, pp. 951–962, Sep. 2017, doi: 10.1016/j.autrev.2017.07.008.

[148] J. Zhang *et al.*, "Endothelial Lactate Controls Muscle Regeneration from Ischemia by Inducing M2-like Macrophage Polarization," *Cell Metab.*, vol. 31, no. 6, pp. 1136-1153.e7, 2020, doi: 10.1016/j.cmet.2020.05.004.

[149] E. Boscolo *et al.*, "AKT hyper-phosphorylation associated with PI3K mutations in lymphatic endothelial cells from a patient with lymphatic malformation," *Angiogenesis*, vol. 18, no. 2, pp. 151–162, 2015, doi: 10.1007/s10456-014-9453-2.

[150] E. Seront, A. Van Damme, L. M. Boon, and M. Vikkula, "Rapamycin and treatment of venous malformations," *Curr. Opin. Hematol.*, vol. 26, no. 3, pp. 185–192, 2019, doi: 10.1097/MOH.0000000000000498.

[151] P. Hillmann and D. Fabbro, "PI3K/mTOR pathway inhibition: Opportunities in oncology and rare genetic diseases," *Int. J. Mol. Sci.*, vol. 20, no. 11, pp. 1–16, 2019, doi: 10.3390/ijms20225792.

[152] A. Soler, A. Angulo-Urarte, and M. Graupera, "PI3K at the crossroads of tumor angiogenesis signaling pathways," *Mol. Cell. Oncol.*, vol. 2, no. 2, pp. 1–10, 2015, doi: 10.4161/23723556.2014.975624.

[153] K. M. Keppler-Noreuil *et al.*, "Pharmacodynamic Study of Miransertib in Individuals with Proteus Syndrome," *Am. J. Hum. Genet.*, vol. 104, no. 3, pp. 484–491, 2019, doi: 10.1016/j.ajhg.2019.01.015.

[154] L. G. Biesecker *et al.*, "Clinical report: one year of treatment of Proteus syndrome with miransertib (ARQ 092)," *Cold Spring Harb. Mol. case Stud.*, vol. 6, no. 1, pp. 1–10, 2020, doi:

10.1101/mcs.a004549.

[155] Y. Yu, T. Hall, S. Eathiraj, M. J. Wick, B. Schwartz, and G. Abbadessa, “In-vitro and in-vivo combined effect of ARQ 092, an AKT inhibitor, with ARQ 087, a FGFR inhibitor,” *Anticancer. Drugs*, vol. 28, no. 5, pp. 503–513, 2017, doi: 10.1097/CAD.0000000000000486.

[156] X. Li *et al.*, “Ponatinib combined with rapamycin causes regression of murine venous malformation,” *Arterioscler. Thromb. Vasc. Biol.*, vol. 39, no. 3, pp. 496–512, 2019, doi: 10.1161/ATVBAHA.118.312315.

[157] S. Ruiz, F. Campagne, and P. Marambaud, “Correcting Smad1/5/8, mTOR, and VEGFR2 treats pathology in hereditary hemorrhagic telangiectasia models Graphical abstract Find the latest version :,” *J. Clin. Invest.*, vol. 130, no. 2, pp. 942–957, 2019.

[158] C. J. Bowen *et al.*, “Targetable cellular signaling events mediate vascular pathology in vascular Ehlers-Danlos syndrome,” *J. Clin. Invest.*, vol. 130, no. 2, pp. 686–698, 2020, doi: 10.1172/JCI130730.

[159] K. Harada, A. B. Truong, T. Cai, and P. A. Khavari, “The Class II Phosphoinositide 3-Kinase C2β Is Not Essential for Epidermal Differentiation,” *Mol. Cell. Biol.*, vol. 25, no. 24, pp. 11122–11130, 2005, doi: 10.1128/mcb.25.24.11122-11130.2005.

[160] A. Wallroth, P. A. Koch, A. L. Marat, E. Krause, and V. Haucke, “Protein kinase N controls a lysosomal lipid switch to facilitate nutrient signalling via mTORC1,” *Nature Cell Biology*, vol. 21, no. 9. Nature Publishing Group, pp. 1093–1101, 01-Sep-2019, doi: 10.1038/s41556-019-0377-3.

[161] L. L. Mandar Deepak Muzumdar, Bosiljka Tasic, Kazunari Miyamichi, Ling Li, “A Global Double-Fluorescent Cre Reporter Mouse,” *Genesis*, vol. 45, no. 2, pp. 593–605, 2007, doi: 10.1002/dvg.

[162] J. Ersching *et al.*, “Germinal Center Selection and Affinity Maturation Require Dynamic Regulation of mTORC1 Kinase,” *Immunity*, vol. 46, no. 6, pp. 1045–1058, 2017, doi: 10.1016/j.immuni.2017.06.005.

[163] A. Efeyan, W. C. Comb, and D. M. Sabatini, “Nutrient-sensing mechanisms and pathways,” *Nature*, vol. 517, no. 7534, pp. 302–310, 2015, doi: 10.1038/nature14190.

[164] K. De Bock, M. Georgiadou, and P. Carmeliet, “Role of endothelial cell metabolism in vessel sprouting,” *Cell Metab.*, vol. 18, no. 5, pp. 634–647, 2013, doi: 10.1016/j.cmet.2013.08.001.

[165] W. Li, M. Petrimpol, K. D. Molle, M. N. Hall, E. J. Battegay, and R. Humar, “Hypoxia-induced endothelial proliferation requires both mTORC1 and mTORC2,” *Circ. Res.*, vol. 100, no. 1, pp. 79–87, 2007, doi: 10.1161/01.RES.0000253094.03023.3f.

[166] A. Ma *et al.*, “Tsc1 deficiency-mediated mTOR hyperactivation in vascular endothelial cells causes angiogenesis defects and embryonic lethality,” *Hum. Mol. Genet.*, vol. 23, no. 3, pp. 693–705, 2014, doi: 10.1093/hmg/ddt456.

[167] S. Sun *et al.*, “Constitutive Activation of mTORC1 in Endothelial Cells Leads to the Development and Progression of Article Constitutive Activation of mTORC1 in Endothelial Cells Leads to the Development and Progression of Lymphangiosarcoma through VEGF Autocrine Signalin,” *Cancer Cell*, vol. 28, no. 6, pp. 758–772, 2015, doi: 10.1016/j.ccell.2015.10.004.

[168] R. Diéguez-Hurtado *et al.*, “Loss of the transcription factor RBPJ induces disease-promoting properties in brain pericytes,” *Nat. Commun.*, vol. 10, no. 1, pp. 1–19, 2019, doi: 10.1038/s41467-019-10643-w.

[169] N. B. Hamilton, D. Attwell, and C. N. Hall, “Pericyte-mediated regulation of capillary diameter: a component of neurovascular coupling in health and disease,” *Front. Neuroenergetics*, vol. 2, no. 5, pp. 1–14, 2010, doi: 10.3389/fnene.2010.00005.

[170] J. Almaça, J. Weitz, R. Rodriguez-Diaz, E. Pereira, and A. Caicedo, “The Pericyte of the Pancreatic Islet Regulates Capillary Diameter and Local Blood Flow,” *Cell Metab.*, vol. 27, no. 3, pp.

630-644.e4, 2018, doi: 10.1016/j.cmet.2018.02.016.

[171] F. Fernández-Klett, N. Offenhauser, U. Dirnagl, J. Priller, and U. Lindauer, "Pericytes in capillaries are contractile in vivo, but arterioles mediate functional hyperemia in the mouse brain," *Proc. Natl. Acad. Sci. U. S. A.*, vol. 107, no. 51, pp. 22290–22295, 2010, doi: 10.1073/pnas.1011321108.

[172] V. Dominguez *et al.*, "Class II phosphoinositide 3-kinase regulates exocytosis of insulin granules in pancreatic β cells," *J. Biol. Chem.*, vol. 286, no. 6, pp. 4216–4225, 2011, doi: 10.1074/jbc.M110.200295.

[173] L. Liu *et al.*, "Rapamycin inhibits cytoskeleton reorganization and cell motility by suppressing RhoA expression and activity," *J. Biol. Chem.*, vol. 285, no. 49, pp. 38362–38373, 2010, doi: 10.1074/jbc.M110.141168.

[174] K. Błajecka, M. Marinov, L. Leitner, K. Uth, G. Posern, and A. Arcaro, "Phosphoinositide 3-Kinase C2β Regulates RhoA and the Actin Cytoskeleton through an Interaction with Dbl," *PLoS One*, vol. 7, no. 9, Sep. 2012, doi: 10.1371/journal.pone.0044945.

[175] N. Sabha *et al.*, "PIK3C2B inhibition improves function and prolongs survival in myotubular myopathy animal models," *J. Clin. Invest.*, vol. 126, no. 9, pp. 3613–3625, Sep. 2016, doi: 10.1172/JCI86841.

[176] I. Mavrommati, O. Cisse, M. Falasca, and T. Maffucci, "Novel roles for class II Phosphoinositide 3-Kinase C2β in signalling pathways involved in prostate cancer cell invasion," *Sci. Rep.*, vol. 6, no. October 2015, pp. 1–15, 2016, doi: 10.1038/srep23277.

[177] A. Chikh *et al.*, "Class II phosphoinositide 3-kinase C2β regulates a novel signaling pathway involved in breast cancer progression," *Oncotarget*, vol. 7, no. 14, pp. 18325–18345, 2016, doi: 10.18632/oncotarget.7761.

[178] N. Tisch *et al.*, "Caspase-8 modulates physiological and pathological angiogenesis during retina development," *J. Clin. Invest.*, vol. 129, no. 12, pp. 5092–5107, 2019, doi: 10.1172/JCI122767.

[179] P. Villacampa *et al.*, "Accelerated oxygen-induced retinopathy is a reliable model of ischemia-induced retinal neovascularization," *PLoS One*, vol. 12, no. 6, pp. 1–11, 2017, doi: 10.1371/journal.pone.0179759.

[180] A. Kurdi, G. R. Y. De Meyer, and W. Martinet, "Potential therapeutic effects of mTOR inhibition in atherosclerosis," *Br. J. Clin. Pharmacol.*, pp. 1267–1279, 2016, doi: 10.1111/bcp.12820.

[181] C. Camaré, M. Pucelle, A. Nègre-Salvayre, and R. Salvayre, "Angiogenesis in the atherosclerotic plaque," *Redox Biol.*, vol. 12, no. February, pp. 18–34, 2017, doi: 10.1016/j.redox.2017.01.007.

[182] G. L. Basatemur, H. F. Jørgensen, M. C. H. Clarke, M. R. Bennett, and Z. Mallat, "Vascular smooth muscle cells in atherosclerosis," *Nat. Rev. Cardiol.*, vol. 16, no. 12, pp. 727–744, 2019, doi: 10.1038/s41569-019-0227-9.

[183] C. Fernández-Hernando *et al.*, "Loss of Akt1 Leads to Severe Atherosclerosis and Occlusive Coronary Artery Disease," *Cell Metab.*, vol. 6, no. 6, pp. 446–457, 2007, doi: 10.1016/j.cmet.2007.10.007.